Nova Scotia

Department of
Natural Resources

PO Box 698 1701 Hollis Street Halifax, Nova Scotia B3J 2T9

OPEN FILE REPORT 92-008

Geological and Geochemical Observations within the Tangier Gold Deposit

M. C. Corey and R. F. Mills

Nova Scotia Department of Natural Resources

Honourable John G. Leefe, Minister

Halifax, Nova Scotia
1992

93-00814/

TABLE OF CONTENTS

Page

1. INTRODUCTION 1

2. EXPLORATION AND MINING HISTORY 1
   2.1 Historical Overview 1
   2.2 Recent Mining and Exploration 4

3. GEOLOGICAL SETTING 6
   3.1 Geology of the Meguma Terrane 6
   3.2 Structure and Deformation 6
   3.3 Metamorphism 8
   3.4 Alteration 8
   3.5 Origin of Gold Deposits 8

4. GEOLOGY OF THE TANGIER DEPOSIT 10
   4.1 Introduction 10
   4.2 Description of Lithologic Units 13
   4.2.1 Pelite 13
   4.2.2 Alteration 18
   4.2.3 Psammite 18
   4.2.4 Alteration 19
   4.2.5 Semi-Pelite 19

5. DESCRIPTION OF QUARTZ VEINS 20
   5.1 Stratabound 20
   5.2 En-Echelon/angular veins 22
   5.3 Quartz-carbonate angulars 22
   5.4 Stratigraphic Variation 29

6. GEOCHEMISTRY 29
   6.1 Whole Rock Lithogeochemistry 31
   6.1.1 Psammite 31
   6.1.2 Pelite 46
   6.1.3 Quartz veins 51
   6.2 Mineral Chemistry 51
   6.2.1 Biotite 54
   6.2.2 Chlorite 54
   6.2.3 Other Minerals 54

7. STRUCTURE AND DEFORMATION 58
   7.1 Faults and Shear Zones 58

Page

8. LOCALIZATION OF GOLD 60

9. DISCUSSION 62

10. CONCLUSIONS 65

11. ACKNOWLEDGEMENTS 66

12. REFERENCES 66

13. APPENDICES 71
13.1 Appendix A. (Lithogeochemistry) 71
13.2 Appendix B. (Mineral Chemistry) 78

14. LiST OF PLATES 85

GEOLOGICAL AND GEOCHEMICAL OBSERVATIONS WITHIN THE TANGIER GOLD DEPOSIT

M. C. Corey and R. F. Mills

1. INTRODUCTION

The Tangier gold deposit is situated within the village of Tangier, Halifax County, Nova Scotia, which is located about 85 kilometers east by northeast of Halifax (Fig. 1.). At the time of writing this report a mining lease for the deposit was held by Coxheath Gold Holdings Ltd.

The landscape of the deposit area consists of drumlins and glacially modified hummocky terrain, terraced by the shoreline in response to glacial isostatic rebound (Stea and Fowler, 1979; Smith, 1988). Today's shoreline is less than 1 kilometre to the south. Average height above sea level is 20 meters. Maximum elevation in the immediate area is 55m above sea level and minimum is sea level. The Tangier mine portal is situated 15 meters above sea level.

The objectives of this project were to compile all previous and current geological data regarding the Tangier mine and to investigate the controls of gold mineralization. This was to be accomplished through detailed geological underground mapping and sampling of existing underground workings and a program of diamond drilling. The project suffered a initial setback when the company currently holding the licence on the property was unable to raise financing to pump out the underground workings. Unable to do underground mapping, the project concentrated on the diamond drill core and data compilation. Since virtually all of the gold bearing zones intersected by Coxheath Gold Holdings Ltd. during underground and surface diamond drilling were removed for assaying purposes the only complete core sections available were from 5 holes drilled by the Sullivan Mining Group in 1983. As part of this study the Nova Scotia Department of Mines and Energy conducted a 4-hole drill program designed to investigate the stratigraphy west of the present underground development as well as provide complete core sections for detailed study. This information was futher supplemented with data compiled from library information, unreleased private company information and geochemical and petrologic investigations of drill core and dump samples. This report presents results of petrological and geochemical investigations and preliminary results of diamond drilling.

2. EXPLORATION AND MINING HISTORY

2.1 Historical Overview

Table 1 lists the sequence of significant events in the mining history of the Tangier mine and the corresponding ounces of gold recovered. As shown, the discovery of gold near Rush Lake in 1860 resulted in production of the regions first gold mine and Nova Scotia's first gold rush. A "wild stampede" of prospective miners applied for leases in the winter of 1861 at Tangier (Malcolm, 1976). The small nature of the claims (20 feet along strike of the veins by 50 across strike) made systematic and coherent mining impossible. The small claims were worked by individuals, each putting down their own shaft to shallow depths. Some 114 shafts were put down on the veins to an average depth of only 20 metres (Forgeron, *et al.*, 1988).

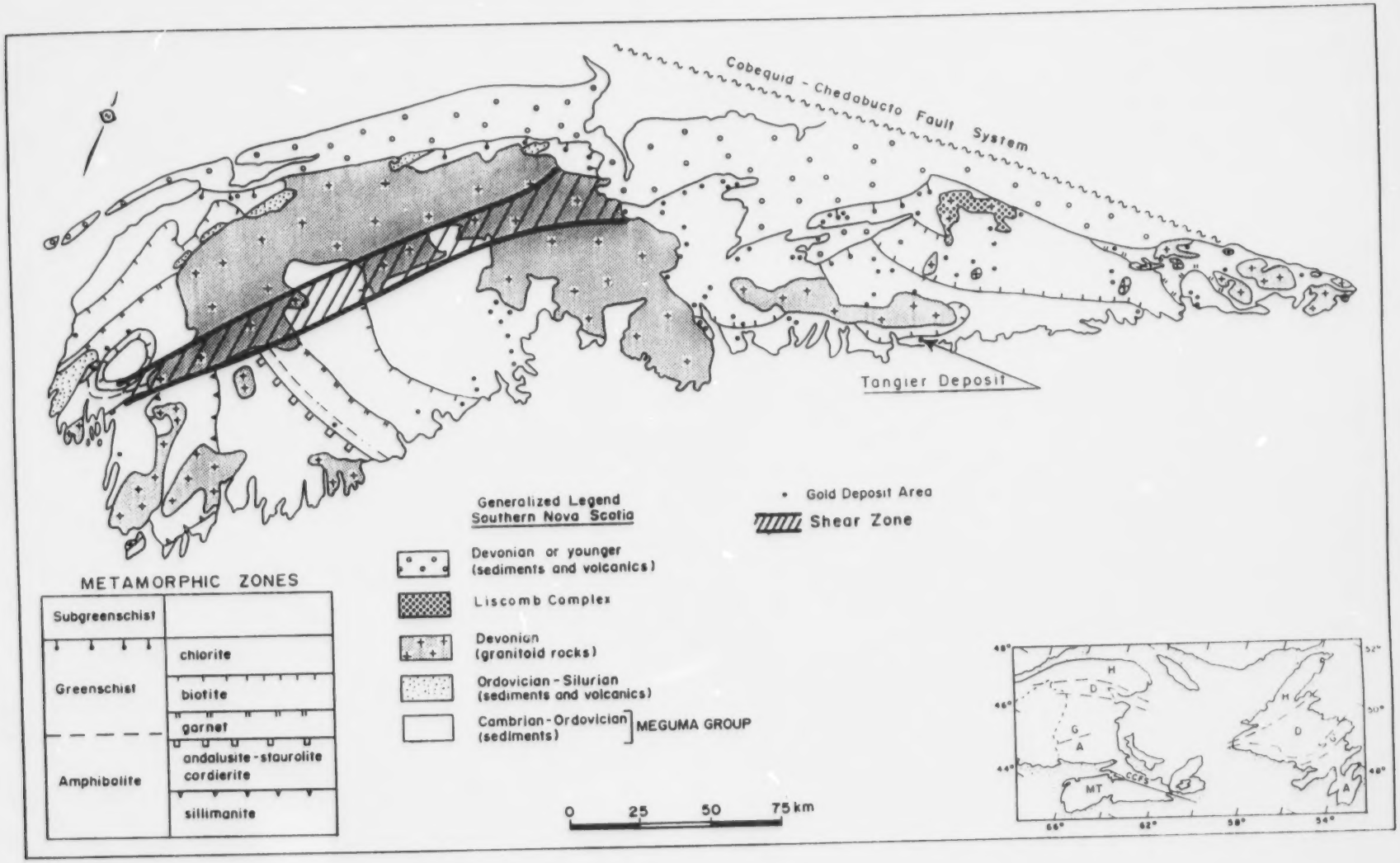

FIGURE 1. Map of N.S. showing location of Tangier and other gold deposits within the Meguma Terrane with respect to general geology and metamorphic zones.

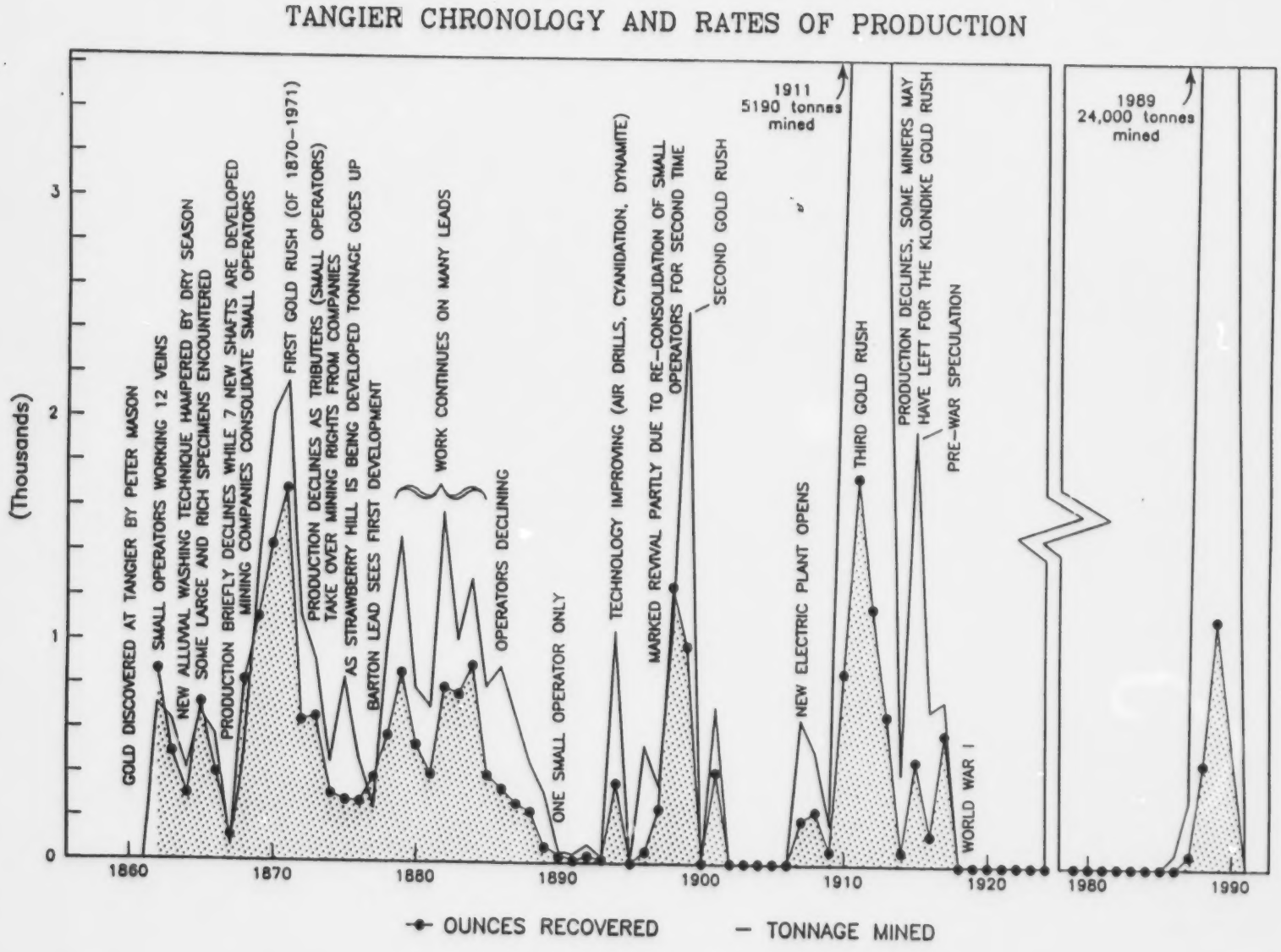

TABLE 1. Chronological history of mining and gold production at Tangier.

Despite the claim problems, initial ore recoveries at the Tangier deposit were spectacular even by historical standards. In 1862 twelve of the richest leads were worked with recoveries averaging 1.25 oz/ton of gold. A change in government policies in 1867 allowing claim holders to sell out or unite with others resulted in 1,240 ounces of gold recovered in 1868 (Malcolm, 1976). The most productive years were 1870-1871 in which 3,907 ounces of gold were recovered from 5,656 tons for an average grade of 0.69 oz./ton (Malcolm, 1976). Small scale mining operations continued at Tangier until the mid 1880's, when an influx of experienced mining people endeavored to reopen some of the idle workings. The combination of mining experience and new technology (cyanide and bromo-cyanide ore treatment) together with financial responsibility, met with some success until roughly the turn of the century. Production and development continued in sporadic fashion until 1921. Production after 1910 appears to have come from the Kent shaft, situated immediately north of Rush Lake. Gold recovery from this shaft reached 2,907 oz. gold from 9,052 tons (0.32 oz./ton) for the period 1910-1911 (Malcolm, 1976). Total production reported from mining at Tangier is 26,287 ounces of gold recovered from approximately 54,000 tons of crushed rock throughout the period 1862-1919. This represents an average grade of 0.48 oz./ton gold (16.6 g/tonne).

2.2 Recent Mining and Exploration

No gold production was reported from the Tangier deposit after 1921. Renewed exploration efforts through the the 1950's to 1980 concentrated on the feasability of mining placer gold from overburden in the vicinity of Copper Lake. This work was preceeded in 1862 when Copper Lake was drained revealing small angular nuggets within glacial drift under the lake bottom sediment. The work was not pursued however due to discouraging results (Malcolm, 1976). Overburden sampling north of Copper Lake in 1958 was also not followed-up. Trenching and pitting by several companies in 1978-1980 also investigated the placer potential of gravels in the immediate vicinity of Copper Lake (Forgeron, *et al.*, 1988). In 1980 the lake-bottom sediments of Copper Lake were tested using a truck-mounted reverse circulation drill. This program reported values $\leq$ 9.50 dollars per m^3 and indicated a source for the gold immediately north of Copper Lake. A drilling program was recommended but never carried out. Regional till exploration by Noranda was conducted in 1982 east and north of the Tangier gold district (Forgeron, *et al.*, 1988).

Prior to the extensive exploration and development by Coxheath Gold Holdings Ltd.(see below) 5 holes totalling 315 m were drilled by the Sullivan Mining Group in 1983 along a north-south line just east of Copper Lake. A 1m long core sample which included a 10 cm gold-bearing quartz vein returned a grade of 20 oz. Au/ton. The overall results however were disappointing.

Coxheaths current stewardship of the Tangier gold district and Tangier mine began on April 1, 1986. The following year exploration and pre-development work began in earnest. Extensive surficial exploration was conducted including large scale prospecting, geophysical surveys and geochemical investigation of the glaciated terrain in the area. A large diamond drilling program initiated on the property outlined ore zones in many of the same quartz leads that had been worked more than a century before (Forgeron *et al.*, 1988). A bulk sample was extracted in 1987 and subsequently led to extensive underground development of the deposit over the next year (Coxheath, 1988). Nova Scotia's first mining lease in 42 years was issued to Coxheath on Dec. 19, 1988. Development in the late 1987-1989 consisted of 30,000 meters of surficial and underground drilling and 5 kilometers of underground development (Fig. 2). Twenty-four thousand (24,000) tons of low grade (development) ore taken from the underground workings were milled at an average grade of 0.07 ounces/ton with a recovery of 90% (Coxheath, 1989). In contrast, 4 mill runs totalling 1513 tons of material taken from a gold-rich ore-

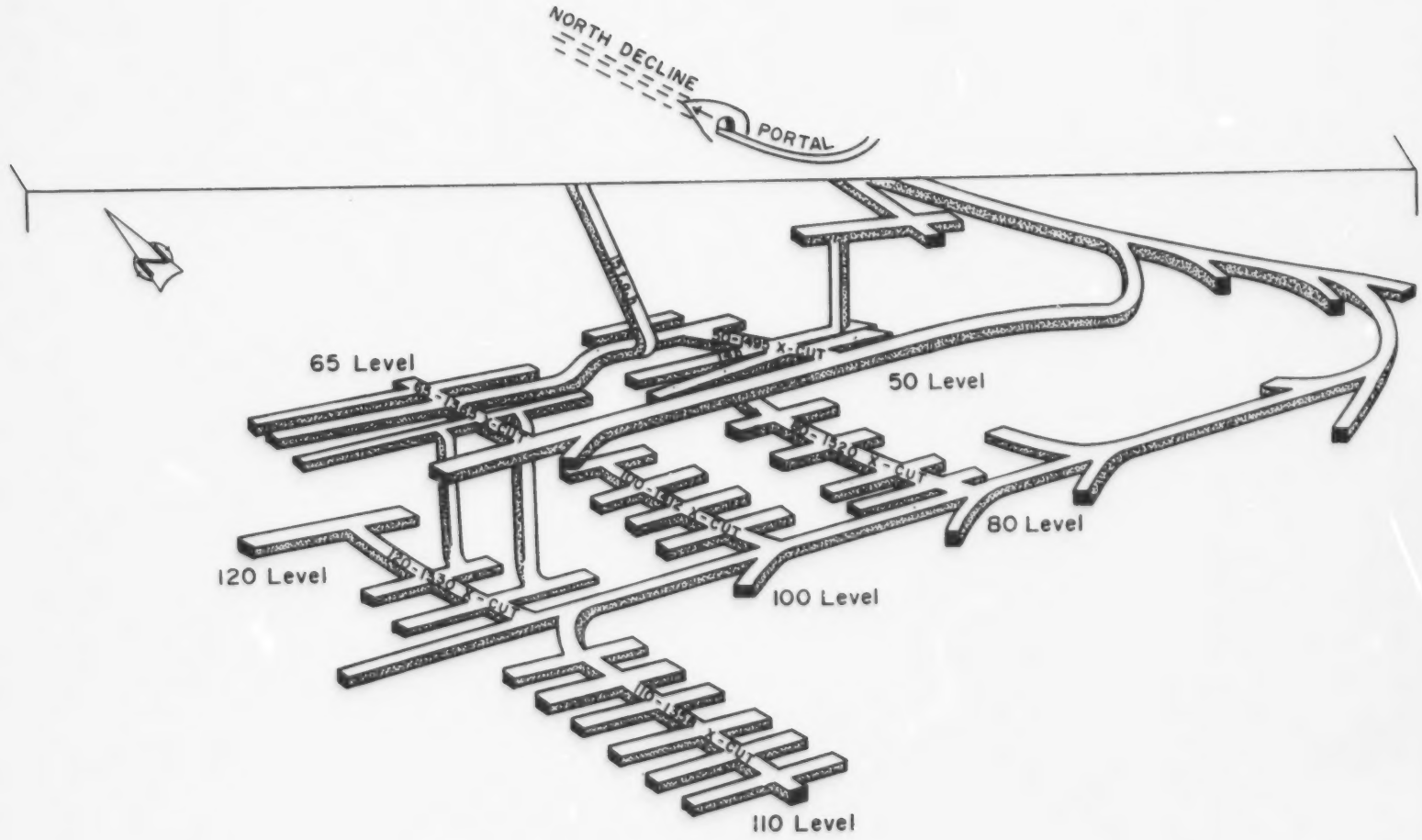

FIGURE 2. Schematic section of underground development at Tangier by Coxheath Gold Holdings Ltd. as of May 1989. No scale intended.

shoot returned an average head grade of 0.58 oz. Au/ton. Gold recovery during these runs ranged from 89-93% (Coxheath, 1989).

Unfortunately, dwindling exploration funds in 1988 combined with legal problems and excessive company debt led Coxheath to suspend operations at Tangier on June 1, 1989. The mine is currently flooded. As of June 1989, proven and probable ore reserves are 144,000 tons grading 0.298 oz. Au/ton (cut) and 1.17 oz. Au/ton (uncut) over a mining width of 3.3 feet (Coxheath, 1990).

3. GEOLOGICAL SETTING

3.1 Geology of the Meguma Terrane

The Meguma Terrane is comprised of three lithotectonic units ranging in age from Cambrian to Devonian. From (areally) most to least abundant these are; metasedimentary rocks of the Cambrian to Ordovician Meguma Group, Late Devonian granitoid intrusions of predominately peraluminous composition and Silurian to Devonian metasedimentary and volcanic rocks scattered along the north margin of the Meguma Terrane in western Nova Scotia. (Fig. 1).

The Meguma Group consists of two dominant formations. These are the Goldenville Formation, consisting of interbedded, regionally metamorphosed, sandstones and siltstones (psammites) and the conformably overlying Halifax Formation, dominated by grey to black slates (pelites) and shales with minor interbedded siltstones. A possibly regionaly correlative third formation has been recognized through detailed mapping by O'Brien (1986) within the Mahone Bay area. Termed the Green Bay Formation this lithostratigraphic package consists of interbedded green to grey-green, Mn-rich siltstones and minor sandstones. This Formation occupies the Goldenville to Halifax transition zone (GHT) and is estimated to have a total thickness of 1-2.5 km. (O'Brien, 1986).

The GHT is poorly exposed throughout the Meguma Zone covering a strike length of approximately 170 kilometres. Where observed, the upper portion of the transition zone is often marked by a banded, highly deformed, calcareous psammite that can contain a high concentration of sulphides and spessartine garnet. This strata has been referred to as a coticule (Sangster, 1990; Graves and Zentilli, 1982). The Tangier gold deposit is believed to be approximately 4.4 kilometres below the GHT (Sangster, 1990).

Synchronous with extensive intrusion of peraluminous granitiods of ca.370 Ma age were mafic intrusions associated with the Liscomb Complex and minor mafic dykes and sills (Fig. 1). The Liscomb Complex, comprised of granulite-facies metavolcanic and metasedimentary rocks and high grade gneisses are of particular interest as they provide a window to rocks of lower crustal compositions (Giles and Chatterjee, 1987). The Liscomb Complex has been indentified as a potential source rock for the gold within Meguma-hosted gold deposits (Chatterjee and Smith, 1991). The Tangier or Popes Harbour Dyke exposed on the east side of Tangier Harbour is approximately 13 metres wide, strikes N-S and dips vertically (Malcom, 1976; Greenough *et al.*, 1988). The dyke contains sapphirine-bearing granulite xenoliths which indicate petrogenesis at approximately 1000°C and 10 Kb. (Chatterjee and Giles, 1991).

3.2 Structure and Deformation

The Meguma Terrane is separated from the Avalon Terrane to the north by the east-west trending Cobequid-Chedabucto Fault, a major regional shear zone trending east-west (Keppie, 1979). Other east-

west faults are present throughout the Meguma, but are rarely seen away from the direct influence of the shear zone (Williams and Hy, 1990). A major northeast-southwest trending post-Visean sinistral shear zone, the Tobiatic shear zone, also traverses the Meguma Terrane from the vicinity of Yarmouth in the west to Liscomb in the east (Giles 1985).

Smith *et al.* (1985), have defined five deformational events (Table 2) associated with, and subsequent to, the Lower Devonian Acadian Orogeny (circa 370 Ma.). The first, or D1 deformation, produced a grain alignment cleavage (S_1) which occurs intermittently throughout the Meguma Terrane.

Table 2. Generalized deformational history of the Eastern Meguma Terrane (after Smith, 1988).

DEFORMATION	CHARACTERISTIC FEATURES	COMMENTS
D_1	rare folds, grain alignment cleavage (flat; folded steep)	variably developed throughout the Eastern Meguma Zone.
D_2	pervasive regional folds; upright slatey and pressure solution cleavages; pre-regional metamorphism	generally transposed into parallelism with S_4 cleavage on fold limbs.
---------METAMORPHISM---------		
D_3	controlled by lithology; no folds; coarse grained biotite foliation; syn- plutonism at ~370 M.Y.A.	subhorizontal orientation except where it is steepened in D_4 shear zones.
---------PLUTONISM---------		
D_4	associated with ductile shear upright cleavage; deforms metamorphic porphyroblasts.	shear zones; may locally be confused with S_2 slatey cleavage.
D_5	crenulations; faults (thrust, reverse, normal, strike slip) kink bands, boudinage.	includes all post D_4 brittle/ ductile structures.

The next deformational event (D_2) involved more intense regional deformation associated with extensive regional, east-west oriented folding. This is reflected by the development of pervasive upright slaty and pressure solution cleavages (S_2) within the pelites and psammites respectively (Smith and Kontak, 1988.c).

The D_3 deformational event, is characterized by subhorizontal biotite foliation (S3) restricted to pelitic assemblages. It is a interpreted to be a contact metamorphic affect associated with the emplacement of granitoid plutons at ca. 370 m.y. (Kontak, *et al.* 1988.c).

The D_4 event is manifested as a strong upright (axial planar) shear cleavage (S4) that deforms porphroblasts (Smith and Kontak, 1988.c). This fabric is associated with ductile shear zones, and is heterogenously developed across the Meguma Terrane. Relative age of this phase of deformation is synchronous with plutonism and contact metamorphism at ca. 370 Ma (Smith and Kontak, 1988.c). This

deformational event was believed to be syn-to post-gold mineralization in the Meguma Group.

The final deformational event (D_5) resulted in development of thrust, reverse and normal faults, kink banding and boudinage. These structures are pervasive throughout the Meguma, and appear to post date gold mineralization (O'Brien, 1983).

Northwest-trending, brittle-ductile faults also occur at high angles throughout the Meguma Group (Fig. 3). These faults which vary in length from tens of metres to tens of kilometers, are present at many Meguma Group gold deposits including Tangier. Movement along them is generally sinistral (Williams and Hy, 1990). These faults manifest themselves on a local scale as shear and breccia zones.

3.3 Metamorphism

Figure 1 shows the approximate location and areal distribution of metamorphic zones throughout the Meguma Group. Two distinct metamorphic events have been described for the Meguma Terrane (Smith and Kontak, 1988.b). The first is a regional greenschist metamorphic event (M_1) characterized by a regional axial planar cleavage (S_2). This M_1 event followed the D_2 regional deformation but preceeded the D_3 (biotite foliation) event. The regional metamorphism is characterized by amphibolite to greenschist-facies which have been locally retrograded to chlorite grade. This was overprinted by a second, dynamo-thermal metamorphic event (M_2) associated with granitoid plutonism but distinct from contact metamorphism, manifested by coarse grained biotite and chlorite overgrowing earlier fabrics and M_1 metamorphic minerals (Smith and Kontak, 1988.b; Douma, 1988, Douma, in prep.). Kontak *et al.* (1990) also report local increase in the metamorphic grade adjacent to some gold deposits due to thermal overprinting associated with quartz veining and gold mineralization. Examples cited are the Beaver Dam, Forest Hills and Cochrane Hill deposits where regional biotite-grade rocks are overprinted with a garnet-andalusite-cordierite-staurolite metamorphic mineral assemblage.

3.4 Alteration

Two stages of alteration (A_1 and A_2) have been recognized (Smith and Kontak, 1988 b.). Of these, A_1 is most pervasive occurring locally on a scale of hundreds of metres. This stage of alteration is distinguished by zones of intense silicification, sericitization, carbonitization and sulphide development. In contrast, the A2 alteration is confined to more restricted zones. It may occur as, sulphide infilling in fractures, small segregated zones bleached from quartz replacement, or coarse arsenopyrite grains with pressure shadows of carbonate and chlorite. There may also be colour mottling in the psammites with no sulphides present. A_2 alteration effects often appear to overprint A_1 alteration.

3.5 Origin of Gold Deposits

Various genetic models have been proposed for these deposits including saddle-reef (Boyle, 1979, 1986; Mawer, 1986, 1987; Henderson and Henderson, 1986), exhalative (Haynes, 1986), hydraulic fracturing and lateral secretion from a unique stratigraphic horizon (Graves and Zentilli, 1982). Current interpretation suggests that incursion of auriferous fluids proceeded along sub-parallel shear zones probably re-activated Acadian breaks, at ca. 370 Ma. (Kontak *et al.*, 1990.a). These authors also note that more recent gold deposition models have a common theme involving crustal instability, magmatism (commonly alkaline), metamorphic devolatization, extensional tectonics and active shearing. Recent isotopic studies by Chatterjee and Smith (1991) eliminate the Meguma Group both alone or in combination with Devonian to Carboniferous magmatism as a source for the gold. Instead, gneisses of

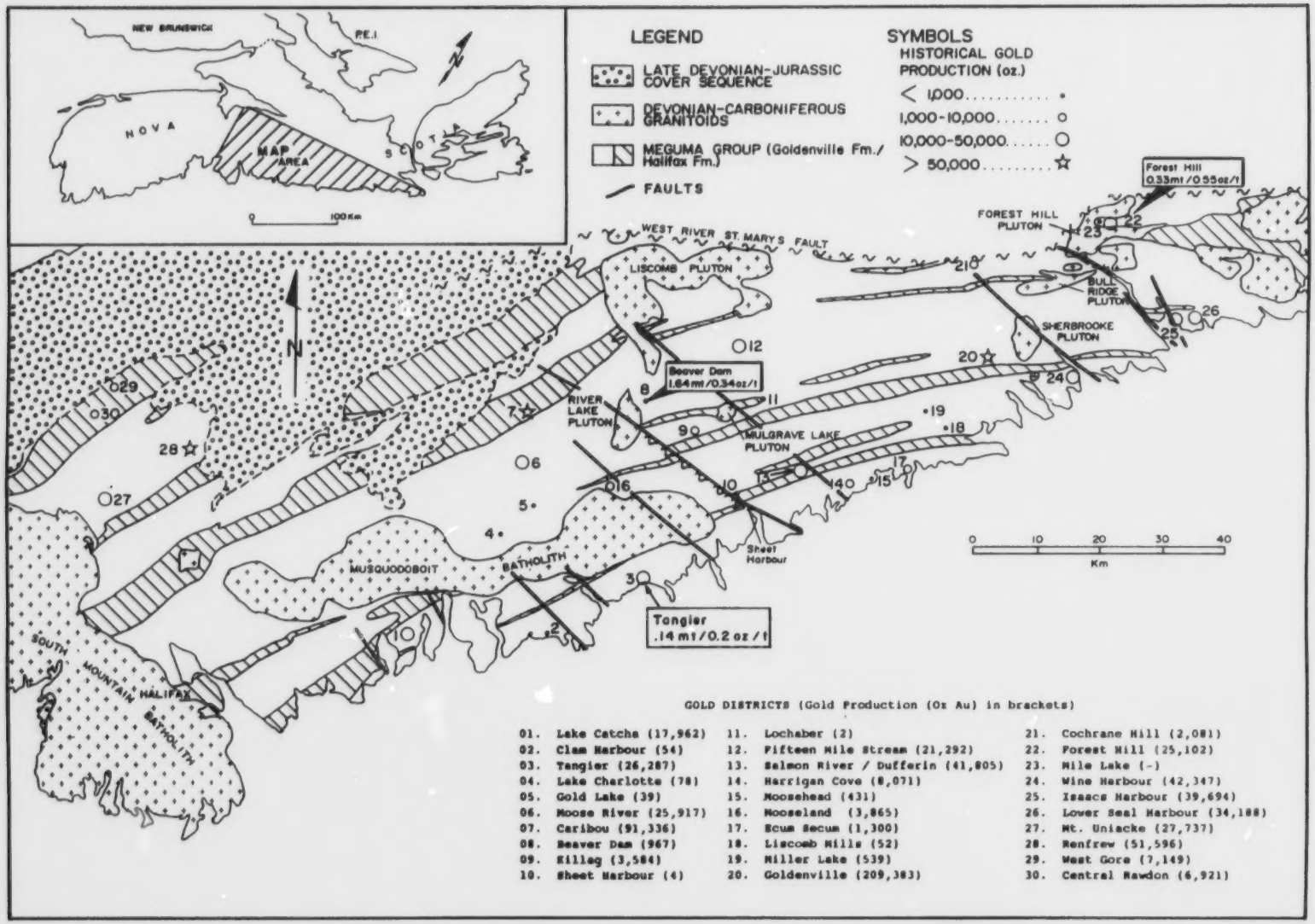

FIGURE 3. General geology map of the eastern Meguma Terrane showing the location of gold deposits and their historical gold production. Modified from Kontak and Smith (1987). Tonnage and grade figures for the Tangier deposit represent proven and probable reserves as stated in Coxheath Gold Holdings annual report 1989. Faults are compiled from Williams and Hy (1990).

the Liscomb Complex are indentified as potential sole source rocks for the hydrothermal fluids from which the gold-bearing quartz veins developed.

The Meguma Group within the eastern Meguma Terrane hosts a total of 30 gold deposits which historically produced approximately 687,000 oz. of gold. Figure 3 shows the location of gold deposits within the eastern Meguma Terrane and lists their respective historical gold production. The reserve estimate for several of the recently developed deposits are also listed.

Although gold occurs within several types of quartz veins, it is usually seen within bedding parallel (BP) veins. Williams and Hy (1990) have postulated that late-syngenetic BP vein systems formed areally extensive competent layers that were faulted and fractured, providing a depositional trap for gold-bearing fluids. Smith and Kontak (1987) have classified veins by relative age relationships to metamorphic and structural events, morphology, mineralogy and texture. These are; bedding parallel, en echelon, irregular (discordant) and AC. The relative geometrical distribution of the vein types is schematically presented in Figure 4.

4. GEOLOGY OF THE TANGIER DEPOSIT

4.1 Introduction

The first geological map of the Tangier gold district was produced by E. R. Faribault through the Geological Survey of Canada (1902). The map (Fig. 5) shows the location shows the location, thickness and structure of the gold-bearing veins observed at the time at Tangier over a strike length of approximately 3 km.

The Tangier gold deposit as defined by recent development and mining by Coxheath Gold Holdings Ltd. is situated on the south limb of the Tangier-Harrigan Cove Anticline immediately north and east of Copper Lake. Stratigraphy dips to the south at 55-70°, with an apparent increase in dip with distance away from the anticlinal axis. Faribaults' map shows the anticline to trend 074° and gently plunge (approx. 12°) in two directions from a dome situated north of Rush Lake. The map also shows that the gold-bearing quartz veins extend to the east approximately 1 km. past the anticlinal dome. While this area was not included in this study the veins were the site of limited exploration by Coxheath and are reported to display similar characteristics to the veins in the study area (Forgeron *et al.*, 1988). Limited diamond drilling of the north limb suggests that although the stratigraphy including quartz veins appears to be continuous north of the anticlinal axis (Forgeron *et al.*, 1988) bedding angles indicate the presence of a minor fold or inflection.

Native gold mineralization is best developed within, but not restricted to, numerous crack-seal textured, bedding-parallel (BP) quartz veins which are confined to black, commonly graphitic, pelite beds. Other quartz vein types occur and may also contain native gold. Many of the auriferous BP quartz veins are described in more detail below.

A cross-section of the south limb of the anticline is shown in Figure 6. This section is compiled from 5 holes drilled by the Sullivan Mining Group in 1983, and a Coxheath hole which deepened a Sullivan hole. The Sullivan holes (T83-1 to 5) were selected because they contained a continuous record of drill core (i.e. no missing core due to whole core geochemical sampling). The Sullivan holes were relogged in detail whereas the geology for the Coxheath hole (TG 86-1) was obtained from a company log. Figures 7a-d present the detailed stratigraphy (true thickness) of the south limb of the Tangier

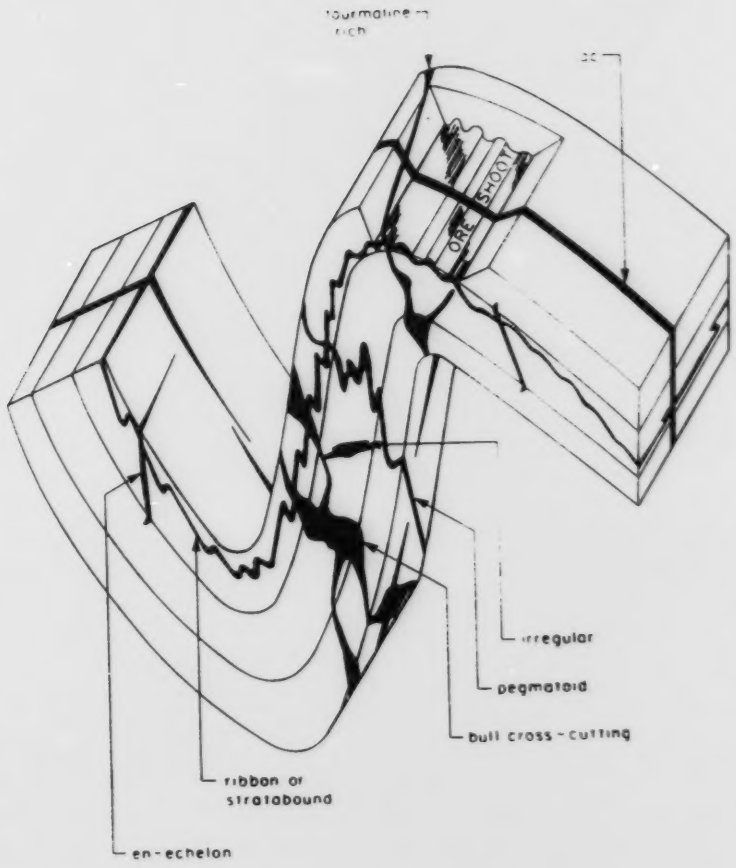

Figure 4. Three-dimensional schematic representing the relative distribution of major vein types within a folded strata. No scale implied. After Smith

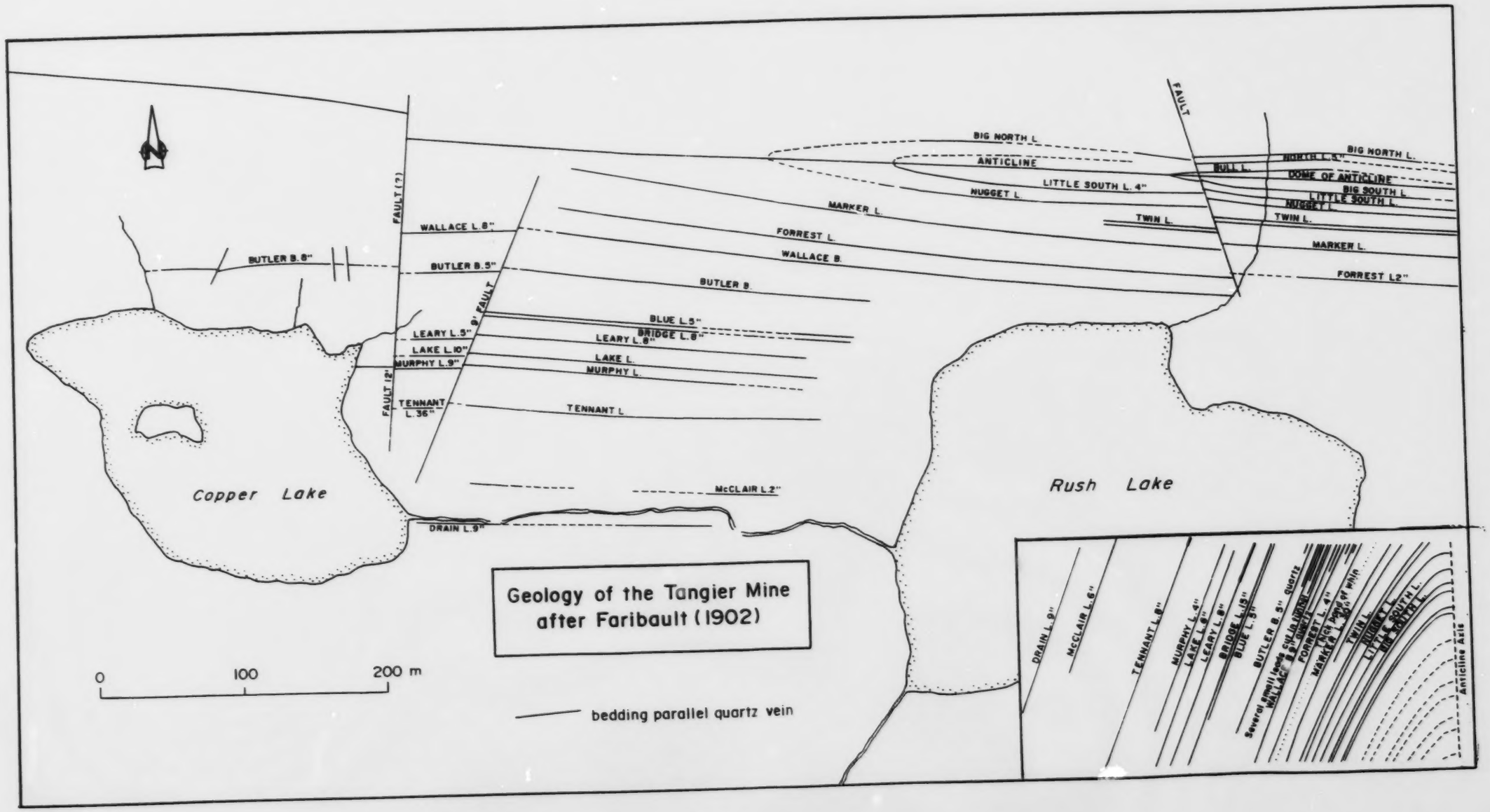

FIGURE 5. Faribault's 1902 geology map of the Tangier gold district.

anticline at several locations. These figures present distance in feet since the holes were drilled in feet, making for a more accurate representation. Figure 7a is a plan map showing the location of the stratigraphic columns relative to the undergroung workings of Coxheath. Figure 7b is the stratigraphy in the area of the portal (north decline) compiled from the Sullivan holes. The N. S. D. M. E holes (TAN 90-3 and 4) provide stratigraphic information in the unexplored area west of Coxheaths underground development (Figs. 7c and d respectively) and tested the extrapolated western extension of the BP quartz vein zones. These figures display approximately 800 ft. (244m) of stratigraphy on the south limb. A detailed description of the drill core from these holes, is available in Mills and Corey (in prep.). The cross-section and stratigraphic columns show the stratigraphy to be comprised of discrete and often quartz vein-bearing pelite beds sandwiched between generally thicker, massive psammite beds. Forgeron *et al.* (1988) report intersecting 69 separate pelite beds during exploration and development on the south limb.

The metamorphic compilation of Nova Scotia by Keppie and Muecke (1979) further shows the deposit to be situated just outside of the zone of biotite-grade metamorphism surrounding the eastern end of the Musquodoboit Batholith. Recent study by Douma (in prep.) and Williams and Hy (1990) have observed the effects of contact metamorphism up to 1.5 km. away from the pluton contact. At Tangier biotite is rare and invariably shows some degree of chloritization.

4.2 Description of Lithologic Units

The following descriptions are based on characteristics observed within diamond drill core and specimens taken from ore and development rock dumps.

4.2.1 Pelite

Within the area of recent development this unit ranges from several millimeter thick bands intercalated with psammite and rare semipelite, to 1-2m thick massive beds. Two types of pelite were observed. Type I is black, invariably graphitic and contains common carbonate with less common accessory biotite, muscovite, chlorite, tourmaline, rutile and sulphides. This type of pelite without exception is host to the gold-bearing BP quartz veins. Adjacent to these veins the pelite often shows fine bedding (?) laminations parallel to the vein margins.

The carbonate usually has a light-brown colouration (weathering?) and occurs as small (1-5mm) oikocrysts oriented parallel to the sub-vertical, axial planar S_4 cleavage (Plate 1a) while framework minerals such as muscovite and chlorite commonly reflect an earlier axial planar cleavage (S_2). These oikocrysts commonly contain small grains of biotite, muscovite, tourmaline, chlorite and opaques (Plate 1b). Analysis of carbonate from several Meguma-type gold deposits by Kontak & Smith (1988a) indicates that the carbonate varies from calcite to ferroan dolomite to ankerite and that the composition does not appear to be host dependant. Limited analysis of the Tangier carbonates indicate that calcite and ferroan-dolomite occur within the deposit (Kontak, pers. comm). Carbonate also occurs as narrow (2cm) bedding parallel bands and irregular swirls. Similar bands have been observed in other gold deposits (Sangster, 1990). Petrographic observations show that these bands are due to a concentration of oikocrysts which also show shear cleavage alighnment (Plates 1c,d). Whether this carbonate is a product of metamorphic, hydrothermal or diagenetic processes is not definitive. However their S_4 orientation and presence of included mineral phases suggests that the oikocrysts overgrew existing mineralogy during syn-plutonic metamorphism/deformation ca. 370 m.y.

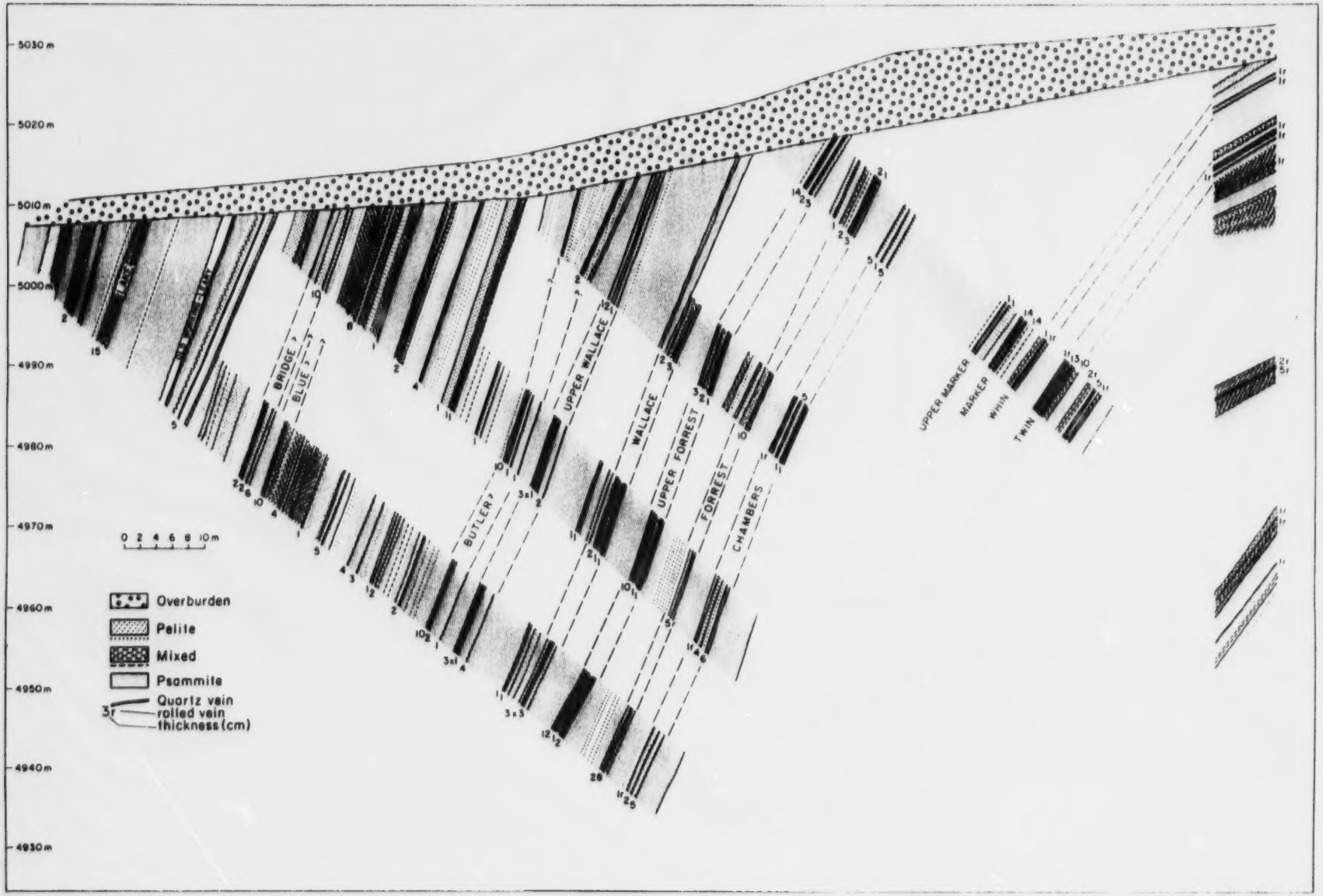

FIGURE 6. Cross-section of south limb of the Tangier deposit showing relative location of quartz veins.

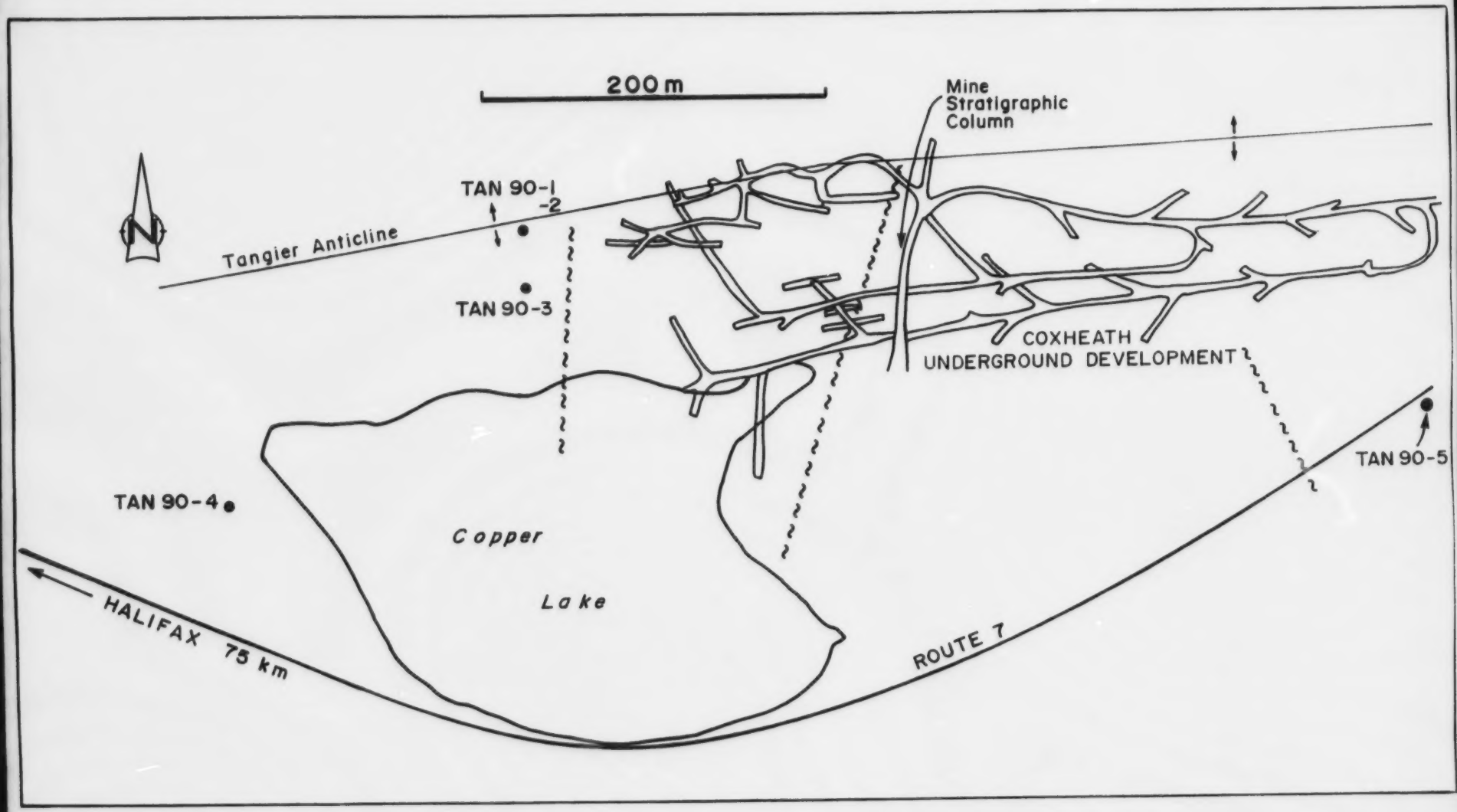

FIGURE 7a. Figure showing location of the cross-section and stratigraphic columns.

FIGURE 7b. Sullivan stratigraphy sequence of the Tangier deposit in the area of the portal (north decline).

FIGURE 7c. Stratigraphy of the Tangier deposit west of the underground workings at the site of N.S.D.M.E. drill hole TAN90-3.

FIGURE 7d. Stratigraphy of the Tangier deposit west of the underground workings at the site of N.S.D.M.E. drill hole TAN90-4.

LEGEND

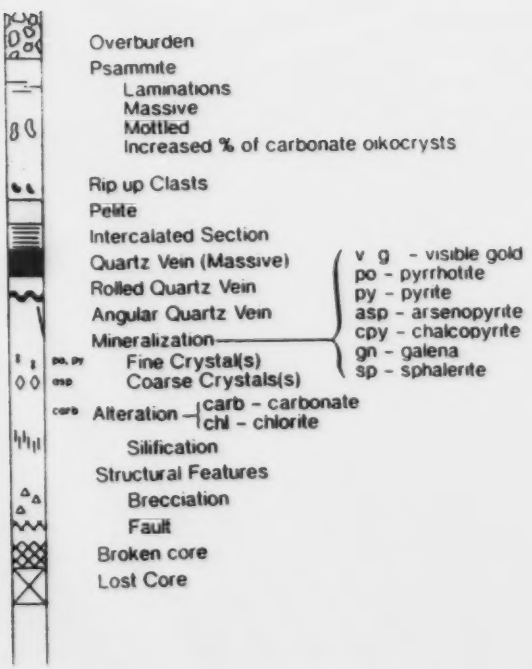

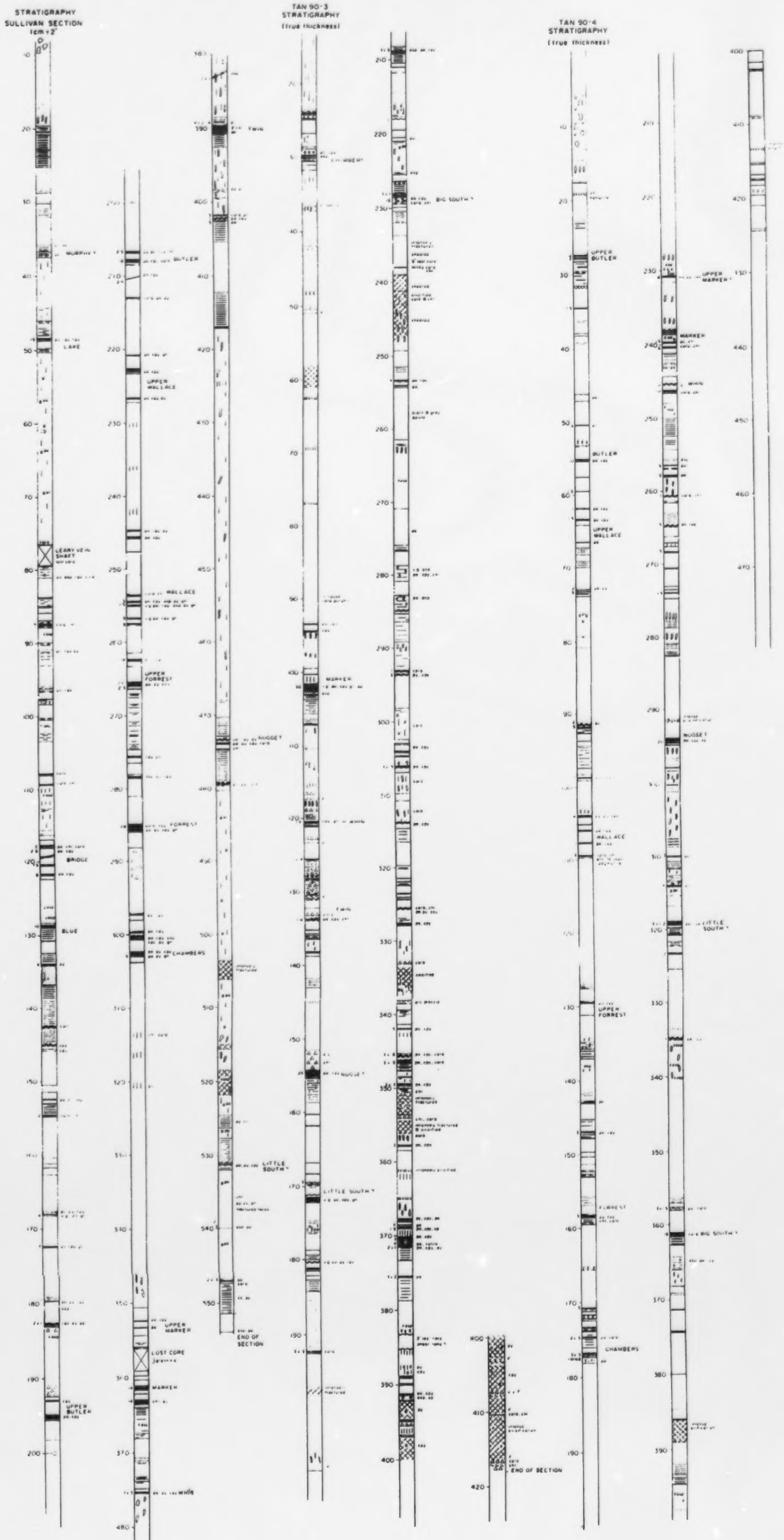
STRATIGRAPHY
SULLIVAN SECTION
(cm +2')
MURPHY
LAKE
LEARY VEIN SHAFT
BRIDGE
BLUE
UPPER BUTLER
BUTLER
UPPER WALLACE
WALLACE
UPPER FORREST
FORREST
CHAMBERS
UPPER MARKER
LOST CORE
MARKER
WHITE
TWIN
NUGGET
LITTLE SOUTH
END OF SECTION
TAN 90-3
STRATIGRAPHY
(true thickness)
MARKER
TWIN
NUGGET
LITTLE SOUTH
BIG SOUTH
HOG
END OF SECTION
TAN 90-4
STRATIGRAPHY
(true thickness)
UPPER BUTLER
BUTLER
UPPER WALLACE
WALLACE
UPPER FORREST
FORREST
CHAMBERS
UPPER MARKER
MARKER
NUGGET
LITTLE SOUTH
BIG SOUTH

Common sulphides present within the pelite include pyrrhotite, pyrite and arsenopyrite. These occur as millimeter sized grains and lenses, thin stringers and rare coarse-grained clots which are commonly oriented parallel to the penetrative axial planar S_4 shear cleavage (Plates 2a-e). The sulphide lenses shown in Plates 2c-e indicate that two generations of sulphide mineralization are present. Early pyrrhotite and pyrite stringers which show intense deformation appear to be overgrown by undeformed, coarse-grained arsenopyrite euhedra.

Type II pelite is dark-grey to bluish-grey, with little or no graphitic alteration or carbonate oikocryst development. This pelite type contains similar accessory mineral phases and is probably the unaltered equivalent of the black-graphitic pelite.

Both types of pelites occur as separate, discrete beds and irregularly interbedded and intercalated lenses which display a well developed axial planar cleavage (S_2). Sharp contacts between the two pelite types were in some cases marked by a thin quartz-carbonate stringer. A similar pelite/pelite contact observed at the Beaverdam deposit by Smith and Kontak (1987) was also thought to be an alteration rather than lithological contact. Irregular clasts of one type within the other were rarely observed (Plate 3).

4.2.2. Alteration

The effects of alteration within the pelite are readily observed within the Tangier deposit. Most prominent is carbonitization, reflected by carbonate enrichment within pelite adjacent to many quartz veins. A good example is shown in Plate 4 where the pelite adjacent to a quartz-carbonate vein shows marked carbonate enrichment. Other types of alteration include; silicification, sericitization, chloritization and carbonization. These alteration types are reflected by a pale greenish-grey colour, abundant sericite, muscovite, abundant chlorite porpyroblasts and intense graphitic alteration respectively. As mentioned above, pelites which host the majority of quartz veins are invariably graphitic; where most intense, the pelite becomes extremely soft and friable and has a 'sooty' texture. However, there does not however appear to be a correlation between intensity of graphitic alteration and concentration of quartz veins (see Geochemistry below).

Another type of alteration affecting graphitic pelite in particular is an enrichment of sulphide minerals (25-50%) within the pelite adjacent to some stratabound quartz veins and massive psammite beds. This can be manifested by the pervasive development of arsenopyrite and pyrrhotite and less common, chalcopyrite, sphalerite and rare galena. Such sulphide enrichment is in sharp contrast to the rest of the pelite which shows only minor dissemminated sulphides ($<5\%$). Sulphide crystals and bands (ribbons) commonly have a preferred dimensional orientation parallel to the S_4 cleavage and may be associated with gold enrichment (see below).

4.2.3 Psammite

This lithology is the most dominate in the study area, represententing approximately 80% of total stratigraphy (Fig. 6). The psammite is generally massive, medium-to-coarse grained, medium -to-dark grey in colour and commonly contains variable amounts of accessory minerals such as muscovite, chlorite, carbonate, biotite, tourmaline and sulphides. As within the pelite these mineral phases display variable textures and orientations (Plate 5 a-e). Sulphide minerals commonly include pyrrhotite and arsenopyrite occurring as pervasive fine-grained (≤ 5mm) disseminations, although arsenopyrite may occur as large (1-4cm) euhedral crystals with well developed quartz-carbonate filled pressure shadows.

In contrast to the pelite, carbonate within this unit is commonly intergrown with quartz and does not form finely interbedded bands. A well developed pressure solution cleavage (Plate 6) was observed within this lithology, a phenomena which appears to increase in intensity as the anticlinal fold axis is approached. Individual psammite beds range from < 1 to 61 feet thick. Some of the thicker beds display well developed graded-bedding, with basal units commonly containing rounded blue-quartz grains. Although the relative thicknesses of some beds allow for their use as stratigraphic markers, they do show lateral and vertical thickness variation. For example, the Marker psammite, a thick massive bed used as a stratigraphic marker is 48' thick in the Sullivan cross-section (Fig. 6) and 61' thick where intersected in N.S.D.M.E drill holes approximately 200m further west (Figs. 7c,d).

Although psammite beds do not host BP quartz veins at Tangier or any gold deposit within the Meguma Terrane, other types of quartz veins do occur. Perhaps the most common are thin (< 5mm), steeply dipping, sub-vertical (shear cleavage (S_3) oriented), quartz-carbonate stringers which crosscut psammite, quartz stockworks and breccias associated with faults and shear zones (Plate 7). Other vein types include discordant, massive milky quartz angulars and en echelon veins which can be of considerable thickness (1-2m). Sulphides (pyrrhotite, pyrite, chalcopyrite, arsenopyrite) often occur within these veins types and in some cases may be associated with gold-enrichment (Sect. 7.2). Sulphide-rich veins (dykes?) also occur within psammites characterized by coarse disseminations of pyrrhotite, chalcopyrite and arsenopyrite within irregular bands. The absence of such zones within pelite presumably indicates that the psammites were more receptive to invasion of hydrothermal fluids due to their coarser grain size. The gold-bearing potential of these dykes has not been investigated.

Primary sedimentary features such as flame structures were observed at pelite/psammite contacts (Plate 8a). Pelite rip-up clasts oriented parallel to shear cleavage are also commonly observed within overlying psammite beds (Plate 8b). The contact may also be the site of dissolution as indicated by the stylolitic contact shown in Plate 8c. Pelite/psammite contacts can also display intense shear cleavage (S_4) attenuation with bedding displacement generally less than 5cm (Plate 8d). Narrow psammitic dykes also occur, commonly within pelite. Such dykes are highly irregular and often contain coarse disseminated chalcopyrite, pyyrhotite and pyrite (Plate 9).

4.2.4. Alteration effects

The most common type of alteration to affect the psammite is silicification. Where most intense, the psammite is commonly finer-grained, has a mottled texture and a bleached pale-grey to green colouration (Plate 10). This alteration may be accompanied by increased fracturing and sulphide minerals. Other types of alteration include; chloritization, carbonitization and sericitization.

4.2.5 Semi-pelite

This lithotype is rare at Tangier and is restricted to thin (< 1.5cm) beds intercalated with pelite and psammite (Plate 11). They are usually biotite and chlorite porphyroblast-rich (5-25%) and have a well developed shear cleavage (S_4). They also have a pale-dark green colouration which perhaps reflect the high concentration of chlorite within this rock-type. Chlorite occurs as sub-rounded grains of probable detrital origin and small acicular crystals oriented parallel to the shear cleavage of probable metamorphic (prograde?) origin. Biotite occurs as dark brown, anhedral rounded grains and subhedral ragged pale yellow laths which show evidence of chloritization and small flakes intergrown with quartz and carbonate. Biotite also displays a strong S_4 alignment. Other mineral phases include small euhedral muscovite laths oriented with the regional S_2 axial-planar cleavage and sub-euhedral rutile, ilmenite and pyrrhotite grains commonly oriented parallel to S_4.

5. DESCRIPTION OF QUARTZ VEINS

The veins at Tangier reflect a variety of styles and textures and are similar in most respects to veins observed at other Meguma-type gold deposits (Fig. 5: Smith, 1987). Many of the textures and characteristics described below are shown in Plates 12 through 16. Figure 8 shows the location of these plates relative to the underground workings. For this study the veins have been divided into 3 classes which are described below.

5.1 Stratabound

This vein class includes the bedding-parallel, crack-seal textured veins also referred to as stratiform, interbedded, ribbon or laminated by other workers. These veins are always hosted by pelite and since they contain the majority of visible gold mineralization are the primary target of exploration and mining at Tangier. These veins commonly show a crack-seal texture characterized by multiple laminations consisting of wall rock fragments and replacements thereof by phyllosilicate, graphite, chlorite, rutile and ilmenite. It is interesting to note that some of the wall-rock inclusions show a well-developed cleavage suggesting that vein emplacement at least post-dated regional D_2 deformation. The bedding-parallel veins also contain areas of massive white quartz which lack laminations. This type of quartz appears to be a later overgrowth/replacement or dilatent infilling as suggested by the presence of vugs in some cases. An unique characteristic of this milky quartz is the occurrence of dark-grey euhedral to subhedral basal quartz sections and tapered columnar quartz crystals oriented perpendicular to the vein wall. These latter features are formed by the stacking of millimetre (or less) thick, inclusion-rich quartz plates oriented parallel to the vein wall (Plates 12a-e). They are thought to represent primary twinned quartz crystals which grew incrementally by crack-seal processes and were later enveloped by the milky quartz (Henderson & Henderson, 1990). Quartz columns of this type at Tangier taper both away and towards the center of the host quartz vein.

The mineralogy of these veins may include accessory biotite, muscovite, carbonate, chlorite, rutile, ilmenite, tourmaline, apatite, and plagioclase (Plates 12f-h). Carbonate and chlorite often occur together as coarse crystal aggregates within boudin necks (see Chapt.7) or discrete veins restricted to a specific horizon within the larger quartz vein (Plate 12i).

Sulphide minerals may include pyrrhotite, chalcopyrite, pyrite, marcasite, arsenopyrite, sphalerite and galena. Native gold occurs as small ($<<$1mm) to very large (6x2x5cm) nuggets commonly associated with the above sulphides, particularly galena. This close association of gold and galena has been observed at other Meguma-type gold deposits (Smith, pers comm., 1991). Almost without exception the gold occurs as discrete grains within the massive milky quartz (Plate 12j). The only exception was a 0.5mm nugget situated within a dark-grey quartz platelet which forms part of a large columnar quartz crystal.

Faribault's 1902 geology map (Fig. 5) of the Tangier deposit identified 18 BP quartz veins south of the fold axis. Coxheath (1989) reported over 40 parallel quartz veins were intersected in the same area during extensive surface and underground diamond drilling. Many of these BP veins have historically been placed within vein packages or zones. (Figs. 6, 7). Table 3 lists the major BP quartz vein(s) occurring at Tangier. The descriptions are based on information compliled from surface and underground drill hole logs, underground geology maps, and company reports. This data represents observations of the quartz veins spanning approximately 360m of strike length and 120m of elevation. In addition,

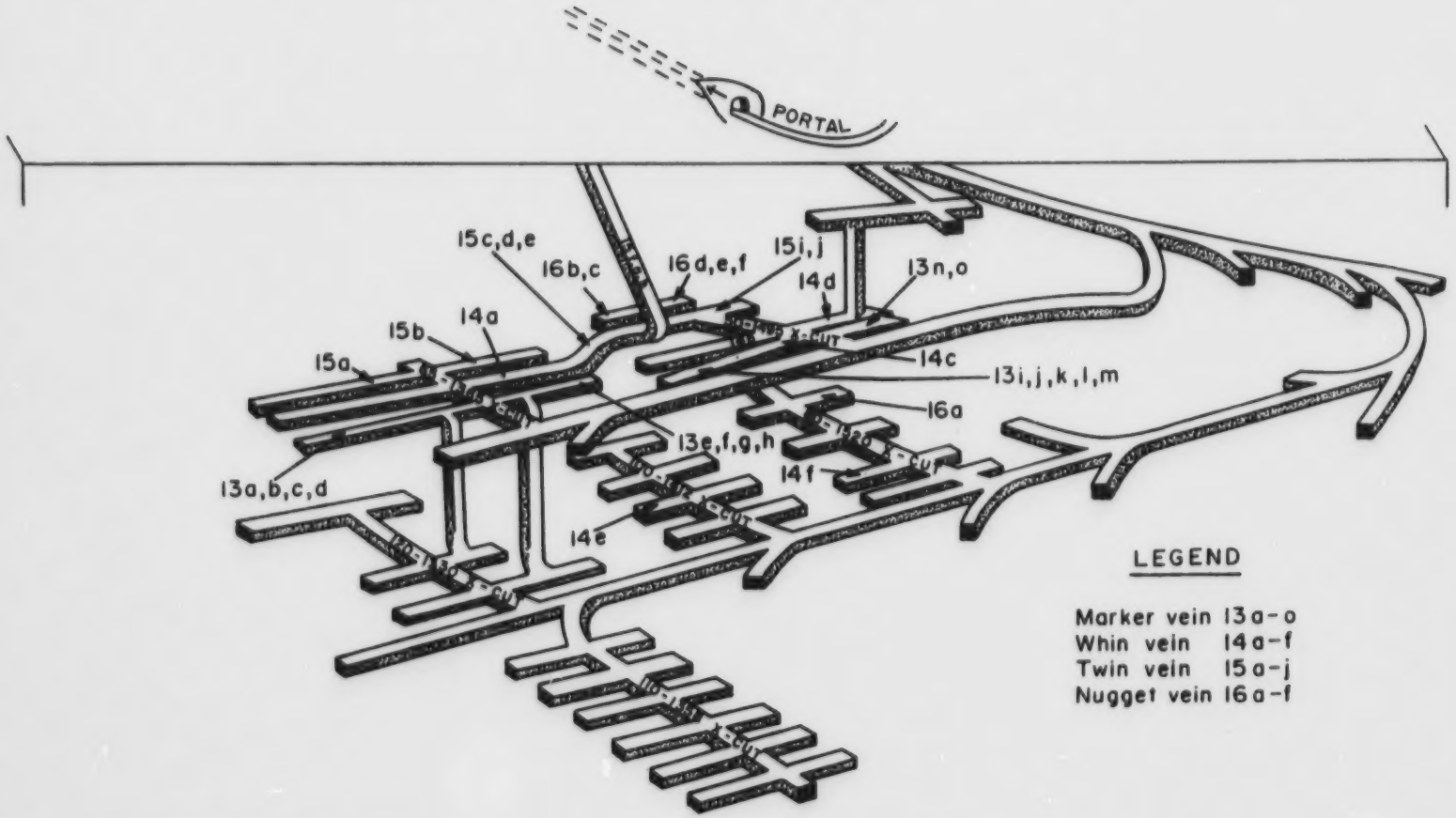

FIGURE 8. Schematic of underground development at Tangier showing relative location of Plates 13 to 16.

preliminary information is included from N.S.D.M.E. drilling approximately 200m further to the west. The veins are described in a sequence from the stratigraphically highest to lowest vein package identified, corresponding with a south to north direction. It should be noted that in addition to the named veins, quartz veins (± gold) also occur between these zones reflecting the discordant nature of some veins.

Athough these veins can persist for hundreds of metres along strike they frequently display variation in thickness and texture. Although these veins are generally stratabound, they can be discordant crossing from one stratigraphic horizon to another (see 5.4 below). Some veins also delaminate from one thick vein to several narrow veins. The veins also display variable types and degrees of deformation which are discussed in detail below (see Chapt. 7).

5.2 En-echelon/angular veins

These veins are very common within the main mine sequence and are usually manifested by clear to milky quartz veins which may contain carbonate and chlorite with accessory pyrrhotite, pyrite and chalcopyrite. This vein type includes irregular stratabound veins which range from < 1 - 8cm thick to apparently random quartz lenses (blows) which can show a wide range of thickness. The largest lense documented is 50cm x 2.5m in a raise on the Twin vein zone. The en echelon veins are thought to represent quartz-filled tension gashes and dilatent extensional fractures which have been rotated and folded in response to compression and faulting (Henderson & Henderson, 1990). This vein type may also be gold-bearing as shown by the Nugget vein (see Table 3) which is thought to represent superimposed and variably rotated en-echelon veins (Sangster, 1990). This particular vein shows wide textural variations along strike and with depth, including massive tension-gap veins which may abruptly pinch-out to crack-seal textured veins which vary in thickness (see Plates 16a-f).

This vein class also includes angular veins which can be very irregular and crosscut stratigraphy (Plate 12k). Observations indicate that some of the angulars may have comprised part of a stratabound vein, contributing to the composite nature and variable textures (i.e. massive and crack-seal) often described within those veins. These angular veins also appear to play a crucial role in the localization and control of high-grade ore shoots with dramatic gold enrichment observed in some stratabound veins adjacent to an angular vein (Coxheath Gold Holdings Ltd, 1989). Such a situation occurs within the Whin vein (Table 3) and is described in detail below (Chapt.7.2).

5.3 Quartz-carbonate angulars

In contrast to the thicker, massive milky quartz angulars described above, these quartz-carbonate angulars are typically < 1cm to 2cm thick. They contain quartz+carbonate and frequently chlorite. These veins are best developed within psammite beds where they can become very abundant. Termed "angulars" because they cross-cut stratigraphy, the histogram in Figure 9 reflects the orientations of 633 such veins compiled from Coxheath diamond drill hole logs. It shows two main populations exists; one at a high angle to bedding the other at a low angle. Sub-populations are also indicated at 10° and 80° to bedding. The veins display several textural varieties, including, mm wide linear veins parallel to joints and fracture cleavage in the psammite and irregular zones of quartz-carbonate-filled tension gashes and breccias (Plate 7a,b). While the former most likely represent AC-veins the latter are probably related to the abundant NW shear/faults indentified at Tangier. The AC-veins formed at a high angle to bedding in response to late extension parallel to the regional fold axis.

TABLE 3. Description of stratabound bedding-parallel quartz veins occurring on the south limb of the Tangier anticline in the area of recent underground exploration and development.

TABLE 3. DESCRIPTION OF QUARTZ VEINS.

VEIN(S)	LOCATION	TYPE & THICKNESS	MINERALOGY	HOST ROCK	COMMENTS
TENNANT	PHASE II (W)	BP-CS vein - 13 cm	po, cpy	graphitic; pelite/30 cm thick	only intersection of vein reported
MURPHY	PHASE I	none present			50 cm of massive pelite occurs but no quartz veins present
	PHASE II (W)	HW: BP vein - 5 mm FW: BP-CS vein - 3 cm	cpy, chl po	graphitic pelite - 2.5 m thick	
LAKE	PHASE I (see Fig. ?)	BP-CS vein - 15 cm	po, cpy, py	graphitic pelite - 60 cm	near hanging wall (HW)
	PHASE II (W)	HW: BP-CS vein - 29 cm FW: BP-CS vein - 8 cm	po, cpy, chl po, cpy, gn, chl	graphitic pelite - 50 cm	not drilled in Phase III
LEARY	PHASE II (W)	5 BP-CS veins - 15-30 cm near HW & FW also con-tains massive milky qtz blows & en echelon veins	po, cpy, gn, chl	graphitic pelite - 3 m	psammite surrounding Leary pelite in both zones shows asp+po enrichment adjacent to pelite. Hanging wall psammite contains 2 thick (17-35 cm) milky en echelon qtz veins. Phase I:
	PHASE III	1 to 9 veins - massive to CS textured - <1 cm - 75 cm	po, py, cpy, gn, cc, chl ±vg - 2 sightings	graphitic pelite - 40 cm to 3 m	based on 18 drill holes; usually 1-2 veins in this zone; 2 holes intersected 9 veins; deepest intersections of this zone reported folded/rolled veins.
BRIDGE	PHASE I	2 BP-CS veins; 8/4 cm	py, po, cpy; ±v.g.?	graphitic pelite - 1.5 m	veins are folded
	PHASE II (W)	1-2 BP-CS veins; 1.5-10 cm assoc. with 10-18 cm thick milky, massive - en echelon vein	po, cpy, carb, chl	graphitic pelite - 1.8 to 3.4 m	zone intersected in holes, associated with angular and en echelon veins
	PHASE III	1 or more - BP-CS to massive - 3.5-10 cm	po, cpy, gn, py, carb, chl, ±v.g.	graphitic pelite - 90 cm to 6.1 m	this zone and Blue zone (below) reported to be combined in pelite in ore intersection
BLUE	PHASE I	BP-CS vein - 4 cm	py, po, cpy, ±v.g.	graphitic pelite - 3 m	5 m below Bridge Zone
	PHASE II (W)	HW: 1-3 BP-CS veins - <1-1.5 cm FW: 1 BP-CS vein 11-26 cm	po, cpy, carb, ±v.g. po, cpy, gn, chl, carb	graphitic pelite - 6.5 m	1.5 m below Bridge Zone; also assoc. 36 cm massive, milky en echelon qtz vein in on intersection
	PHASE III	1 BP-CS-massive vein <1-9 cm near HW	py, gn, asp, carb, ±v.g.	graphitic pelite - 1-6 m	- 4 m below Bridge - v.g. sited in <1 cm vein

BP = bedding parallel
CS = crack-seal
HW = hanging wall
po = pyrrhotite
py = pyrite
cpy = chalcopyrite
sp = sphalerite
asp = arsenopyrite
chl = chlorite
carb carbonate
v.g. visible gold
FW = footwall
gn = galena
cc = calcite

TABLE 7 DESCRIPTION OF QUARTZ VEINS (CONT'D).

VEIN(S)	LOCATION	TYPE & THICKNESS	MINERALOGY	HOST ROCK	COMMENTS
HISTORICAL UPPER BUTLER	PHASE I (see Fig.)	1 BP vein 5 cm	py, po, chl, carb	graphitic pelite - 5 m	
	PHASE II	2-4 BP-CS veins <1-14 cm thick vein at F.W.	po, cpy, py, chl, carb	graphitic pelite - 3 to 6 m	
	PHASE III	1-8 BP-CS to massive veins <1-4.7 cm	po, cpy, py gn, ±v.g.	graphitic pelite - 2.3 to 5.1 m	zone usually contained 3 veins - other veins were intersected but were discontinuous from hole to hole - some intersections were sheared/faulted
HISTORICAL BUTLER	PHASE I (see Fig.)	3 BP veins <1-4 cm	po, py, cpy, gn ±v.g.	graphitic pelite - 6 m	
	PHASE II	2-4 BP veins <1-3 cm varies from CS-massive	po, cpy, chl, carb ±v.g.	graphitic pelite - .4 to 3 m	- v.g. reported in 5 mm BP, HW vein - 3 m thick pelite incl. 2 m of intercalated pelitic/psammite
	PHASE III	2-3 BP-CS veins near H.W. .4-7 cm	po, cpy, py, gn, carb ±v.g.	graphitic pelite - .2 to .7 m	v.g. observed in 1 out of 18 intersections
UPPER BUTLER	PHASE I (see Fig.)	4 BP veins <1-1.5 cm	po, py, cpy	pelite - 3.5 m	coarse diss. asp reported in pelite
	PHASE II	1-4 BP veins <1-2.5 cm	po, py, cpy, chl, carb	pelite - approx. 1.5 m	pelite contains 2mm - thick BP po stringers
	PHASE III	1-3 BP-CS veins <1-8 cm	po, cpy, gn, chl, carb ±v.g.	pelite - .6 to 1.5 m	- v.g. sited in one intersection - veins can be discontinuous
	NSDME (90-4)	2 BP-CS veins 4,7 cm	po, py	graphitic pelite - .7 m	1 mm po stringer in pelite
BUTLER	PHASE I	3 BP-CS veins; 1/2.5/8 cm	py, po, cpy	pelite - .5 m	- 2 narrow veins are rolled - associated with 10 cm shear zone
	PHASE II	varies from; 1 BP-CS to massive vein near F.W. 10-19 cm thick - to 5 BP veins 1-3 cm	po, cpy, py, chl	pelite - approx. 1 m	coarse disseminated asp reported in pelite
	PHASE III	H.W.: 1-4 BP-CS veins - <1-6 cm F.W.: 1-3 BP-CS veins - <1-3 cm	po, cpy, py, gn, carb, chl ±v.g.	pelite - .5 to 1.6 m, usually 1.2 m thick	
	NSDME (90-4)	1 BP-CS vein -10 cm	po, cpy	graphitic pelite - .4 m	

TABLE 3 DESCRIPTION OF QUARTZ VEINS (CONT'D).

VEIN(S)	LOCATION	TYPE & THICKNESS	MINERALOGY	HOST ROCK	COMMENTS
UPPER WALLACE	PHASE I	4 - BP-CS veins <1-2 cm	py, cpy	graphitic pelite - 1 m	
	PHASE II	1 BP-CS vein 1-5 cm western intersections 20/22 cm thick	po, py, cpy, asp, chl	graphitic pelite ~ .8 m	- po can occur as mm stringers - minor intercalated psammite
	PHASE III	H.W.: 1-2 BP-CS veins .3-2.5 cm F.W.: 1 BP-CS vein 4-25 cm	po, cpy, gn, sp, py ± v.g.	graphitic pelite - .3 to .6 m	v.g sited in most westerly intersections
	NSDME (90-4)	3 BP-CS veins 1-1.5 cm	po, cpy, py	graphitic pelite	zone consists of 3 thin pelite bands 5-30 cm thick over approx.
WALLACE	PHASE I	4-5 BP-CS veins <1-1 cm	py, po, cpy ±v.g.	graphitic pelite - .6 m	small scale boudins observed; surface diamond-drilling intersected numerous narrow rolled BP veins
	PHASE II	varies from 1-2 BP-CS veins .5-5 cm thick in western intersections - 3-8 BP-CS? veins in eastern drilling - 2 mm - 2 cm thick	po, cpy, chl, carb	graphitic pelite - .2 to .3 m in west and 1.5-3 m in eastern drilling	12 cm thick massive en echelon qtz vein inter- sected within this zone in one eastern drill hole
	PHASE III	1-4 BP-CS to massive veins .3-13 cm	po, cpy, py, gn ±v.g.	graphitic pelite - .13 to .6 m	- folded/rolled veins reported in some inter-sections - v.g. sited in one intersection
	NSDME (90-4)	4 - BP-CS veins 1-4 cm	po, py, cpy, carb, chl	graphitic pelite - 1.7 m	minor intercalated psammite
UPPER FORREST	PHASE I	1 BP-CS vein - 15 cm	py, po, cpy	graphitic pelite - .5 to 1 m	
	PHASE II	1-3 BP-CS veins <1-10 cm	py, po, cpy, chl, carb, v.g.	graphitic pelite - .5 to 1 m	- veins absent from zone in one westerly drill hole
	PHASE III	2-8 BP-CS to massive veins <1-5 cm	po, cpy, py, gn, chl, carb ±v.g.	graphitic pelite - 1 to 2.5 m	- v.g. more common in eastern intersections - veins show rare folding/rolling
	NSDME (90-4)	1 - BP-CS vein - 3 cm	po, cpy	graphitic pelite - .5	

TABLE 3 DESCRIPTION OF QUARTZ VEINS (CONT'D).

VEIN(S)	LOCATION	TYPE & THICKNESS	MINERALOGY	HOST ROCK	COMMENTS
FORREST	PHASE I	1 BP-CS to massive vein 8-30 cm thick	py, po, cpy, gn, chl, carb ±v.g.	graphitic pelite - 1.5 m	associated with massive milky qtz en echelon veins in some intersections
	PHASE II	1BP-CS to massive vein - 15-40 cm 2-3 BP veins <1 cm	po, cpy, gn, chl, carb, ±v.g.	graphitic pelite - .6 to 2 m	
	PHASE III	1 BP-CS to massive vein 4-28 cm 1-2 BP veins <1-3.5 cm	po, cpy, gn, py, chl, carb	graphitic pelite - .4 to .9 m	variable thickness probably due to boudin development
	NSDME (90-4)	1 BP-CS vein - 5 cm 1 BP-massive vein - 3 cm	py, cpy carb, chl	graphitic pelite - 1 m	very minor intercalated psammite
CHAMBERS	PHASE I	4 BP-CS veins <1 cm	py, po, cpy	graphitic pelite - .5 m	
	PHASE II	2 BP-CS veins .5-4 cm	po, cpy, py, chl	graphitic pelite - 1 to 1.5 m	
	PHASE III	1-3 BP-CS veins 1.5-13 cm	po, cpy, py, gn, sp, chl, carb, ±v.g.	graphitic pelite - .7 to 1.3 m	H.W. vein is the thickest - may also be rolled - thick carbonate veins also observed. v.g. in one intersection
	NSDME	3-4 BP-CS veins <1 cm	po, py, carb	graphitic pelite - .4 to .7 m	- veins folded/rolled - coarse po+cpy+asp blebs in HW psammite
UPPER MARKER	PHASE I	1 BP-CS vein - 3-4 cm	py, po, cpy ±v.g.	graphitic pelite/psammite (60:40) - .5 to .7 m	- veins folded/rolled and can be discontinuous - graphitic alteration can be intense
	PHASE II	1-3 BP-CS to massive veins <1-1.5 cm	po, cpy, py, asp, carb, chl, ±v.g.	graphitic pelite - .8 to 1.5 m	- veins folded/rolled and can be discontinuous - graphitic alteration can be intense
	NSDME	1-2 BP-CS veins 1.5-8 cm	po, py, cpy, carb, chl	graphitic pelite - .3 m	pelite contains abundant carbonate orbs
MARKER (See Plate 13)	PHASE I	1-2 BP-CS to massive veins - 20-60 cm	py, po, cpy, gn, ±v.g.	graphitic pelite - 1.5 to 2 m	- vein displays dramatic boudinaging - v.g. appeared to be consentrated folds/rolls and boudins
	PHASE II	1-2 BP-CS to massive veins - 7-40 cm 1 intersection of 1 BP-CS vein 1.6 m thick	po, cpy, py, asp, gn, chl, carb ±v.g.	graphitic pelite - 1.5 to 2.5 m	- zone usually comprised of 1 thick vein; 2 veins 5-15 cm thick are observed; maybe a function of depth - refer to Plate 12

TABLE 3 DESCRIPTION OF QUARTZ VEINS (CONT'D).

VEIN(S)	LOCATION	TYPE & THICKNESS	MINERALOGY	HOST ROCK	COMMENTS
MARKER	PHASE III	1 BP-CS to massive vein 11-31 cm	po, cpy, py, gn, chl, carb, ±v.g.	graphitic pelite - 1 to 1.6 m	- low angle angulars intersecting zone observed - minor psammite
	NSDME	1 BP-CS - massive vein - 30 cm or 2 BP-CS veins 1.5/6 cm	po, py, cpy, gn, carb, chl, ±v.g.	graphitic pelite - .3 to .5	2 vein zone is folded/rolled
WHIN	PHASE I	2 BP-veins - <1/5 cm	po, py, cpy	graphitic pelite - .5 m	intensely folded/rolled
(Plate 14)	PHASE II	1-4 BP-CS to massive veins <1-4 cm	po, cpy, py, asp, gn, chl, carb, ±v.g.	graphitic pelite - .6 to 1.5 m	- folded/rolled - minor psammite
	PHASE III	3-7 BP-CS to massive veins <1-3 cm	po, cpy, py, asp, gn, chl, carb ±v.g.	graphitic pelite - .25 to .8 m	- fewer (3) and thicker veins in most westerly intersections - folded/rolled - minor psammite
	NSDME	1-2 BP-CS veins - 1.5-10 cm	cpy, gn, ±sp	graphitic pelite .8 to 1 m	- veins folded/rolled - minor psammite in zone
TWIN	PHASE I	2 BP-CS veins - 5-7 cm approx. 10-15 cm apart in N. decline surficial drilling in same area intersected 1-8 veins; .2-5 cm wide within this zone	py, cpy, po, gn ± v.g.	graphitic pelite 1 to 2 m minor psammite	commonly 2 veins separated by psammite bed. 30-40 cm thick - veins can be intensely folded/rolled - underground workings report
(Plate 15)	PHASE II	2-8 BP-CS veins; .5-7 cm with 2 pelite beds. H.W. vein(s) - .5-7 cm may pinch out completely	po, cpy, py, gn, chl ± v.g.	graphitic pelite - 1 to 2 m - 2 pelite bed separated by psammite	- thick veins usually have C-S texture - thin veins are commonly massive and folded/rolled - v.g. usually in H.W. vein(s)
	PHASE III	H.W.: 1-5 BP-CS veins; .4-3.5 cm when single veins F.W.: 1 BP-CS vein - 3.7-12 cm + thickest in most westerly hole	po, cpy, py, gn	graphitic pelite - .8 to .9 m 2 beds separated by approx. 30 cm psammite	- veins are folded/rolled
	NSDME	1 BP-CS vein; .5-4 cm	po, cpy, chl	2 graphitic pelite beds .3 m separated by 20 cm of psammite	up-dip intersection marked by associated with 6 m wide zone of intense shearing/brecciation
NUGGET	PHASE I	1 massive vein; 15-85 cm en echelon + tension gap veins 1 rolled C-S vein common at H.W. .1-2.5 cm	po, py, cpy, asp ± v.g. carb, chl	extremely graphitic pelite .3 to 3.5 m may contain minor narrow psammite bands	- zone characterized by presence of massive en echelon + tension-gap quartz veins, which can contain large angular pelite fragments - pelite host contains disseminated asp + py
(Plate 16)	PHASE II	≤10 BP-CS, to massive en echelon and tension gap veins .2-25 cm	asp, po, cpy, py ± gn ±v.g. pink carb, chl	extremely graphitic pelite and minor interbedded psammite .5 to 2.5 m	veins may be absent from this zone due to boudinaging effects - pelite host contains disseminated asp; crystals ≤ 2.5 cm - veins can be folded and contain abundant angular pelite fragments - v.g. occurs usually in H.W. vein(s)

TABLE 3 DESCRIPTION OF QUARTZ VEINS (CONT'D).

	PHASE III	1-4 BP-CS to massive vein(s) .8-4.5 cm two zones at H.W. uppermost contains 2-4 folded veins 2.5-4.5 cm lower set of 1-2 folded veins .8-2.5 cm	asp, po, cpy, py ± v.g.	interbedded graphitic pelite and psammite .8 to 1.2 m	may be intensely sheared
	NSDME	1 BP-CS to massive vein; 20 cm C-S textured at vein margins, inner portion is massive and vuggy ± columnar quartz crystals	po, cpy	extremely graphitic pelite with minor psammite .5 m	- vein contains angular pelite fragments - slickensides (S_3?) visible on graphitic pelite
LITTLE SOUTH	PHASE I	≤7 BP-CS to massive veins .1 to 13 cm	po, py, cpy ± v.g.	graphitic pelite .3 to 1.0 m minor intercalated psammite	- veins may be folded/rolled
	PHASE II	≤5 BP-CS to massive veins .5 to 5 cm	po, cpy, py, chl	graphitic pelite .4 to 1.3 m minor intercalated psammite	
	PHASE III	1-5 BP-CS veins 2 to 5.5 cm	po, cpy, py	graphitic pelite .2 m	- veins are folded/rolled
	NSDME	up-dip: 2 x .2 cm folded BP veins at H. W. followed by 1 BP-CS vein - 25 cm down-dip: 4-6 BP-CS veins - .5 to 2 cm	po po + cpy + gn ± v.g. po ± cpy	graphitic pelite .4 m minor intercalated psammite	H. W. vein is carbonate-rich
BIG SOUTH	PHASE I	1-4 folded BP-CS veins .1 to 5 cm at H. W. followed by 1 BP-CS to massive vein 13 to 50 cm	po, py, cpy, ± asp ± v.g.	interbedded graphitic pelite and psammite 1 to 2 m	- pelite often contains diss. sulphides - v.g. in H. W. veins
	PHASE II	1-3 folded BP-CS to massive veins 1-5 cm at H. W. followed by BP-CS vein - 10 cm and 1 BP-massive vein - 21 cm	po, py, cpy, asp ± v.g. asp	interbedded graphitic pelite and psammite 1 to 2 m	- v.g. in H. W. veins
	PHASE III	1-5 folded BP-CS-massive veins 1 to 8 cm at H. W. followed by 1-2 BP-massive - CS vein(s) 10 to 25 cm	po, py, cpy, ± asp ± v.g.	interbedded graphitic pelite and psammite 1 to 2 m	
	NSDME	3 x 1 cm folded BP veins at H. W. followed by 1 BP-CS to massive vein 26 cm - down-dip intersection contained 3 x 1.5 cm folded BP-CS veins in massive pelite approx. 1 m above a 50 cm BP-CS-massive vein	po ± cpy chl, carb near F. W. po, carb	interbedded graphitic pelite and psammite .5 to 1 m	- columnar quartz crystals in thick vein veins in down-dip intersection separated by 1 m of massive psammite

These veins may contain pyrite, pyrrhotite and chalcopyrite and where most abundant may be associated with zones of gold enrichment, as noted by the occurrence of anomalous gold values within some quartz-carbonate enriched psammite beds situated both above and below some of the B.P quartz vein zones (see 7.2 below).

5.4 Stratigraphic Variation

Based on compilation of Coxheath drilling and the stratigraphic columns presented in Figure 7 there appears to be dramatic variation in thickness and stratigraphic continuity of individual beds and relative position of quartz veins. Examples of this are shown by the stratigraphic sequences; TAN90-3, 0-260ft.; TAN90-4, 170-400ft.; and 303-550ft. of the Sullivan sequence. All sequences begin with what is assumed to be the Chambers zone.

It is evident that the three sections display striking differences. The Sullivan-sequence for instance, begins with three discrete pelite beds hosting a total of 6 sulphide-bearing quartz veins which are separated by massive psammite. The same package further west, along strike and down-dip (TAN90-4) is represented by a zone of mixed psammite and pelite and only 1 vein. The section up-dip (TAN90-3) from TAN90-4 is also interbedded, but has a thin semipelite horizon and 6 veins. This zone bottoms out in the Marker psammite which ranges from a true thickness of 46-52ft. in the Sullivan-sequence to 61ft. approximately 400ft. along strike and 100ft. up-dip in TAN90-3. The dramatic thickening up-dip is consistent with underground observations by Coxheath geologists which indicate local thickening of beds close to the hinge of the fold axis. The footwall of the Marker psammite is represented by two 30cm wide pelite bands in the Sullivan-sequence and TAN90-4, and a single 30cm pelite bed in TAN90-3. These particular pelite beds are host to the 'Upper Marker' vein(s) which occur as, a folded 3cm hanging wall and a 1.5 cm footwall BP-vein in TAN90-3 and as a single 8cm hangingwall BP-vein in the hangingwall pelite bed in the Sullivan-section. Similar variation is also shown by the Marker vein which is stratigraphically, the next vein package down section.

Also noted was that the pelite beds hosting these veins may show as much thickness variation as the veins. For example Forgeron *et al.* (1988) report that the Marker vein in one hole is 20cm thick in a 1.2m thick pelite; approximately 200 m east and 20 m down-dip the vein is 25cm thick within a 4.65m thick pelite and 40cm. thick in a 1.9m thick pelite another 20m down-dip. This variation implies that the veins likely formed by both the crack-seal mechanism and a process of progressive silicification and replacement of wall rock (Smith 1988a; Henderson and Henderson, 1990).

Further down section, the Whin and Big South veins show a difference of 10ft. and 13ft. in their respective stratigraphic locations within drill holes TAN90-3 and 4, as does the Little South vein package which occurs at a lower statigraphic level within TAN90-3 compared to its location in TAN90-4. Also observed based on the stratigraphic columns is that zones of intense alteration and fracturing appear to correlate well up-dip and along strike as shown by sections TAN90-3, 240-242ft. and TAN90-4, 386-389ft.

6. GEOCHEMISTRY

A total of 53 drill core samples were collected for lithogeochemical analyses. The purpose was to define the geochemical characteristics of the Tangier deposit and indentify both interdeposit and intradeposit geochemical variation and trends. The 53 samples are comprised of 24 psammites, 19 pelites

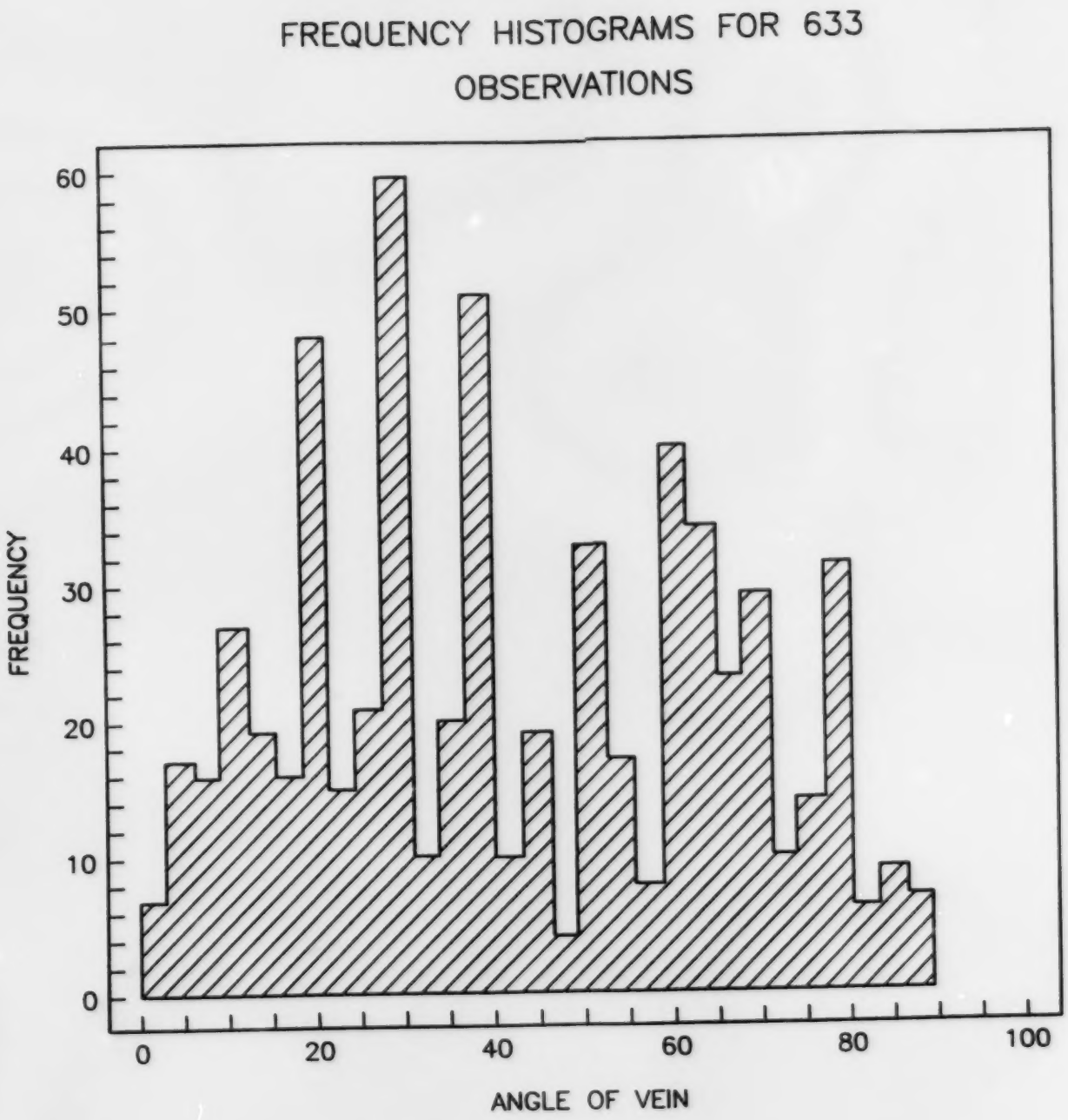

FIGURE 9. Histogram showing the orientation of 633 quartz+-carbonate angular veins compiled from Coxheath Gold Holdings Ltd. diamond drill records.

and 10 quartz veins. In order to compensate for the random occurrence of sulphides and gold within the quartz veins these samples were crushed and hand-picked to remove all visible mineralization and wall-rock fragments thereby minimizing artificial geochemical variation.

All samples were analysed at the Minerals Engineering Centre, Technical University of Nova Scotia, Halifax employing the following analytical techniques. Major oxides: FeO, NaO, CaO, MgO, TiO_2, and Al_2O_3 (AA); P_2O_5 and SiO_2 (colourmetric); CO_2, S, and organic C (LECO); Fe_2O_3 (titration); $\pm$ H_2O (gravimetric). Trace elements: As-W (colourmetric), Cu-Pb-Zn-Ni-Co-Cr-Li-Rb-V (total acid leach followed by AA), Au-Ag-Cd (aqua-regia leach followed by AA), F(specific ion electrode), La-Ba-Sr-Zr-Y-Sc-Ga-Bi-B-Sb-Sn-Mo (emmision spectrometry) and Hg (cold-vapour AA). All samples were jaw crushed and pulverized to -150 mesh prior to analysis.

6.1 Whole rock lithogeochemistry

Appendix A lists, minimum, maximum and mean concentrations for Tangier psammite, pelite and quartz vein samples as well as those from the eastern Meguma terrane (EMT) after Douma (in prep.). The 'altered' group refers to those samples which display visible effects of hydrothermal alteration such as colour change and or textural or mineralogical modification. It is possible that some of the samples labelled as unaltered may have been only mildly altered thereby lacking any visual expression. Also included are major-oxide and trace element geochemical analysis for the Tangier samples. The samples are indentified according to drill hole number and depth where sampled (e.g. T3-54 represents, drill hole T3, at 54 ft. down hole)

The ternary diagrams (Fig. 10) show that Tangier pelites and psammites possess distinct geochemical signatures characterized by generally lower concentrations of SiO_2, Na_2O, total Fe% (Fe_2O_3), CaO, and CO_2 and higher K_2O in the pelites. Figures 10a,b show how the Tangier samples groups plot with respect to similar samples collected by Douma (in prep.) within the EMT. The geochemical characteristics and variation of the psammites, pelites and quartz veins are discussed below.

6.1.1 Psammite

The variation in mean major-oxide and trace element concentrations for the unaltered and altered psammites collected at Tangier and also those encompassing all Tangier psammite samples and EMT samples are shown in Figures 11a and 11b. Figure 11a shows similar to only minor variation in mean concentrations of Si-Ti-Al-Ca-C-oxides for the sample groups. Wide variation occurs in the mean concentration (wt.%) of; Fe_2O_3 which is highest (1.66) in the EMT and lowest (.338) in the altered Tangier samples; MnO which ranges from a high of .08 in the EMT to a low of .039 in the altered group; K_2O which is highest in the EMT (2.89) and lowest in the altered mean (1.47) and CO_2 which ranges from approximately 1.0 in the Tangier samples to .34 in the EMT mean. Less dramatic variations occur in; FeO and MgO which are lowest in the altered mean and, Na_2O and P_2O_5 which are lowest in the EMT mean. The C concentration is similar for both Tangier sample groups and was not analysed in the EMT samples.

The widest variations in mean trace element concentration (ppm; Au-ppb) within the sample groups (Fig. 11b) occur for: As which ranges from a high of 601.89 in the unaltered mean to 77.5 in the altered mean, to 14.89 in the EMT mean and W, which varies from 74.17 in the altered mean to 5.78 in the unaltered mean, and 2.48 in the E.M.T. mean. The extremely high As unaltered mean is attributed to one sample which contained fine grained disseminated arsenopyrite. Au concentration is highest in altered

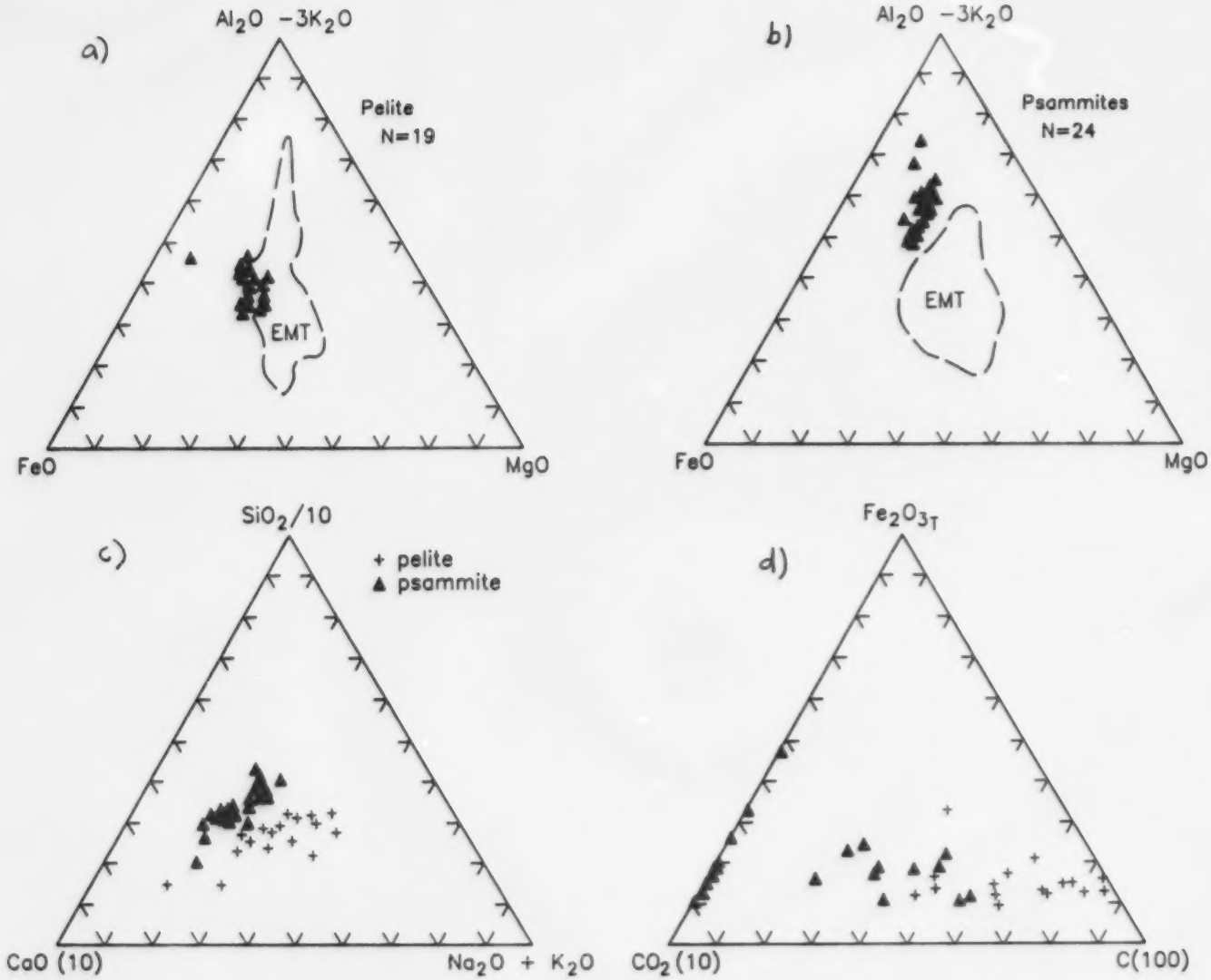

FIGURE 10. Ternary plots of Tangier psammite and pelite samples:
a. AKFM plot of pelite samples

b. AKFM plot of psammite samples

e)

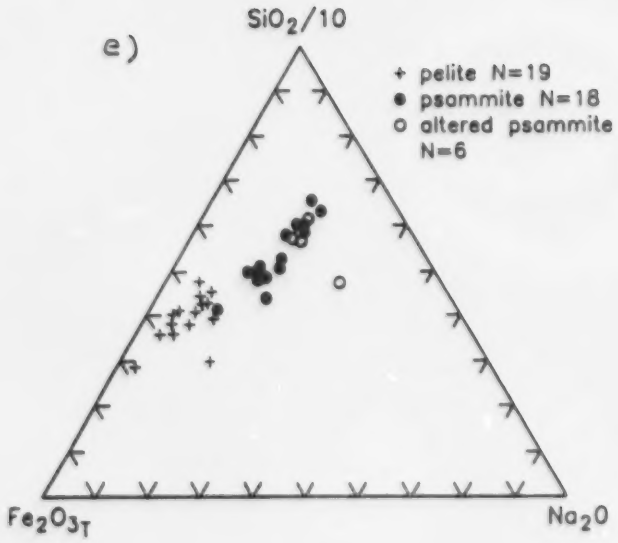
$SiO_2/10$
+ pelite N=19
● psammite N=18
○ altered psammite N=6
Fe_2O_{3T}
Na_2O

f)

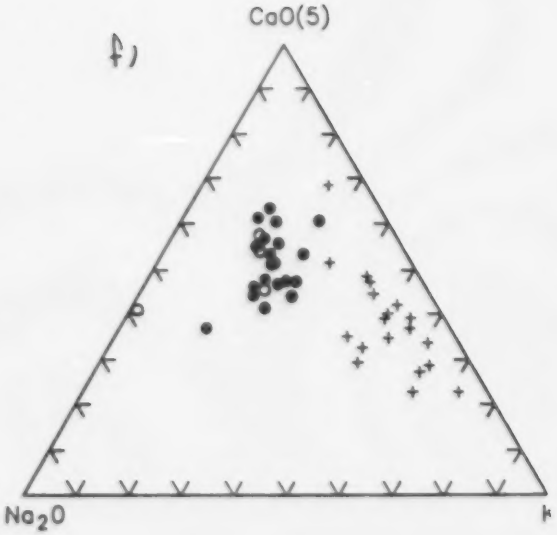
CaO(5)
Na_2O

g)

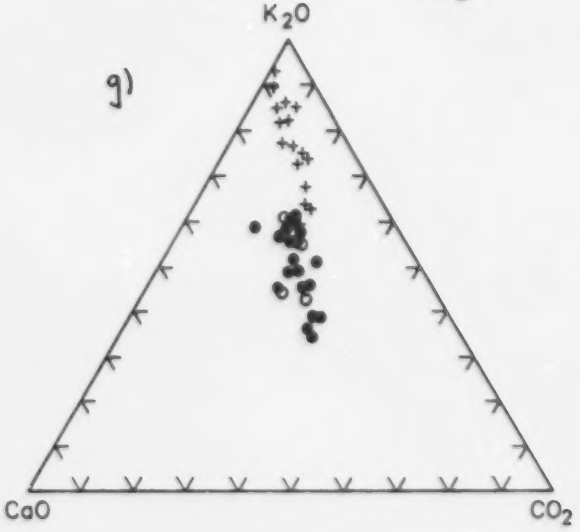
K_2O
CaO
CO_2

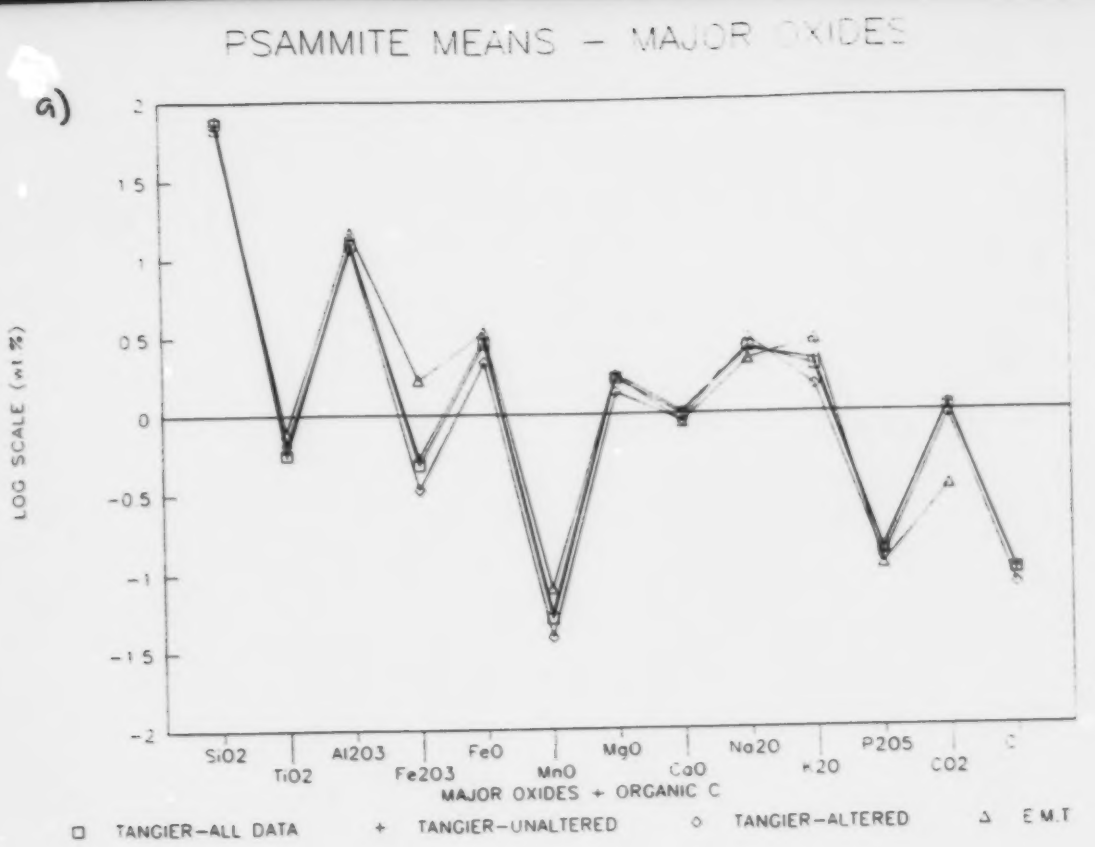

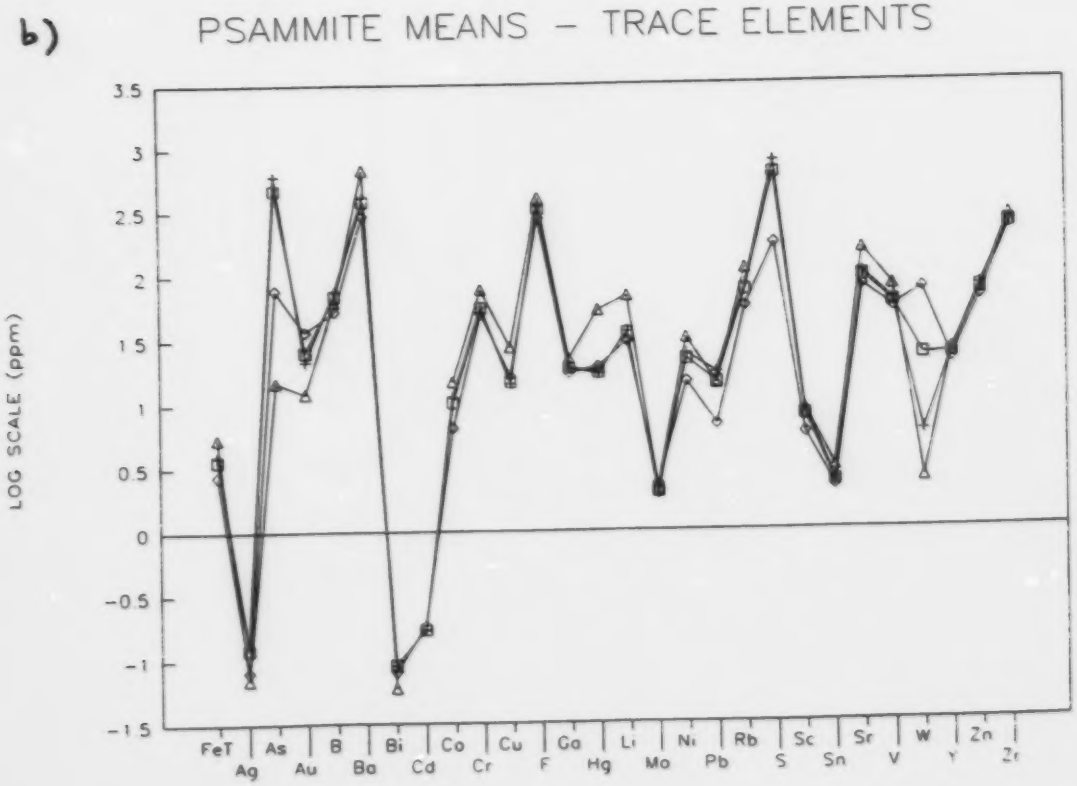

FIGURE 11a. Variation in mean major-oxide concentrations for psammite sample groups

b. Variation in trace element concentrations for psammite sample groups

TABLE 4. List of samples used for comparison of major-oxides and trace elements and the relative enrichments and depletions of each.

TABLE 4: RELATIVE ENRICHMENT/DEPLETION OF MAJOR-OXIDES AND TRACE ELEMENTS

		Si	Ti	Al	Fe	FeO	Mn	Mg	Ca	Na	K	P	CO_2	C	FeT
FIG. 14	UNALTERED MEAN (a)	72.81	0.58	12.58	0.53	3.05	0.06	1.79	1.03	2.53	2.16	0.14	1.11	0.10	3.92
	ALTERED MEAN (b)	77.45	0.65	11.62	0.34	2.15	0.04	1.37	0.90	2.98	1.47	0.12	0.95	0.08	2.73
	ENRICH/DEPL FACTOR (a/b)	1.06	1.12	0.92	0.64	0.71	0.70	0.77	0.87	1.18	0.68	0.86	0.86	0.80	0.70
	LOG (a/b)	0.03	0.05	-0.03	-0.20	-0.15	-0.16	-0.12	-0.06	0.07	-0.17	-0.06	-0.07	-0.10	-0.16
FIG. 16	T-4-176	80.97	0.31	9.84	0.24	1.53	0.031	0.78	0.66	2.36	1.48	0.097	0.71	N.D	1.94
	T-4-166	79.70	0.44	10.30	0.05	1.68	0.039	0.73	1.09	2.77	1.65	0.109	1.46	N.D	1.92
	ENRICH/DEPL FACTOR	1.02	0.70	0.96	4.86	0.91	0.79	1.07	0.61	0.85	0.90	0.89	0.49	0.00	1.01
	LOG	0.01	-0.15	-0.02	0.69	-0.04	-0.10	0.03	-0.22	-0.07	-0.05	-0.05	-0.31	0.00	0.00
	T-4-166	79.70	0.44	10.30	0.05	1.68	0.039	0.73	1.09	2.77	1.65	0.109	1.46	N.D.	1.92
	T-4-142.4	70.86	0.65	13.10	0.69	3.79	0.054	1.76	1.10	2.36	2.08	0.130	1.35	N.D	4.91
	ENRICH/DEPL FACTOR	1.12	0.68	0.79	0.07	0.44	0.72	0.41	0.99	1.17	0.79	0.84	1.08	0.00	0.39
	LOG	0.05	-0.17	-0.10	-1.15	-0.35	-0.14	-0.38	-0.00	0.07	-0.10	-0.08	0.03	0.00	-0.41
FIG. 15	90-3-465	77.40	0.44	10.81	0.32	2.51	0.034	1.23	0.78	5.36	0.13	0.130	0.61	0.05	3.12
	90-3-475	68.08	0.60	14.95	0.81	3.43	0.061	2.13	0.97	2.59	2.97	0.198	0.98	0.05	4.63
	ENRICH/DEPL FACTOR	1.14	0.73	0.72	0.40	0.73	0.56	0.58	0.80	2.07	0.04	0.66	0.62	1.00	0.67
	LOG	0.06	-0.13	-0.14	-0.40	-0.14	-0.25	-0.24	-0.09	0.32	-1.36	-0.18	-0.21	0.00	-0.17
FIG. 17a	T-4-142.4	70.86	0.65	13.10	0.69	3.79	0.054	1.76	1.10	2.36	2.08	0.130	1.35	0.05	4.91
	90-3-184.6	70.32	0.64	13.69	0.95	3.13	0.039	2.15	0.73	2.29	2.47	0.146	0.82	0.05	4.44
	ENRICH/DEPL FACTOR	1.01	1.02	0.96	0.72	1.21	1.38	0.82	1.51	1.03	0.84	0.89	1.65	1.00	1.11
	LOG	0.00	0.01	-0.02	-0.14	0.08	0.14	-0.09	0.18	0.01	-0.07	-0.05	0.22	0.00	0.04
FIG. 17b	T-3-102.5	76.55	0.65	11.14	0.47	2.21	0.050	1.51	0.99	2.45	1.90	0.133	1.30	N.D.	2.93
	T-4-28.8	76.31	0.54	11.01	0.15	2.61	0.046	1.66	1.05	2.63	1.73	0.130	1.29	N.D.	3.06
	ENRICH/DEPL FACTOR	1.00	1.20	1.01	3.07	0.85	1.09	0.91	0.94	0.93	1.10	1.02	1.01	0.00	0.96
	LOG	0.00	0.08	0.01	0.49	-0.07	0.04	-0.04	-0.03	-0.03	0.04	0.01	0.00	0.00	-0.02
FIG. 20a	T-4-134	60.00	0.78	19.46	1.26	4.57	0.054	2.47	1.07	1.09	4.77	0.149	1.68	0.32	6.35
	T-4-145	47.71	0.93	23.36	1.94	5.71	0.079	3.48	1.85	2.73	5.97	0.190	2.27	0.57	8.30
	ENRICH/DEPL FACTOR	1.26	0.84	0.83	0.65	0.80	0.68	0.71	0.58	0.40	0.80	0.78	0.74	0.56	0.77
	LOG	0.10	-0.08	-0.08	-0.19	-0.10	-0.17	-0.15	-0.24	-0.40	-0.10	-0.11	-0.13	-0.25	-0.12
FIG. 20b	90-3-624	51.20	0.99	23.98	1.91	5.58	0.070	3.64	0.51	1.04	5.70	0.178	0.42	0.41	8.13
	90-3-538.5	58.89	0.89	19.63	1.24	5.21	0.077	2.84	0.65	1.99	4.09	0.140	0.53	0.09	7.04
	ENRICH/DEPL FACTOR	0.87	1.11	1.22	1.55	1.07	0.91	1.28	0.78	0.52	1.39	1.27	0.79	4.56	1.15
	LOG	-0.06	0.05	0.09	0.19	0.03	-0.04	0.11	-0.11	-0.28	0.14	0.10	-0.10	0.66	0.06

TABLE 4 : RELATIVE ENRICHMENT/DEPELTION OF MAJOR-OXIDES AND TRACE ELEMENTS

		Ag	As	Au	B	Ba	Bi	Cd	Co	Cr	Cu	F	Ga	Hg	Li	Mo
FIG. 14	UNALTERED MEAN (a)	0.13	601.89	21.65	74.56	408.89	0.09	0.17	11.44	57.11	14.28	346.11	19.28	16.89	36.50	1.88
	ALTERED MEAN (b)	0.08	77.50	36.83	52.67	294.50	0.08	0.18	6.50	50.50	16.67	278.33	17.33	19.17	30.33	2.27
	ENRICH/DEPL FACTOR (a/b)	0.62	0.13	1.70	0.71	0.72	0.89	1.06	0.57	0.88	1.17	0.80	0.90	1.13	0.83	1.21
	LOG (a/b)	-0.21	-0.89	0.23	-0.15	-0.14	-0.05	0.02	-0.25	-0.05	0.07	-0.09	-0.05	0.05	-0.08	0.08
FIG. 16	90-3-465	0.05	7.00	5.00	3.00	17.00	0.09	0.01	5.00	52.00	17.00	150.00	19.00	28.00	17.00	2.70
	90-3-475	0.13	51.00	2.00	70.00	390.00	0.09	0.04	10.00	75.00	7.00	410.00	22.00	16.00	31.00	1.60
	ENRICH/DEPL FACTOR	0.38	0.14	2.50	0.04	0.04	1.00	0.25	0.50	0.69	2.43	0.37	0.86	1.75	0.55	1.69
	LOG	-0.41	-0.86	0.40	-1.37	-1.36	0.00	-0.60	-0.30	-0.16	0.39	-0.44	-0.06	0.24	-0.26	0.23
FIG. 15	T-4-176	0.10	290.00	10.00	75.00	290.00	0.09	0.01	5.00	34.00	12.00	280.00	14.00	16.00	20.00	3.10
	T-4-166	0.15	300.00	7.00	86.00	380.00	0.08	0.04	5.00	31.00	22.00	360.00	15.00	16.00	18.00	1.70
	ENRICH/DEPL FACTOR	0.67	0.97	1.43	0.87	0.76	1.13	0.25	1.00	1.10	0.55	0.78	0.93	1.00	1.11	1.82
	LOG	-0.18	-0.01	0.15	-0.06	-0.12	0.05	-0.60	0.00	0.04	-0.26	-0.11	-0.03	0.00	0.05	0.26
	T-4-166	0.15	300.00	7.00	86.00	380.00	0.08	0.04	5.00	31.00	22.00	360.00	15.00	16.00	18.00	1.70
	T-4-142.4	0.10	1100.00	45.00	95.00	360.00	0.09	0.02	14.00	63.00	12.00	340.00	18.00	12.00	30.00	1.50
	ENRICH/DEPL FACTOR	1.50	0.27	0.16	0.91	1.06	0.89	2.00	0.36	0.49	1.83	1.06	0.83	1.33	0.60	1.13
	LOG	0.18	-0.56	-0.81	-0.04	0.02	-0.05	0.30	-0.45	-0.31	0.26	0.02	-0.08	0.12	-0.22	0.05
FIG. 17a	T-4-142.4	0.10	1100.00	45.00	95.00	360.00	0.09	0.02	14.00	63.00	12.00	340.00	18.00	12.00	30.00	1.50
	90-3-184.6	0.15	1300.00	55.00	87.00	360.00	0.09	1.52	29.00	72.00	14.00	390.00	28.00	20.00	52.00	2.10
	ENRICH/DEPL FACTOR	0.67	0.85	0.82	1.09	1.00	1.00	0.01	0.48	0.88	0.86	0.87	0.64	0.60	0.58	0.71
	LOG	-0.18	-0.07	-0.09	0.04	0.00	0.00	-1.88	-0.32	-0.06	-0.07	-0.06	-0.19	-0.22	-0.24	-0.15
FIG. 17b	T-3-102.5	0.10	73.00	2.00	66.00	340.00	0.09	0.01	8.00	55.00	7.00	260.00	14.00	12.00	34.00	1.60
	T-4-28.8	0.10	57.00	2.00	16.00	360.00	0.09	0.02	9.00	50.00	8.00	260.00	19.00	12.00	35.00	1.90
	ENRICH/DEPL FACTOR	1.00	1.28	1.00	4.13	0.94	1.00	0.50	0.89	1.10	0.88	1.00	0.74	1.00	0.97	0.84
	LOG	0.00	0.11	0.00	0.62	-0.02	0.00	-0.30	-0.05	0.04	-0.06	0.00	-0.13	0.00	-0.01	-0.07
FIG. 20a	T-4-134	0.25	900.00	34.00	95.00	830.00	0.08	0.05	12.00	74.00	48.00	560.00	31.00	12.00	58.00	1.60
	T-4-145	0.25	5100.00	5.00	84.00	1200.00	0.13	0.08	17.00	104.00	40.00	690.00	29.00	12.00	66.00	0.80
	ENRICH/DEPL FACTOR	1.00	0.18	6.80	1.13	0.69	0.62	0.63	0.71	0.71	1.20	0.81	1.07	1.00	0.88	2.00
	LOG	0.00	-0.75	0.83	0.05	-0.16	-0.21	-0.20	-0.15	-0.15	0.08	-0.09	0.03	0.00	-0.06	0.30
FIG. 20b	90-3-624	0.20	29.00	2.00	87.00	1680.00	0.08	0.04	20.00	119.00	37.00	520.00	36.00	20.00	67.00	1.30
	90-3-538.5	0.15	34.00	29.00	72.00	460.00	0.05	0.04	19.00	109.00	14.00	180.00	32.00	20.00	42.00	1.30
	ENRICH/DEPL FACTOR	1.33	0.85	0.07	1.21	3.65	1.60	1.00	1.05	1.09	2.64	2.89	1.13	1.00	1.60	1.00
	LOG	0.12	-0.07	-1.16	0.08	0.56	0.20	0.00	0.02	0.04	0.42	0.46	0.05	0.00	0.20	0.00

TABLE 4 : RELATIVE ENRICHMENT/DEPELTION OF MAJOR-OXIDES AND TRACE ELEMENTS

		Ni	Pb	Rb	S	Sc	Sn	Sr	V	W	Y	Zn	Zr
FIG. 11	UNALTERED MEAN (a)	24.39	17.06	80.72	763.78	8.73	2.44	99.72	60.89	5.78	23.78	77.11	237.78
	ALTERED MEAN (b)	14.67	6.67	55.67	172.00	5.67	2.17	79.17	53.33	74.17	21.00	63.17	223.33
	ENRICH/DEPL FACTOR (a/b)	0.60	0.39	0.69	0.23	0.65	0.89	0.79	0.88	12.83	0.88	0.82	0.94
	LOG (a/b)	-0.22	-0.41	-0.16	-0.65	-0.19	-0.05	-0.10	-0.06	1.11	-0.05	-0.09	-0.03
FIG. 14	90-3-465	16.00	6.00	8.00	20.00	8.00	1.4	85.00	48.00	9.00	13.00	39.00	215.00
	90-3-475	19.00	9.00	100.00	200.00	4.00	2.7	95.00	67.00	2.00	23.00	67.00	150.00
	ENRICH/DEPL FACTOR	0.84	0.67	0.08	0.10	2.00	0.52	0.89	0.72	4.50	0.57	0.58	1.43
	LOG	-0.07	-0.18	-1.10	-1.00	0.30	-0.29	-0.05	-0.14	0.65	-0.25	-0.24	0.16
FIG. 15	T-4-176	12.00	3.00	59.00	170.00	6.00	2.9	85.00	44.00	30.00	14.00	21.00	195.00
	T-4-166	11.00	11.00	71.00	1500.00	9.00	1.8	130.00	47.00	12.00	19.00	19.00	155.00
	ENRICH/DEPL FACTOR	1.09	0.27	0.83	0.11	0.67	1.61	0.65	0.94	2.50	0.74	1.11	1.26
	LOG	0.04	-0.56	-0.08	-0.95	-0.18	0.21	-0.18	-0.03	0.40	-0.13	0.04	0.10
	T-4-166	11.00	11.00	71.00	1500.00	9.00	1.8	130.00	47.00	12.00	19.00	19.00	155.00
	T-4-142.4	31.00	12.00	74.00	1100.00	12.00	2.4	142.00	57.00	2.00	23.00	63.00	330.00
	ENRICH/DEPL FACTOR	0.35	0.92	0.96	1.36	0.75	0.75	0.92	0.82	6.00	0.83	0.30	0.47
	LOG	-0.45	-0.04	-0.02	0.13	-0.12	-0.12	-0.04	-0.08	0.78	-0.08	-0.52	-0.33
FIG. 17a	T-4-142.4	31.00	12.00	74.00	1100.00	12.00	2.4	142.00	57.00	2.00	23.00	63.00	330.00
	90-3-184.6	41.00	25.00	88.00	1100.00	1.00	2.4	75.00	68.00	1.00	22.00	380.00	225.00
	ENRICH/DEPL FACTOR	0.76	0.48	0.84	1.00	12.00	1.00	1.89	0.84	2.00	1.05	0.17	1.47
	LOG	-0.12	-0.32	-0.08	0.00	1.08	0.00	0.28	-0.08	0.30	0.02	-0.78	0.17
FIG. 17b	T-3-102.5	17.00	5.00	77.00	180.00	4.00	2.0	55.00	53.00	390.00	24.00	36.00	305.00
	T-4-28.8	16.00	12.00	72.00	100.00	5.00	2.1	62.00	57.00	14.00	34.00	39.00	180.00
	ENRICH/DEPL FACTOR	1.06	0.42	1.07	1.80	0.80	0.95	0.89	0.93	27.86	0.71	0.92	1.69
	LOG	0.03	-0.38	0.03	0.26	-0.10	-0.02	-0.05	-0.03	1.44	-0.15	-0.03	0.23
FIG. 20a	T-4-134	41.00	48.00	167.00	5300.00	18.00	3.3	130.00	110.00	2.00	22.00	83.00	80.00
	T-4-145	45.00	15.00	204.00	4100.00	23.00	3.4	170.00	150.00	5.00	24.00	113.00	115.00
	ENRICH/DEPL FACTOR	0.91	3.20	0.82	1.29	0.78	0.97	0.76	0.73	0.40	0.92	0.73	0.70
	LOG	-0.04	0.51	-0.09	0.11	-0.11	-0.01	-0.12	-0.13	-0.40	-0.04	-0.13	-0.16
FIG. 20b	90-3-624	41.00	6.00	219.00	870.00	11.00	3.8	35.00	144.00	1.00	23.00	107.00	155.00
	90-3-538.5	34.00	3.00	122.00	180.00	6.00	3.0	61.00	96.00	1.00	23.00	106.00	140.00
	ENRICH/DEPL FACTOR	1.21	2.00	1.80	4.83	1.83	1.27	0.57	1.50	1.00	1.00	1.01	1.11
	LOG	0.08	0.30	0.25	0.68	0.26	0.10	-0.24	0.18	0.00	0.00	0.00	0.04

TABLE 4 : RELATIVE ENRICHMENT/DEPELTION OF MAJOR-OXIDES AND TRACE ELEMENTS

		Si	Ti	Al	Fe	FeO	Mn	Mg	Ca	Na	K	P	CO2	C	FeT
FIG. 21a	90-3-317	98.85	0.005	0.12	0.05	0.59	0.008	0.063	0.13	0.003	0.011	0.024	0.23	1.00	0.71
	T-4-37.5	96.78	0.006	0.23	0.37	0.69	0.007	0.044	0.12	0.008	0.047	0.012	0.52	1.00	1.14
	ENRICH/DEPL FACTOR	1.02	0.83	0.52	0.14	0.86	1.10	1.43	1.08	0.38	0.23	2.00	0.44	1.00	0.62
	LOG	0.01	-0.08	-0.28	-0.85	-0.07	0.04	0.16	0.03	-0.43	-0.63	0.30	-0.35	0.00	-0.21
FIG. 21b	90-3-317	98.85	0.005	0.12	0.05	0.59	0.008	0.063	0.13	0.003	0.011	0.024	0.23	1.00	0.71
	90-3-183	99.02	0.003	0.12	0.15	0.33	0.005	0.046	0.09	0.011	0.015	0.004	0.13	1.00	0.52
	ENRICH/DEPL FACTOR	1.00	1.67	1.00	0.35	1.79	1.54	1.37	1.44	0.27	0.73	6.00	1.77	1.00	1.37
	LOG	0.00	0.22	0.00	-0.46	0.25	0.19	0.14	0.16	-0.56	-0.13	0.78	0.25	0.00	0.14
FIG. 22	90-3-182.2	56.25	0.93	20.45	1.22	4.62	0.060	3.52	1.21	1.29	5.21	0.231	1.73	0.23	6.37
	T-4-145	47.71	0.93	23.36	1.94	5.71	0.079	3.48	1.85	2.73	5.97	0.190	2.27	0.57	8.30
	ENRICH/DEPL FACTOR	1.18	1.00	0.88	0.63	0.81	0.76	1.01	0.65	0.47	0.87	1.22	0.76	0.40	0.77
	LOG	0.07	0.00	-0.06	-0.20	-0.09	-0.12	0.00	-0.18	-0.33	-0.06	0.08	-0.12	-0.39	-0.11
	90-3-183	99.02	0.003	0.12	0.15	0.33	0.005	0.046	0.09	0.011	0.015	0.004	0.13	1.00	0.52
	T-4-145.6	98.43	0.004	0.12	0.02	0.59	0.017	0.109	0.34	0.009	0.023	0.008	0.46	1.00	0.68
	ENRICH/DEPL FACTOR	1.01	0.75	1.00	6.70	0.56	0.29	0.42	0.26	1.22	0.65	0.50	0.28	1.00	0.76
	LOG	0.00	-0.12	0.00	0.83	-0.25	-0.53	-0.37	-0.58	0.09	-0.19	-0.30	-0.55	0.00	-0.12

TABLE 4: RELATIVE ENRICHMENT/DEPELTION OF MAJOR-OXIDES AND TRACE ELEMENTS

		Ag	As	Au(ppb)	B	Ba	Bi	Cd	Co	Cr	Cu	F	Ga	Hg	Li	Mo
FIG. 21a	90-3-317	0.20	2.00	3800.00	15.00	4.00	0.10	0.24	1.00	76.00	10.00	48.00	1.00	24.00	2.00	13.00
	T-4-37.5	0.73	12.00	313.00	104.00	11.00	0.50	0.04	7.00	61.00	294.00	52.00	1.00	16.00	1.00	8.30
	ENRICH/DEPL FACTOR	0.27	0.17	12.14	0.14	0.36	0.20	6.00	0.14	1.25	0.03	0.92	1.00	1.50	2.00	1.57
	LOG	-0.56	-0.78	1.08	-0.84	-0.44	-0.70	0.78	-0.85	0.10	-1.47	-0.03	0.00	0.18	0.30	0.19
FIG. 21b	90-3-317	0.20	2.00	3800.00	15.00	4.00	0.10	0.24	1.00	76.00	10.00	48.00	1.00	24.00	2.00	13.00
	90-3-183	0.05	29.00	9.00	14.00	5.00	0.09	0.13	1.00	26.00	34.00	80.00	1.00	19.00	2.00	5.00
	ENRICH/DEPL FACTOR	4.00	0.07	422.22	1.07	0.80	1.11	1.85	1.00	2.92	0.29	0.60	1.00	1.26	1.00	2.60
	LOG	0.60	-1.16	2.63	0.03	-0.10	0.05	0.27	0.00	0.47	-0.53	-0.22	0.00	0.10	0.00	0.41
FIG 22	90-3-182.2	0.15	310.00	4.00	85.00	800.00	0.07	0.97	13.00	94.00	17.00	560.00	29.00	24.00	75.00	2.30
	T-4-145	0.25	5100.00	5.00	84.00	1200.00	0.13	0.08	17.00	104.00	40.00	690.00	29.00	12.00	66.00	0.80
	ENRICH/DEPL FACTOR	0.60	0.06	0.80	1.01	0.67	0.54	12.13	0.76	0.90	0.43	0.81	1.00	2.00	1.14	2.88
	LOG	-0.22	-1.22	-0.10	0.01	-0.18	-0.27	1.08	-0.12	-0.04	-0.37	-0.09	0.00	0.30	0.06	0.46
	90-3-183	0.05	29.00	9.00	14.00	5.00	0.09	0.13	1.00	26.00	34.00	80.00	1.00	19.00	2.00	5.00
	T-4-145.6	0.13	16.00	10.00	12.00	10.00	0.10	0.05	1.00	56.00	11.00	58.00	1.00	12.00	1.00	8.00
	ENRICH/DEPL FACTOR	0.38	1.81	0.90	1.17	0.50	0.90	2.60	1.00	0.46	3.09	1.38	1.00	1.58	2.00	0.63
	LOG	-0.41	0.26	-0.05	0.07	-0.30	-0.05	0.41	0.00	-0.33	0.49	0.14	0.00	0.20	0.30	-0.20

TABLE 4 : RELATIVE ENRICHMENT/DEPELTION OF MAJOR-OXIDES AND TRACE ELEMENTS

		Ni	Pb	Rb	S	Sc	Sn	Sr	V	W	Y	Zn	Zr
FIG. 21a.	90-3-317	6.00	2.00	5.00	39.00	1.00	2.3	1.00	1.00	3.00	20.00	27.00	100.00
	T-4-37.5	15.00	131.00	7.00	2700.00	1.00	2.9	1.00	1.00	1.00	19.00	12.00	55.00
	ENRICH/DEPL FACTOR	0.40	0.02	0.71	0.01	1.00	0.79	1.00	1.00	3.00	1.05	2.25	1.82
	LOG	-0.40	-1.82	-0.15	-1.84	0.00	-0.10	0.00	0.00	0.48	0.02	0.35	0.26
FIG. 21b	90-3-317	6.00	2.00	5.00	39.00	1.00	2.3	1.00	1.00	3.00	20.00	27.00	100.00
	90-3-183	5.00	3.00	6.00	100.00	1.00	2.4	1.00	1.00	1.00	16.00	22.00	95.00
	ENRICH/DEPL FACTOR	1.20	0.67	0.83	0.39	1.00	0.96	1.00	1.00	3.00	1.25	1.23	1.05
	LOG	0.08	-0.18	-0.08	-0.41	0.00	-0.02	0.00	0.00	0.48	0.10	0.09	0.02
FIG. 22	90-3-182.2	34.00	9.00	177.00	1100.00	6.00	2.7	80.00	140.00	1.00	26.00	236.00	245.00
	T-4-145	45.00	15.00	204.00	4100.00	23.00	3.4	170.00	150.00	5.00	24.00	113.00	115.00
	ENRICH/DEPL FACTOR	0.76	0.60	0.87	0.27	0.26	0.79	0.47	0.93	0.20	1.08	2.09	2.13
	LOG	-0.12	-0.22	-0.06	-0.57	-0.58	-0.10	-0.33	-0.03	-0.70	0.03	0.32	0.33
	90-3-183	5.00	3.00	6.00	100.00	1.00	2.4	1.00	1.00	1.00	16.00	22.00	95.00
	T-4-145.6	4.00	1.00	8.00	92.00	1.00	2.4	8.00	1.00	1.00	19.00	14.00	58.00
	ENRICH/DEPL FACTOR	1.25	3.00	0.75	1.09	1.00	1.00	0.13	1.00	1.00	0.84	1.57	1.64
	LOG	0.10	0.48	-0.12	0.04	0.00	0.00	-0.90	0.00	0.00	-0.07	0.20	0.21

mean (36.8) and lowest in the EMT (12.1). The range in concentration of major-oxides and trace elements for the unaltered and altered Tangier psammite sample groups are shown in Figures 12 and 13 respectively. Significant variation in the concentration of major oxides (wt.%) within the unaltered psammites (Fig. 12a) are indicated for; Fe_2O_3 (max-1.12/min-.05), MgO (2.9/.73), CaO (1.77/.54) and K_2O (3.81/1.24). Major-oxides within the altered psammite sample group (Fig. 12b) which show significant variation are, Na_2O (5.36/2.36) and K_2O (1.9/.13). Trace elements in the unaltered psammites (Fig. 13a) which show a wide range in concentration are; As (max-2000/min-13), Au (140/2), B (114/14), Cd (1.52/.01), Cu (35/4), Li (100/18), Pb (123/2), S (2200/10), W (20/1) and Zn (380/19). Significant trace element variation within altered psammites (Fig. 13b) are indicated by; As (max-290/min-7), Au (200/2), B (80/3), Ba (420/17), Cu (47/7), Pb (12/3), Rb (77/8), S (500/20), W (390/1) and Zn (202/21).

Although visually, there are dramatic differences between altered and unaltered psammites at Tangier (e.g., colour, texture), it is important to note that comparisons of corresponding oxide and trace element concentration ranges, show no clear geochemical distinction is possible between the two sample groups. The least amount of range overlap for the sample groups (and therefor best discriminator) is shown by K_2O which has range of 1.24 - 3.81 wt.% for the unaltered and .13 - 1.9 wt.% for the altered sample group. Trace elements which show a relatively low amount of range overlap include B, Ba, Rb and W. With the exception of W, which can be sharply enriched, these elements are present in lower concentrations within the altered samples. These differences are also reflected in Figure 14, in which the altered psammite mean was normalized to the unaltered mean. This figure shows relative differences in oxide and trace element concentrations between the two sample groups. It should be stressed that this comparison shows only general geochemical changes in response to hydrothermal alteration of psammites at Tangier and does not reflect the effect of a particular alteration type on a particular sample. This will only be revealed by comparing samples from the same bed or stratigraphic location. For example, the geochemical effects of hydrothermal alteration within the Tangier psammites are displayed in Figure 15 which shows the effect of progressive silicification within a single psammite bed. This was accomplished by plotting the relative geochemical difference of; a moderately silicified sample (79.7 wt.% SiO_2) normalized by an unaltered sample (70.86 wt.% SiO_2) and, a intensely silicified psammite (80.97 wt.% SiO_2) normalized by the moderately silicified sample. The samples used for comparison and a the relative % change for each major-oxide and trace element is listed in Table 4.

As can be seen, the moderate/no silicification comparison is characterized by strong relative enrichment of W, with weaker enrichments of Cd, Cu, Ag. Si_2O shows only weak relative enrichment. By comparison, strong relative depletions are shown by Fe_2O_3, Au, As, Zn, Ni, Co, total Fe, FeO and MgO with weaker depletion of Zr, Cr, Li, TiO_2, MnO, K_2O, Sc and Sn. Although increased silicification displays many of the characteristics shown by the above, some elements show opposite behavior. These include enrichment in Fe_2O_3, Mo, Sn, Au, Zr, Li, Zn and SiO_2, and depletion of S, Cd, Pb, CO_2, Cu, CaO, Ag, Ba, F and Sr.

Figure 16 also shows relative geochemical changes in response to intense silicification of a psammite. Although this comparison reflects many changes which are similar to those above such as enrichment in W, Mo and Au and depletion of Cd, S, Ag, and CO_2, there are significant differences. These include enrichment of; Na_2O, and strong depletion of; K_2O, B, Ba, F, Rb and Sn.

While the above has established that the concentration of oxide and trace elements in psammites can vary in response to hydrothermal alteration, this study also indicates geochemical variation exists between Tangier psammites which show no visible alteration effects. Examples of this are presented in Figure

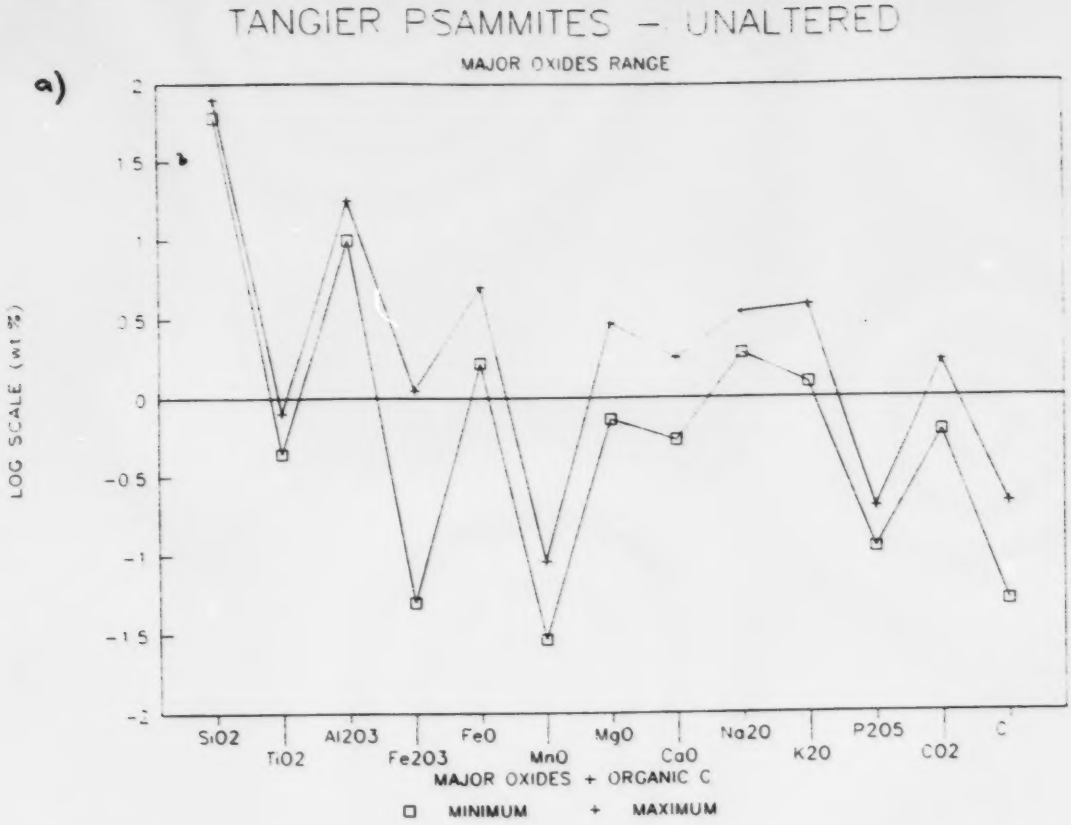

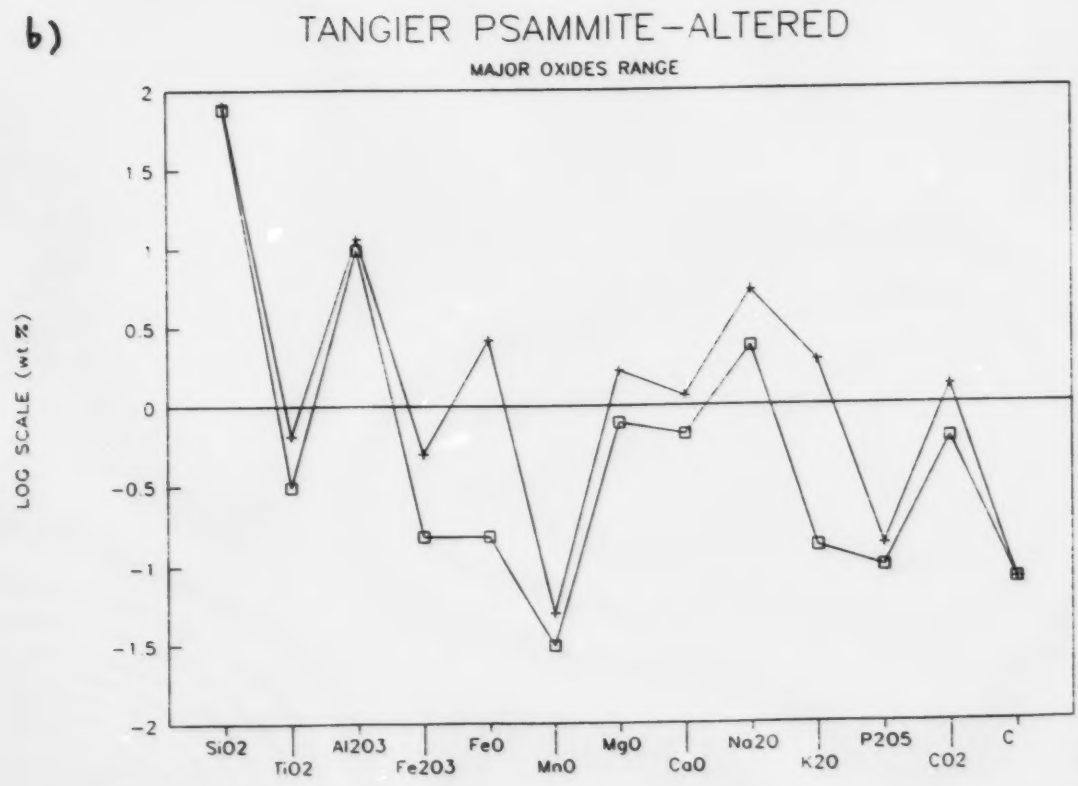

FIGURE 12a. Range in concentration of major-oxides within unaltered psammites

b. Range in concentration of major-oxides within altered psammites

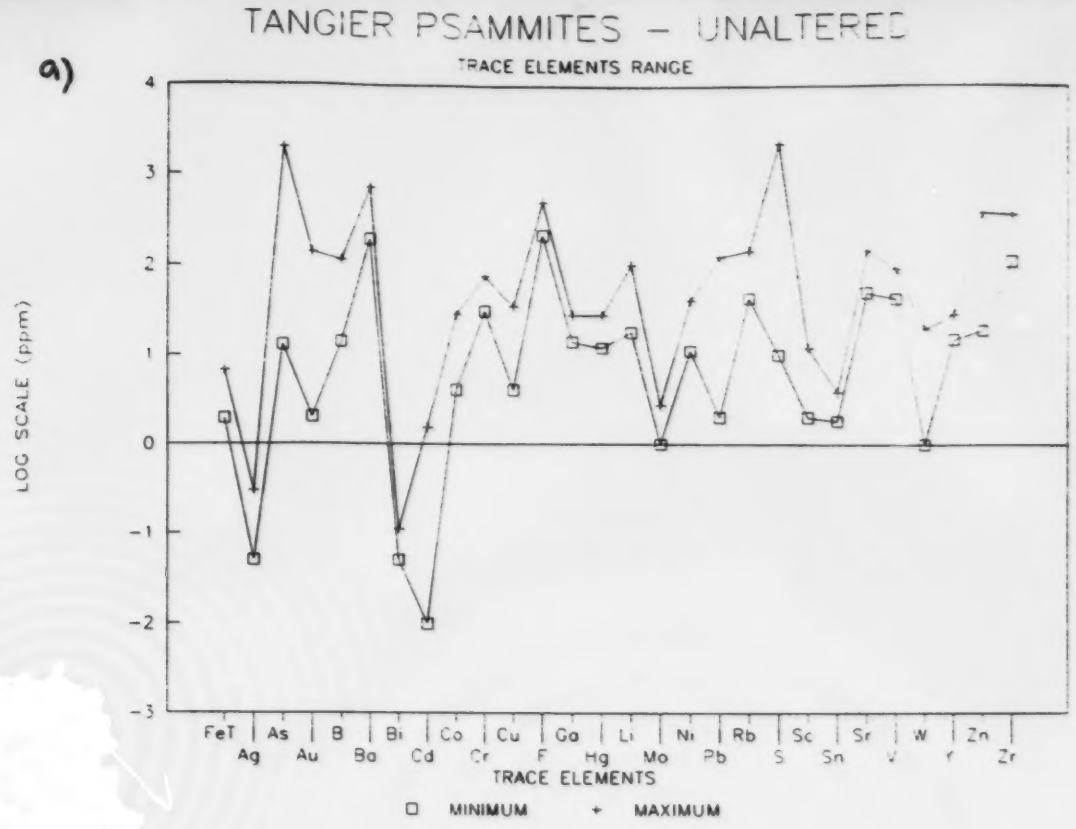

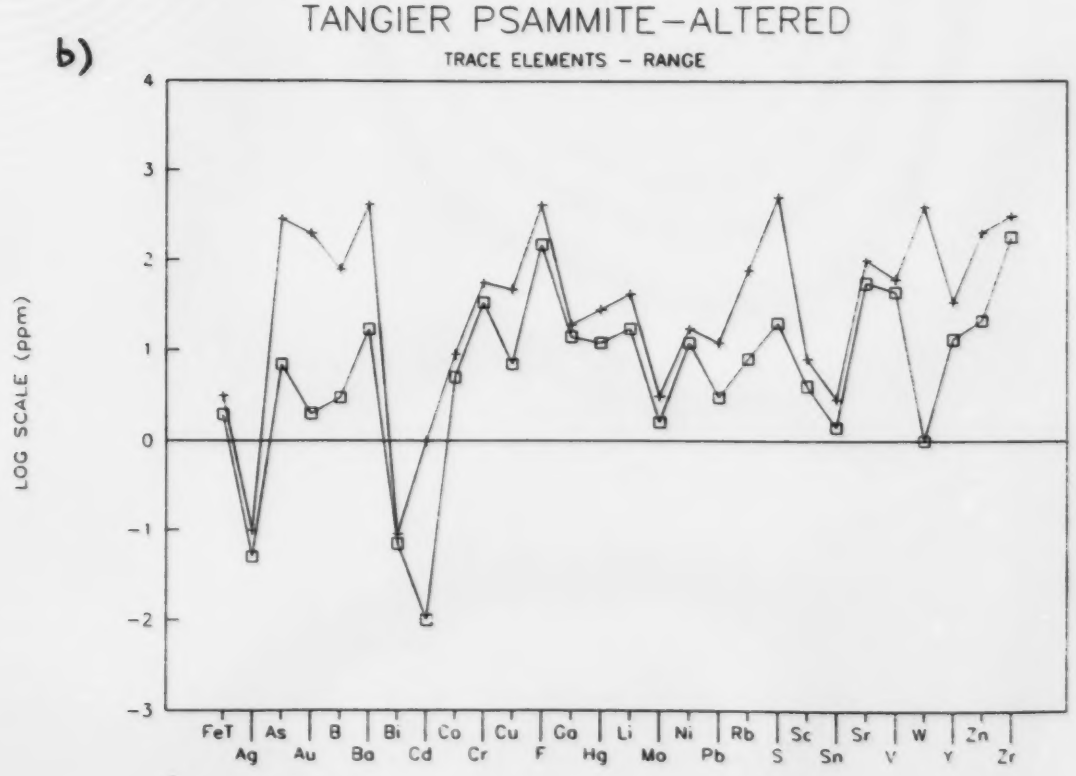

FIGURE 13a. Range in concentration of trace elements within unaltered psammites

b. Range in concentration of trace elements within altered psammites

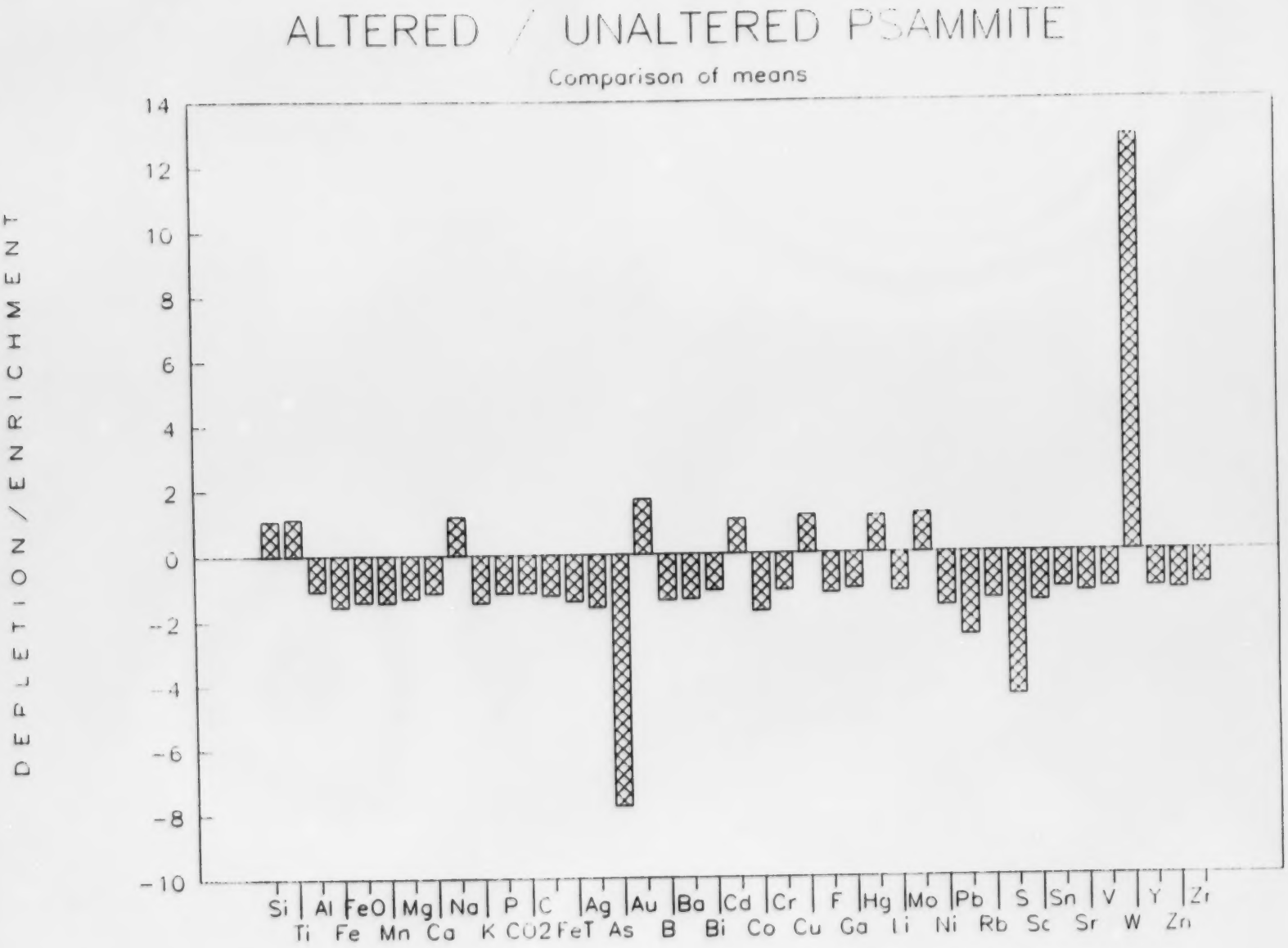

FIGURE 14. Bar diagram showing relative enrichment and depletion of major-oxide and trace element concentrations for unaltered psammite mean compared to the altered psammite mean.

15)

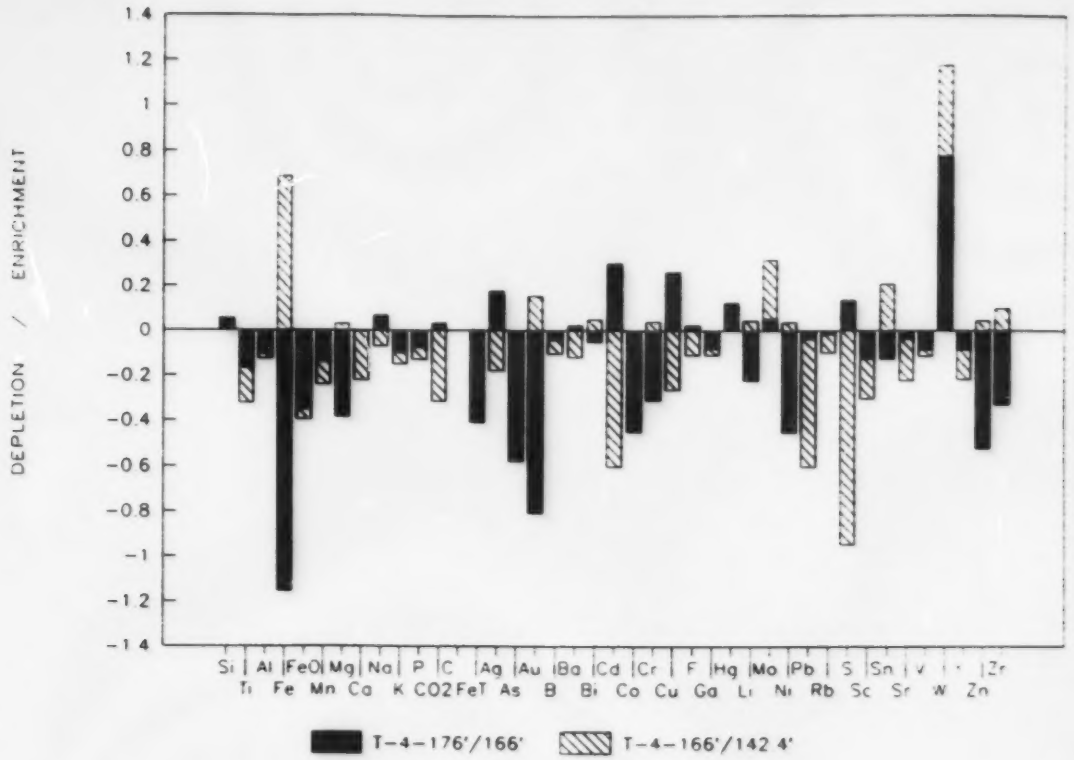

16)

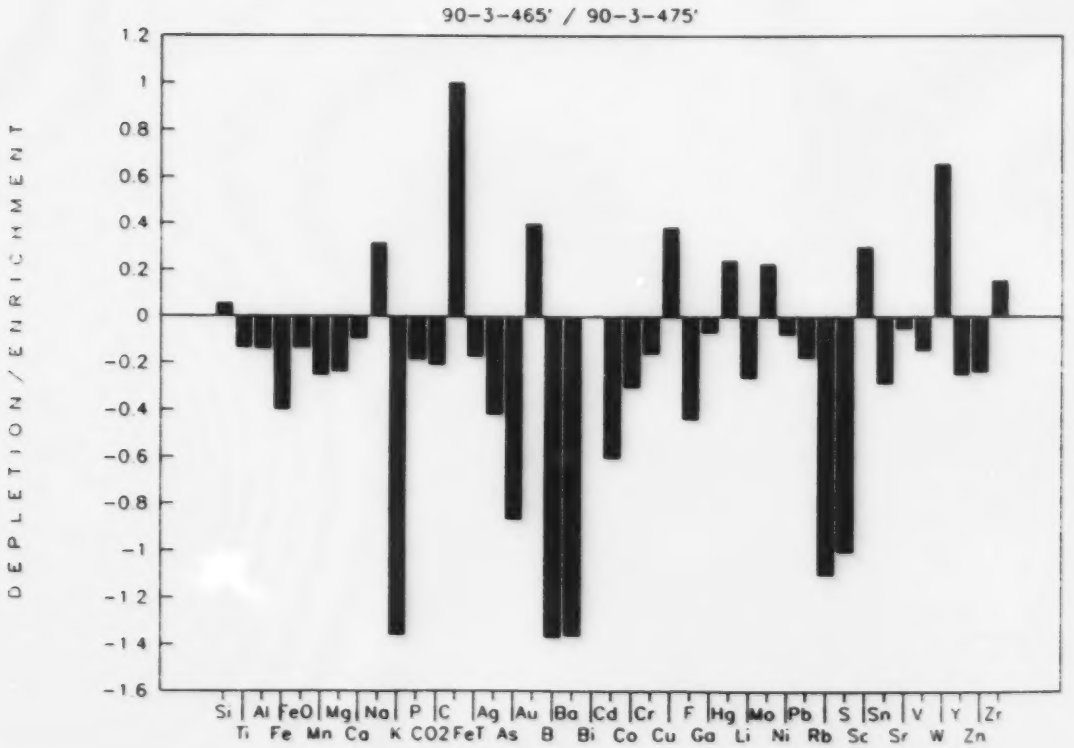

FIGURE 15. Bar diagram showing relative enrichment and depletion of major-oxide and trace element concentrations within psammite bed in response to progressive silicification.

FIGURE 16. Bar diagram showing relative enrichment and depletion of major-oxide and trace element concentrations in response to silicification.

17a, which reflects the relative geochemical difference between two psammites from the same stratigraphic location approximately 300m apart along strike and Figure 17b which compares two samples with a dip separation of approximately 30m. The former compares two unaltered psammites from below the Marker vein-pelite and shows for the most part only minor relative geochemical difference between the two samples. Exceptions are Cd, Co, Pb, Sc and Zn. Figure 17b which compares two silicified psammites from the same stratigraphic location, also shows only minor geochemical differences for the majority of elements. The most significant exceptions are Fe_2O_3, B, Pb and W. The strong enrichment in W in sample T3-102.5 is consistent with the W enrichment shown in other silicified samples. The above disparity, which is much less than that which occurs via alteration is thought to be attributed to stratigraphic variation rather than superimposed metasomatic modification.

6.1.2 Pelite:

Appendix A lists the basic statistics for all Tangier pelite samples. Figure 18 compares the mean oxide and trace element concentrations of Tangier, eastern Meguma Terrain (Douma, in prep) and Moose River pelites (Tuoquoy zone; Smith, unpublished data). Carbon (wt.%) is not included because it was not analyzed within the Moose River or E.M.T samples. With respect to the major oxides (Fig.18a), the three sample groups show little variation with the exception of lower MnO in the Tangier mean (.06 wt.% compared to .13wt.% for E.M.T.) and higher CaO (1.64 wt.% / Tangier = .91) and CO_2 (1.88 wt.% / Tangier = .97) in the Moose River pelite mean.

Average trace element concentrations (Fig.18b) which show significant variation include; As which is highest in the Tangier mean (576.11) ppm) and lowest in the E.M.T. (11.71 ppm), Au which is highest in the Moose River mean (102.5 ppb) and lowest (4.9 ppb) in the E.M.T. mean and Ba and W which are highest (1307.89 and 5.79 respectively) in the Tangier mean. The AKFM ternary plot (Fig. 10) shows the Tangier pelites correlate well with the field defined by Douma (in prep.) for pelites of the E.M.T.

The range in concentration of major oxides and trace elements within Tangier pelites is shown in Figure 19. Major oxides which display wide variability include MgO (max-4.27/min-.64), CaO (max-2.64/min-.42), Na_2O (max-2.9/min-.56), CO_2 (max-2.28/min-.07) and C (max-.57/min-.09). Most of this variation is likely attributed to the variable concentration of carbonate within the pelite. Trace element variability within the Tangier pelites is most extreme for As (max-5100/min-4), Au (max-34 ppb/min-2 ppb), Cu (max-75/min-4), F (max-1320/min-80), Pb (max-48/min-3), W (max-20/min-1), Ba (max-2400/min-460) and Zn (max-429/min-76).

Geochemical modification within pelites in response to metasomatic processes is evident from Figures 20a and 20b and listed in Table 4. The former compares an intensely silicified pelite (60 wt.% SiO_2) to that of a unsilicified pelite (47.7 wt.% SiO_2) located 10' below while the latter presents changes attributed to carbonization. As can be seen in Figure 20a, relative geochemical differences between the two samples include enrichment of; Au, Pb and Mo and depletion of As, W, Na_2O, C and CaO. The apparent antithetic relationship between Au and As is also reflected by silicification alteration trends within the psammites. The negative SiO_2 and W correlation however is opposite to that shown by the psammites.

Figure 20b presents geochemical changes derived through intense carbonization. At Tangier, this alteration process where most intense results in a friable, graphite-rich, black pelite which commonly shows evidence of intense deformation such as slickensides and a well developed cremulation cleavage

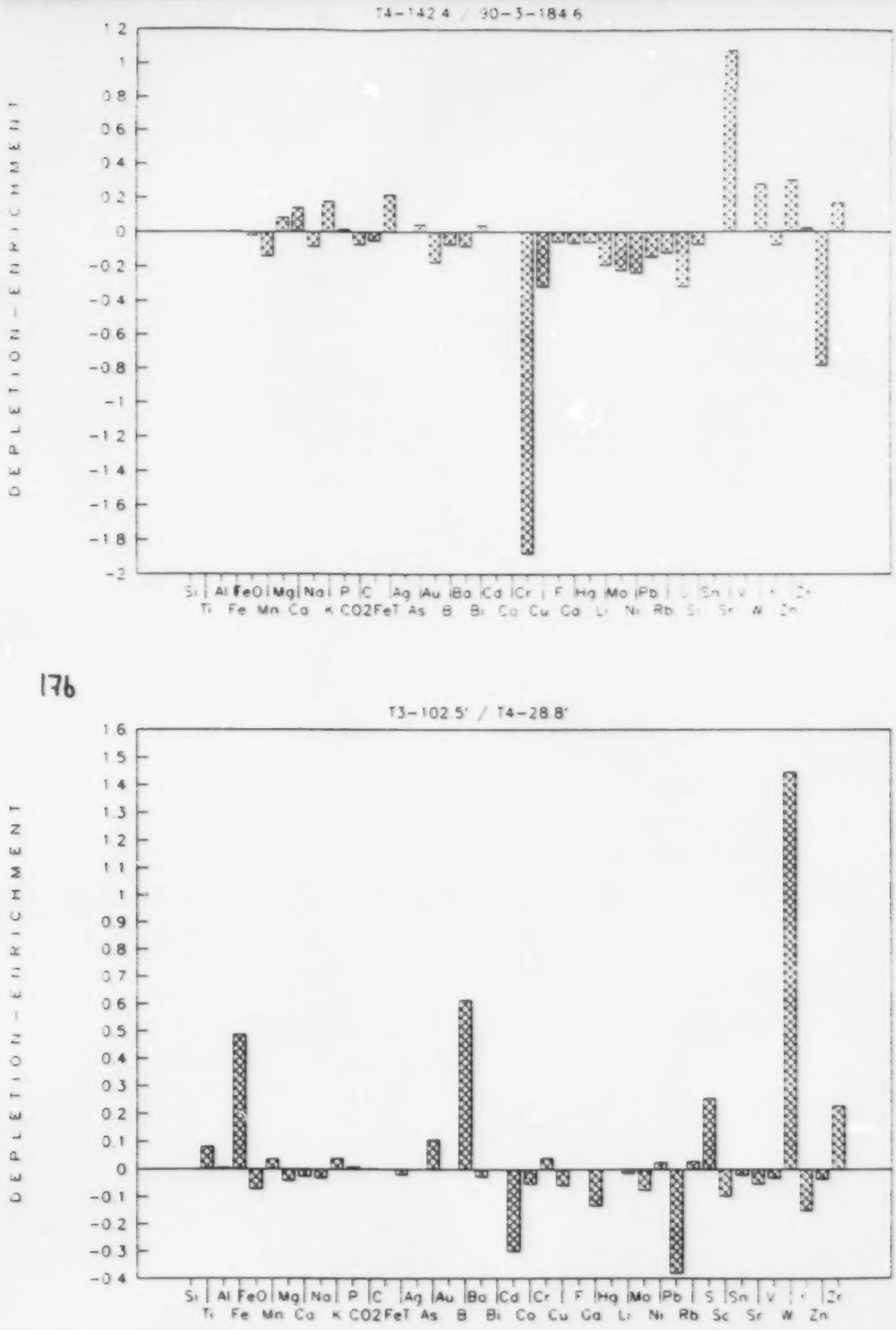

FIGURE 17a. Bar diagram showing relative enrichment and depletion of major-oxide and trace element concentrations in psammites at same stratigraphic level but separated horizontally.

b. Relative geochemical differences shown by stratigraphically separated psammites.

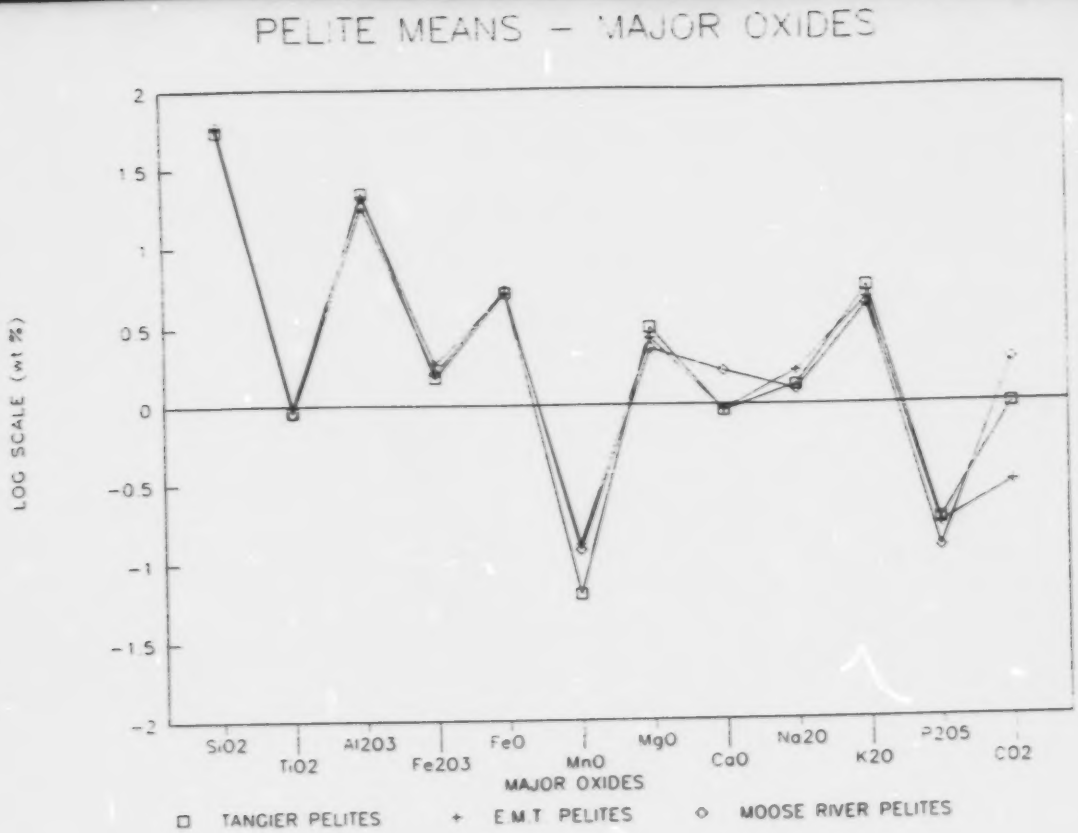

18b.

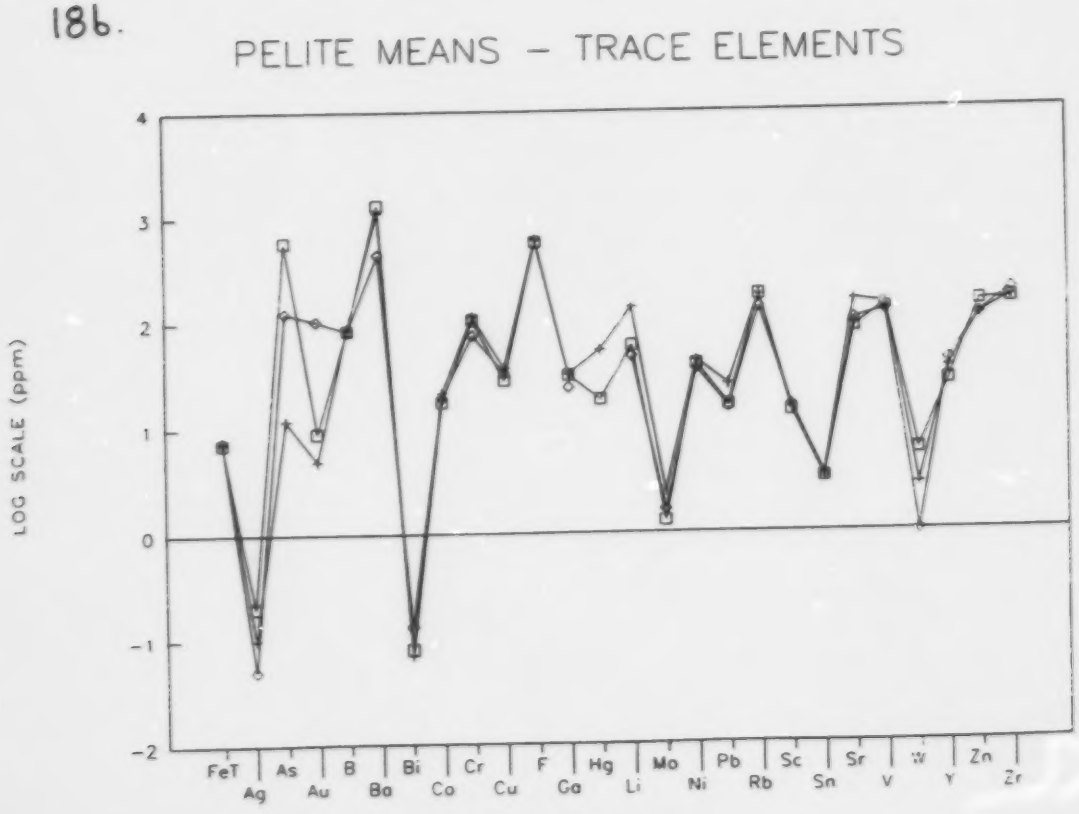

FIGURE 18a. Variation in average major-oxide concentrations for pelite sample groups

b. Variation in average trace element concentrations for pelite sample groups

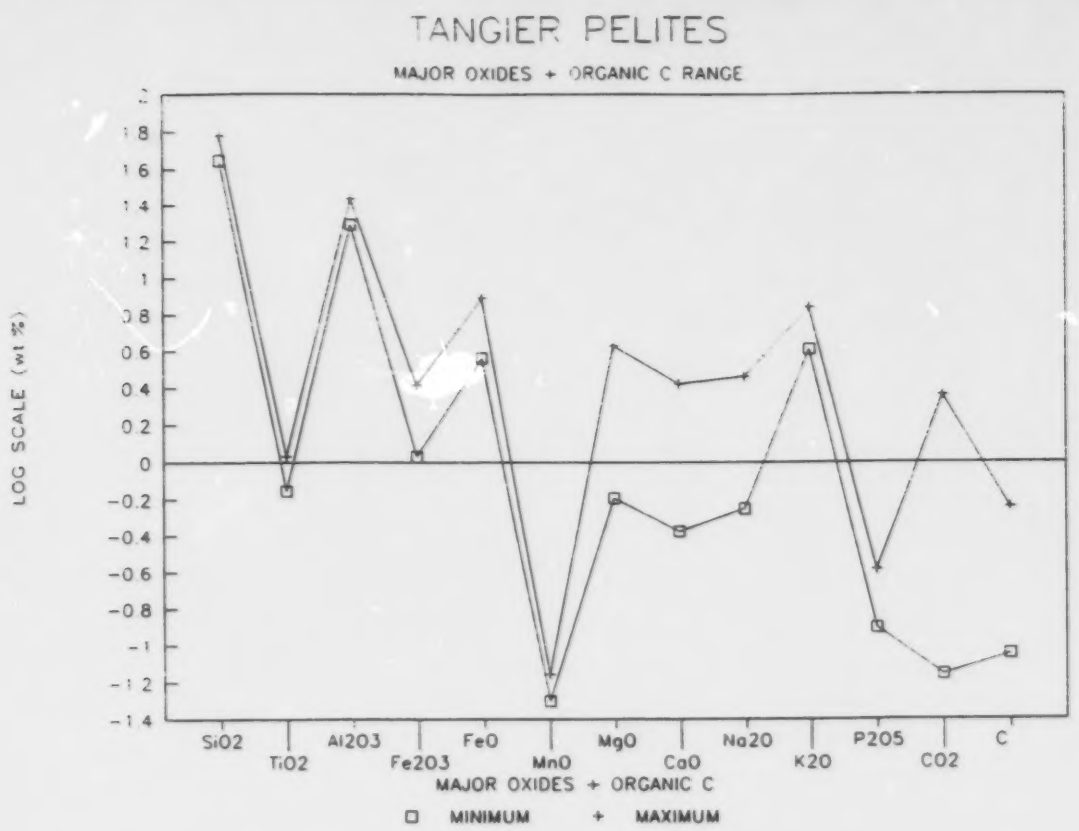

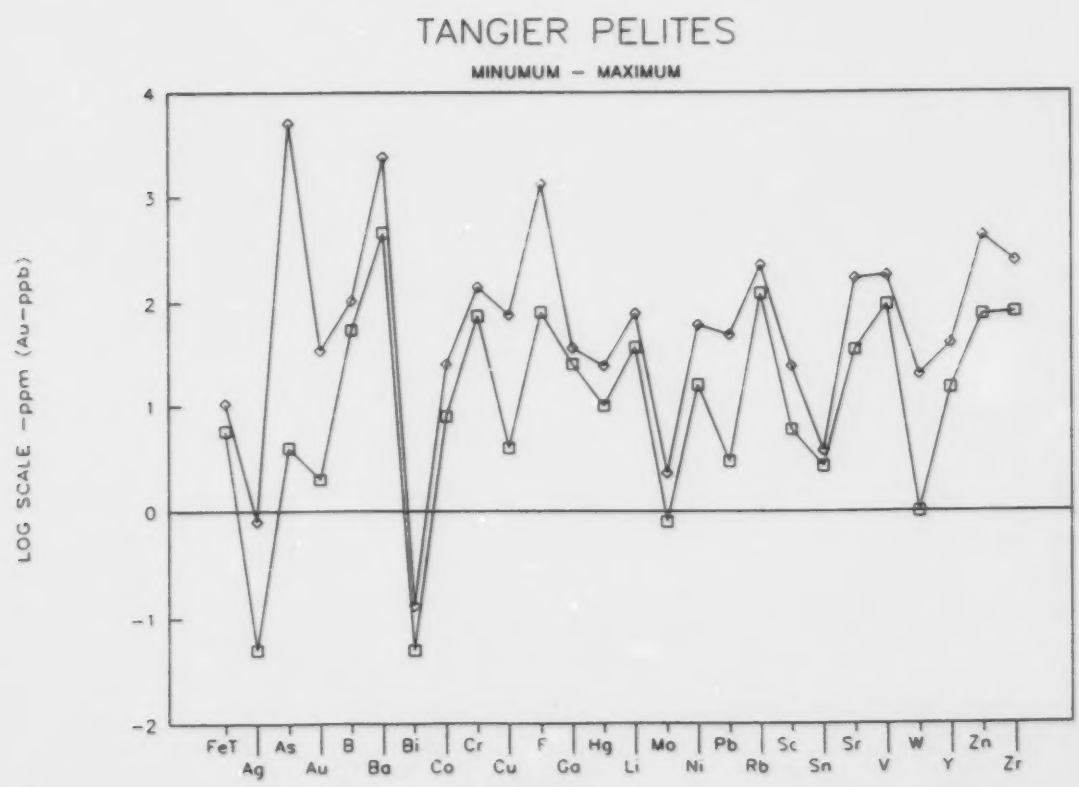

FIGURE 19a. Range in concentration of major-oxides in Tangier pelites

b. Range in concentration of trace elements in Tangier pelites

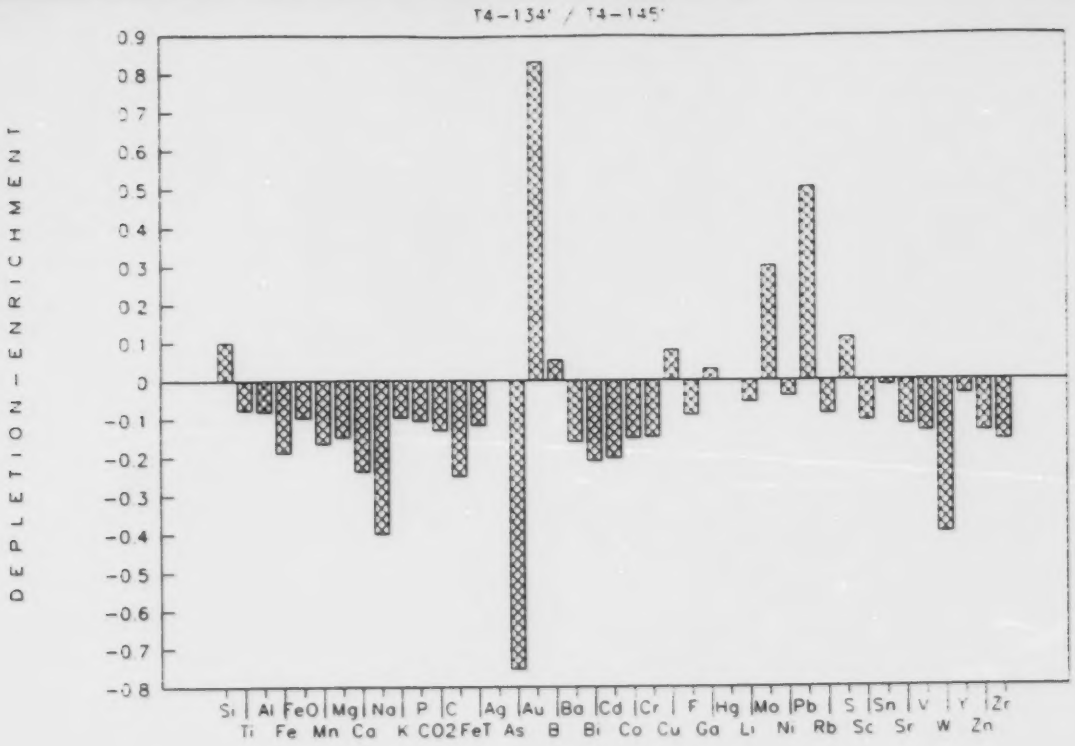

20b.

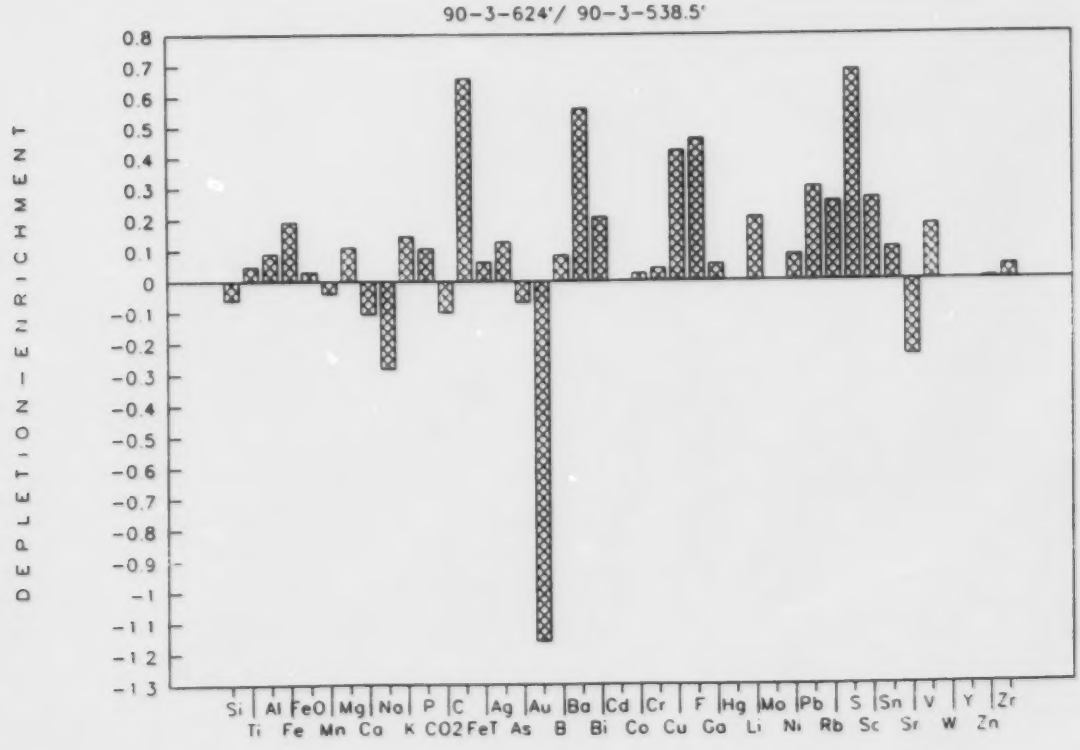

FIGURE 20a. Bar diagram showing relative enrichment and depletion of major-oxide and trace element concentrations in silicified pelite compared to unaltered pelite.

b. Bar diagram showing relative enrichment and depletion of major-oxide and trace element concentrations in pelite in response to carbonization.

(S_5). The carbonization process is characterized by relative enrichment of S, C, Ba, F and Cu accompanied by strong relative depletion of Au and minor Na_2O and Sr. The apparent negative correlation between C and Au is curious since gold-bearing quartz veins at Tangier occur within graphitic, black pelites.

6.1.3 Quartz Veins:

The relative geochemical differences between several types of quartz veins are illustrated in Figure 21 and listed in Table 4. Figure 21a compares the two vein samples most enriched in Au (3000 ppb / 313 ppb). The sample with 3000 ppb which contained visible gold in hand-sample (removed for analysis) was normalized to the 313 ppb sample which was barren. Significant geochemical differences between them include enrichment of Au, Cd, W and Zn with depletion of S, Pb, Cu, Co, B, As, Fe_2O_3, and Bi within the gold-bearing sample. Athough the apparent negative correlation between Au and As-Pb-Bi is surprising due to the common association of gold with galena, arsenopyrite and Bi-enrichment in many gold deposits (Smith and Kontak, 1987). However, the negative Au-As correlation is consistent with their relationship within the Tangier psammites.

The antithetic relationship between Au and As is also shown in Figure 21b which is a plot of the gold-enriched vein sample (3000 ppb) normalized to that of a low Au bearing sample (9 ppb). This comparison is characterized by significant Au and minor P_2O_5 and Ag enrichment along with relative depletion of As, Na_2O and Cu within the gold enriched sample. The minor relative enrichment of P_2O_5 in both figures may be attributed to the presence of apatite which can be a common accessory phase in the quartz veins.

To demonstrate geochemical variability within a specific quartz vein two samples from the Marker vein approximately 200 m apart were compared (Fig. 22). Also shown are the relative geochemical differences within pelite from each veins hanging-wall contact. The purpose of this comparison was to determine if intra-vein geochemical variation is a product of fluid-rock interaction with geochemical variable wall-rock or due to inherent geochemical heterogeneity within the veins. If there was significant fluid-infiltration or wall-rock assimilation the respective vein and wall-rock comparisons should reflect similar relative geochemical differences. Figure 22 shows the two vein samples differ most significantly with respect to Fe_2O_3, CaO, CO_2, Sr, Cu and Pb. A slight negative Au-As correlation is also apparent. With repect to the pelite comparison, similar trends are shown by F_2O_3, Sr, Cu and Pb; with CaO and CO_2 showing contrary behavior. The similar trends within both vein and wall rock suggests that either the pelite was altered by interaction with fluids attending quartz-veining or the quartz vein chemistry was influenced by assimilation of host-rock. The difference in the CaO and CO_2 reflects a higher concentration of carbonate within one of the pelites.

6.2 Mineral Chemistry:

As part of this study, the chemistry of chlorite and biotite phases were determined in order to characterize the nature of the fluid phase attending their crystallization. These mineral phases were selected because they display several different habits and occur in both quartz veins and host-rock at Tangier. Oxide concentrations and cation proportions for the mineral phases are listed in Appendix B. All analyses were determined using the Jeol 733 electron microprobe - Link system located at Dalhousie University.

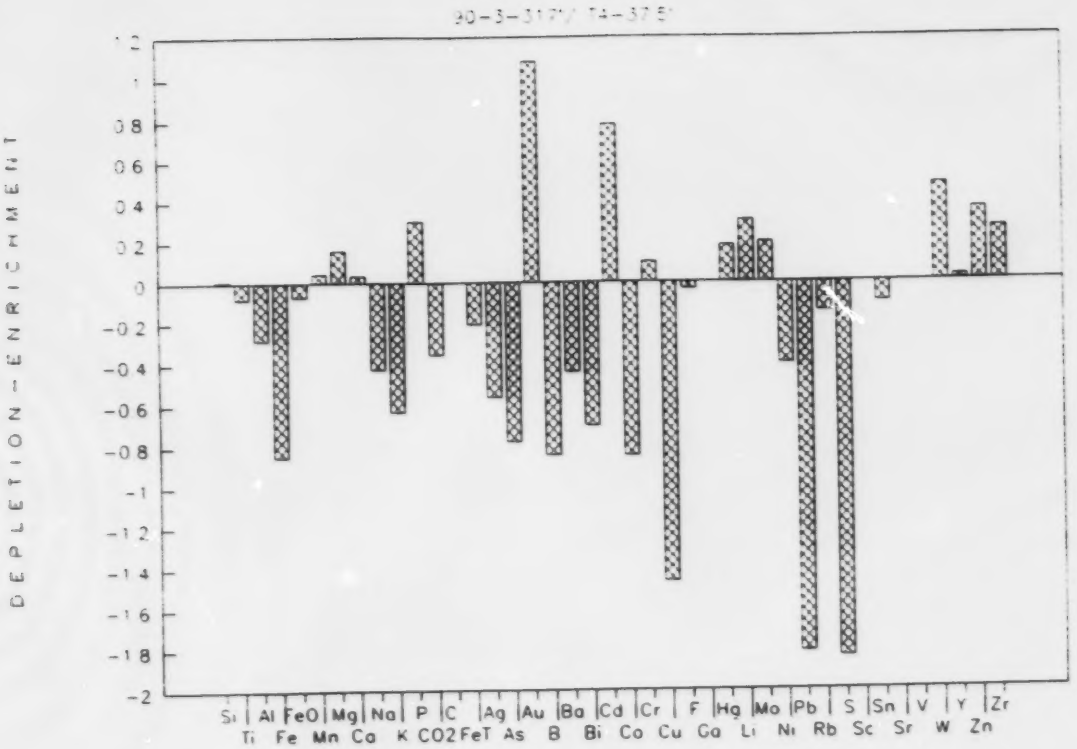

21b

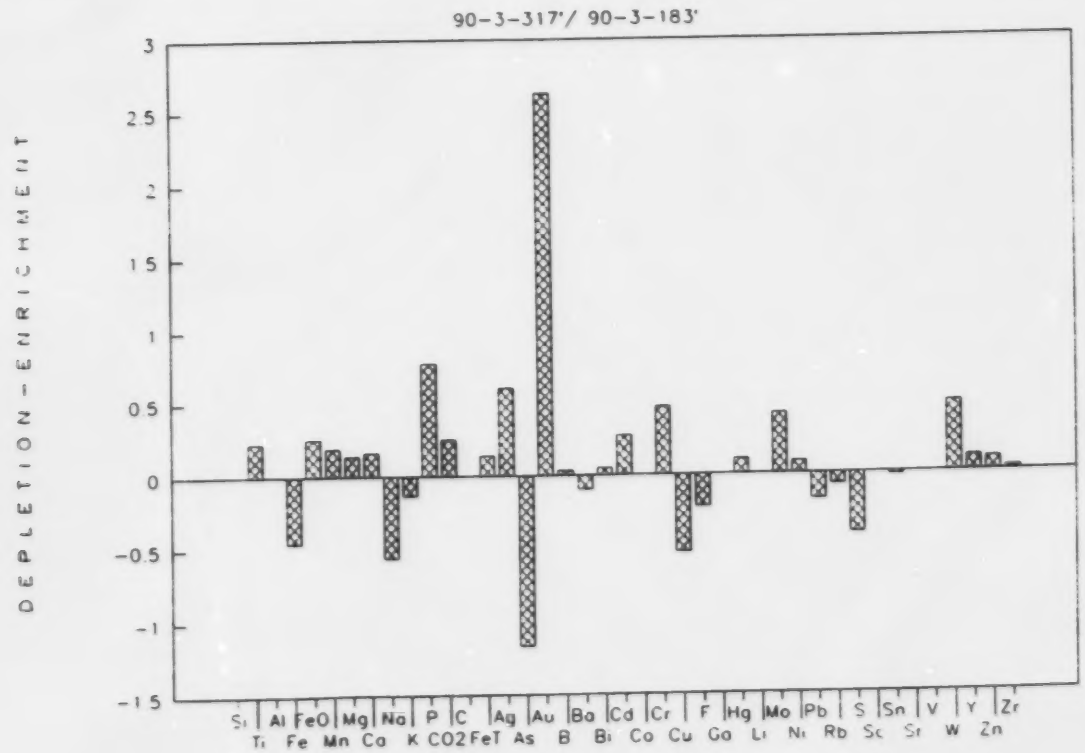

FIGURE 21a. Bar diagram showing relative differences of major-oxide and trace element concentrations between two gold-enriched quartz veins.

b. Bar diagram showing relative enrichment and depletion of major-oxide and trace element concentrations in gold-bearing quartz vein compared to barren quartz vein.

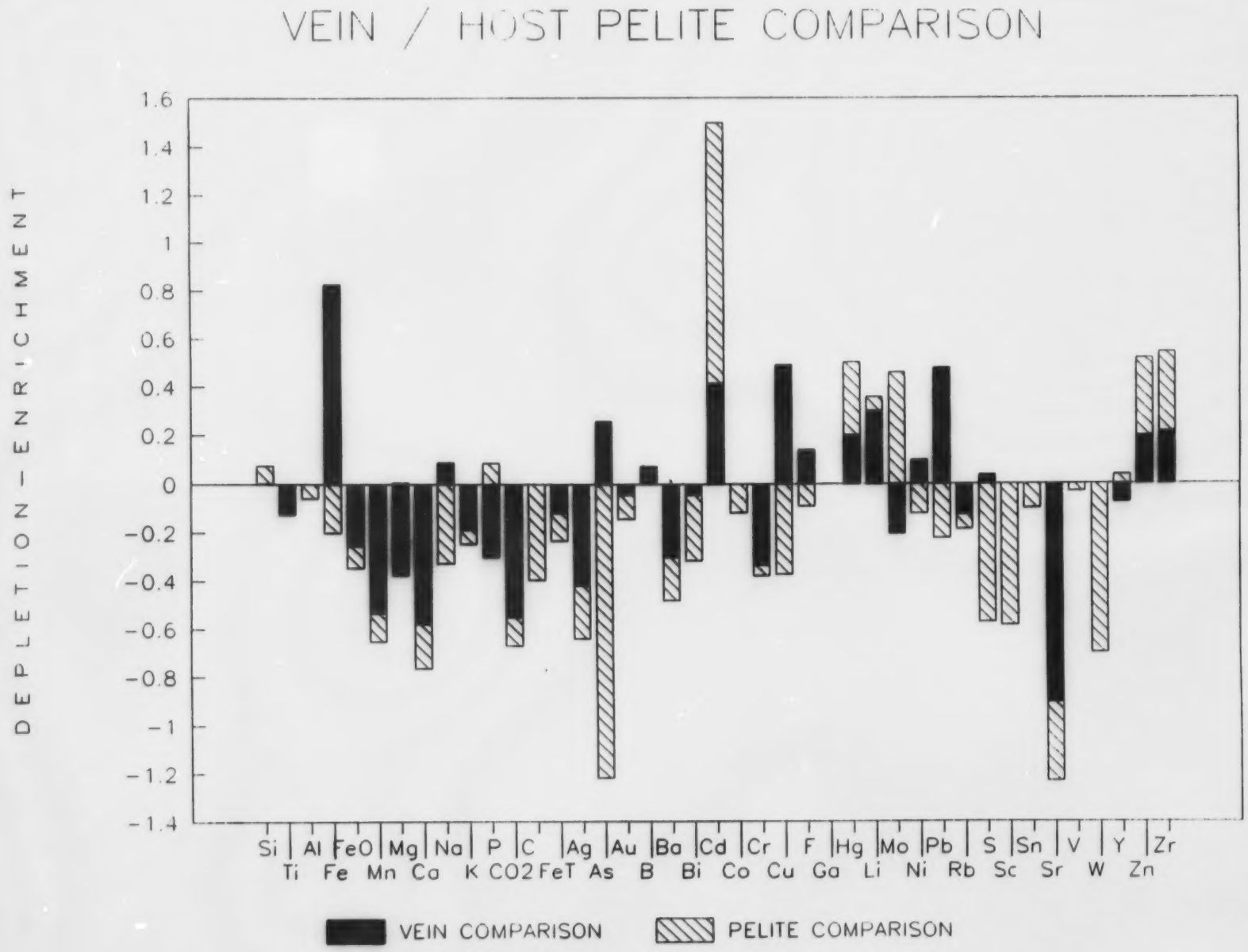

FIGURE 22. Bar diagram comparing the relative geochemical differences of the vein samples in Fig.21 to their respective pelite host rocks.

6.2.1 Biotite

This mineral phase is not common at Tangier. All textural types of biotite (rounded grains, flakes) invariably show some degree of chloritization.

The Al^{iv}, Fe/(Fe+Mg) and Fe/(Fe+Mg), Ti binary plots (Figs. 23a,b) show the biotites to have a restricted Fe/(Fe+Mg) range of .58 -.61, a Al^{iv} range of 2.16 - 2.46 and a Ti range of .204 -.266. No distinction can be made between the two textural types.

Compared to biotites within biotite-zone E.M.T. samples analysed by Douma (in prep.), the Tangier biotites contain lower Al^{iv} but comparable Fe/(Fe+Mg) and Ti. Compared to biotites from chlorite-zone psammites analysed by Douma the Tangier biotites contain less Ti and Fe/(Fe+Mg) but comparable Al^{iv}. They also contain slightly more Fe/(Fe+Mg) than vein and wall-rock biotites from the Beaverdam Au deposit which range from .47 to .57. The Beaverdam deposit is in part hosted by biotite-grade metasediments (Kontak and Smith, 1988b).

6.2.2 Chlorite

Three distinct textural types of this mineral were observed: 1) rounded and oriented metamorphic porphyroblasts within psammites and pelites, 2) large euhedral laths and 3)irregular "wormy" aggregates within quartz veins and quartz-carbonate flooded shear zones and angular veins. The latter most likely owe their presence to hydrothermal processes. Pervasive chloritization of biotite suggests that some of the chlorite may represent completely chloritized biotite and or possibly retrograde biotite.

Figure 24a displays the composition of the three textural types based on the classification of Hey (1954). Except for a few samples from each group, the textural types show two distinct fields. The psammite-hosted chlorite porphyroblasts cluster just within the Fe-enriched side of the ripidolite field whereas quartz-vein hosted hydrothermal chlorite laths and wormy aggregates plot within the pychnoclore field. The composition of the Tangier porphyroblasts is comparable to that for chlorites from biotite and chlorite zone metasediments (Douma, in prep). The distinct composition of vein and wall rock chlorites at Tangier suggests that the two types were derived from chemically different fluids. Distinct compositional differences are also reflected by chlorites (and biotites) at other Meguma-hosted Au deposits (Kontak and Smith, 1988a; Kontak, pers. comm).

Based on the composition of the chlorites their approximate temperatures of crystallization can be estimated (Jowett, 1991). The calculated temperatures for the Tangier chlorites (Fig. 24b) show a temperature range of 376.6 - 254.3 °C. Average temperatures are 357.2° for the porphyroblasts, 302.3° for the laths and 275.9° for the 'worms'. These temperatures are consistent with the 300$\pm$ 50°C range estimated by Kontak and Smith (1990) using fluid inclusions and geothermometry for formation of similar minerals in other Meguma gold deposits.

6.2.3 Other minerals

Preliminary analysis of pyrrhotite (Appendix B) indicate the presence of at least two compositionally distinct types within the quartz veins. These particular samples differ with respect to Fe_2O_3, Ag, Bi, Cu and Pb. More study is warranted to determine if there is any correlation with pyrrhotite composition and texture to gold mineralization.

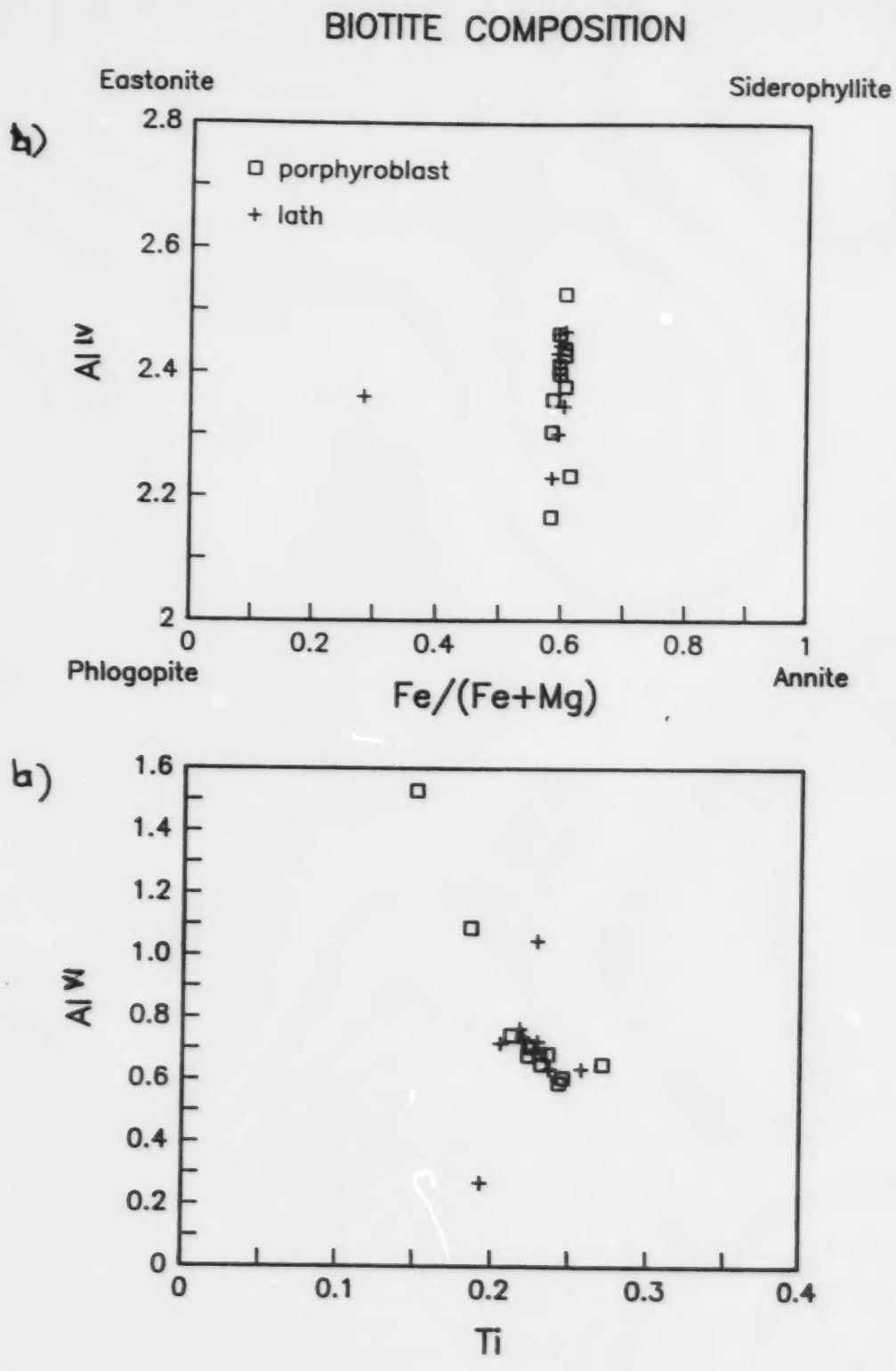

FIGURE 23a. Al^{IV} - Fe/(Fe+Mg) binary plot of biotites from Tangier rock samples with superimposed fields for biotites from Douma (in prep.).

b. Fe/(Fe+Mg) - Ti binary plot of biotites from Tangier rock samples with superimposed fields for biotites from Douma (in prep.)

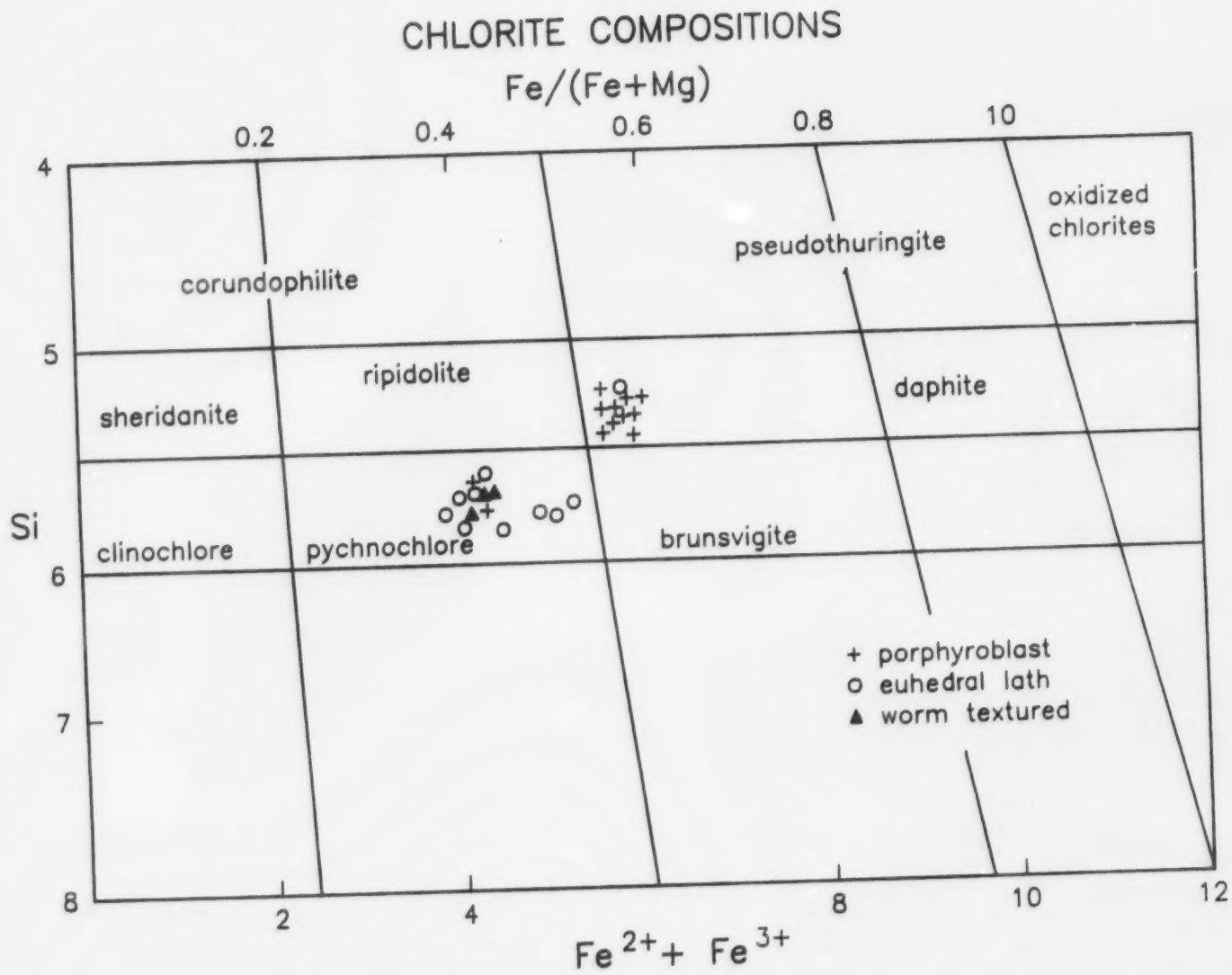

FIGURE 24a. Hey (1954) diagram showing composition of Tangier chlorites.

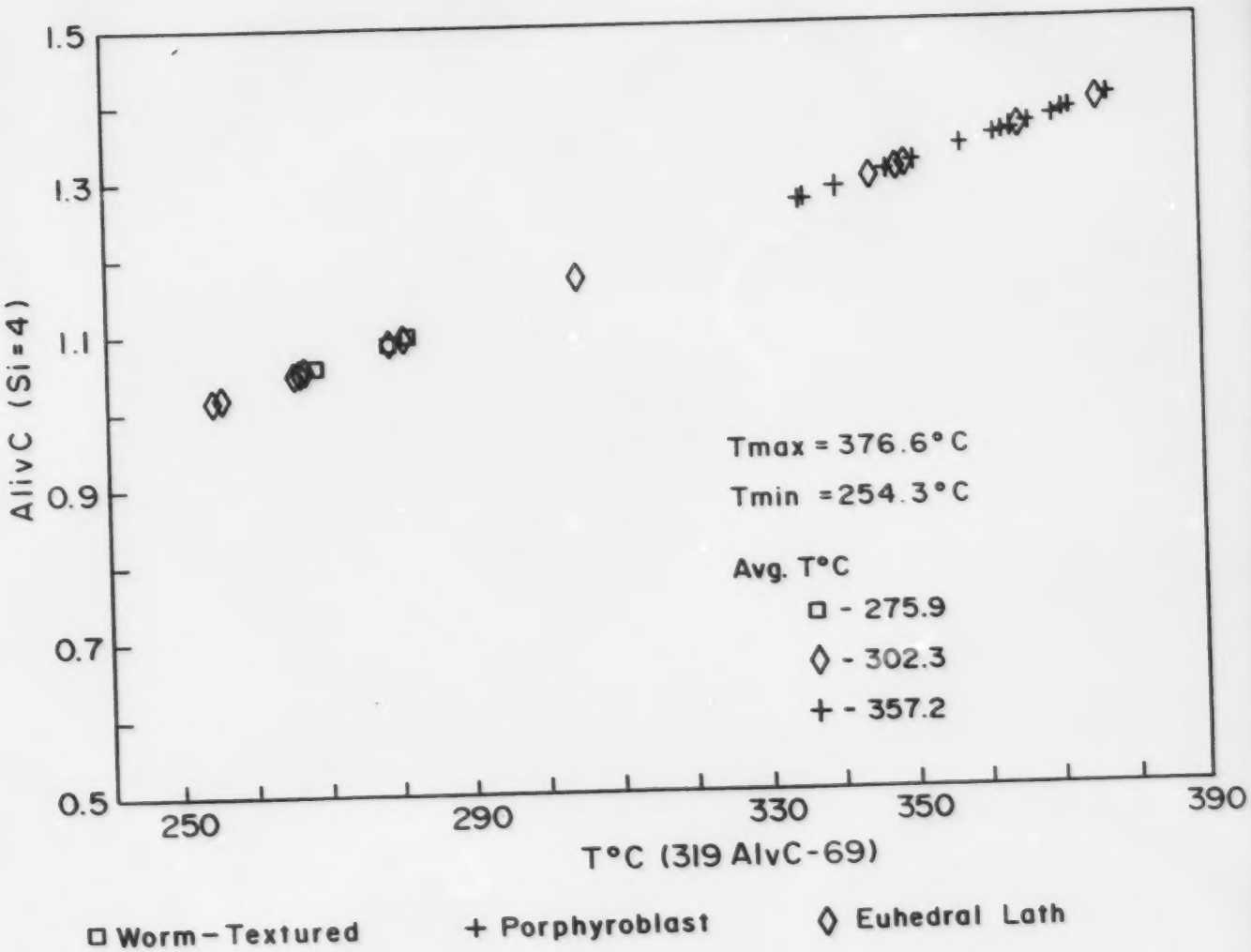

FIGURE 24b. Crystallization temperature estimates for Tangier chlorites after Jowett (1991).

7. STRUCTURE AND DEFORMATION

The Tangier Au deposit displays many of the deformation features documented from other Au deposits within the eastern Meguma Terrain. Table 5 below, lists the deformational events which occurred at Tangier and how they are manifested. It is important to note that occurrence of these features is often intermittant and of variable intensity.

Observations at Tangier indicate that the bedding parallel quartz veins often display intermittant folding and deformation. Features such as secondary folds, boudins, slickensided wall rock, recrystallized and undulose extinction of quartz grains, and brecciated and/or crenulated wall rock inclusions indicate a complicated deformational history (Plates 17a-g). Although all veins are folded to some degree, such a feature may not be characteristic of the particular vein. In some however, folds are very common and may be used as a character trait with which to reliably identify a particular vein package (e.g. Whin and Nugget veins; Plates 14 and 16). Observations by Coxheath geologists of drill core and underground mapping indicate that the folds have a 12° to 15° plunge to the west, with the fold axis generally parallel to the anticlinal axis (Plate 18). These minor folds were also noted to have an overall down-dip extension at 45°.

Coxheath geologists also report that the veins are generally more deformed in the area of the fold hinge than on the limbs (Forgeron *et al.*, 1988). This observation has also been documented on a regional scale within the eastern Meguma Terrain by Williams and Hy (1990). In the area of recent N.S.D.M.E. drilling close to the fold hinge (TAN90-1) it appears that the bedding parallel veins do not continue over the hinge but instead are pinched-out at some unknown distance down dip. This is consistent with Coxheath drilling near the hinge approximately 200m further east which indicates that although the veins occur on the north side of the axis they are intensely folded and pinched or absent at the hinge. Coxheath geologists attributed this observation to compression along the fold axis.

Boudinaged veins are also frequently seen where the results are dramatic pinch and swell textures (Plate 19). For example, the Marker which has the best developed boudins varies from 35-25-60-20-35-60 cm over 30m of exposure in a sub-drift close to surface. Sangster (1990) describes the boudins as the "chocolate-tablet type" since they extend along strike and down-dip. Coxheath geologists report one set of boudins strike 15°N with a 12°-15° plunge with the second set having a near vertical to slightly east trending orientation. The boudin necks where the vein is pinched often contains massive coarse crystalline quartz with associated with chorite and carbonate. These 'blows' of quartz are thought to represent both en echelon type extensional veins and recrystallized quartz. This would account for the fact that the quartz blows often extend slightly into the wall rock.

7.1 Faults and Shear Zones

There is ample evidence of late stage faulting and shearing (S_5) within the Tangier deposit. Most obvious are the presence of numerous sub-vertical, N-W trending, narrow (< 1m) brittle-ductile faults. They are characterized by intense shearing and or brecciation of wall rock and massive quartz-carbonate-+chlorite deposition within the fault zone (Plate 20a-c). The faults cross-cut and commonly displace both stratigraphy and statabound quartz veins. Where a fault intersects a quartz vein, the vein may be displaced and or dramatically reduced in thickness as shown by the Marker vein in Plate 21 which reflects dip-slip faulting.

Table 5. Deformation and cleavage development at Tangier.

Deformation/cleavage	Evidence	Comments
D_1-S_1	not observed	
D_2-S_2	- reflected by matrix-groundmass muscovite laths and chlorite - slaty cleavage in pelites and pressure solution cleavage in psammite - oriented quartz-carbonate stringers	- overprinted by well developed penetrative D_4 shear cleavage - intermittant - not well preserved
D_3-S_3	- coarse biotite foliation in semi-pelite bands? and oriented chlorite porphyroblasts	- controlled by lithology - intermittant - not well perserved
D_4-S_4	- aligned chlorite/carbonate/ sulphides crystals overprinting D_2 mineralogy - minor folds in quartz veins - quartz-carbonate stringers oriented parallel to S_4 cleavage	- near vertical axial plane - mimicks S_2 regional fold orientation in many cases - present in all rock-types
D_5-S_5	- crenulation cleavage in pelites - slickensides - boudinaged stratabound quartz veins - crenulated stylolites and wall rock in stratabound quartz veins - ductile/brittle shear-fault zones - quartz-carbonate brecciated wall rock and quartz veins - crenulated and kinked sulphides - apparent kinked stratigraphy north of F.A. and also on south limb as suggested by variable bedding orientations.	- slickensides, and boudins display subhorizontal plunge similar to that of anticline

Although brittle faults predominate, rare, narrow ductile shear zones also occur as shown in Plate 22a. This particular shear zone located east of the portal is characterized by a 1cm wide quartz-carbonate+chlorite vein within a 2cm. wide chlorite-rich ultramylonite which contains 1mm ribbons of pyrite (Plate 22b). Displacement along the faults is normally minor (<3m) and sinistral in nature, however there is evidence of dextral movement and locally substantial offset. For example, Coxheath geologists report a total of 17.5m of sinistral displacement over approximately 160m of strike length near the western limit of underground development (see Fig. 2) based on the relative position of the Forrest vein in a series of underground drill holes. This of course assumes that the vein was entirely stratabound.

In contrast, in the eastern half of the underground workings dextral faulting predominates with displacements of 20cm to 3m recorded. These faults are all northwest trending, and sub-vertical and contain a 0.5cm to 50cm (generally 25cm) wide quartz-carbonate-pyrite+pyrrhotite fissure vein. The apparent local spatial segregation of dextral and sinistral faults has also been documented regionally by Williams and Hy (1990) in the eastern Meguma Terrane. Faulting is also commonly associated with abundant, similarly oriented, narrow ($\leq$ 1cm) quartz+carbonate angular veins which may display minor displacement of several centimeters (Plate 23).

Shearing within the pelites is reflected by the development of slickensides and creulation cleavage (S_5; Plate 24). Slickensides often occur within extremely graphitic and friable pelite associated with bedding parallel quartz veins as wall rock or included fragments, and have a 12°- 15° plunge parallel to that of the anticline. Crenulation cleavage is present as narrow ($<$ 1cm) wide zones which penetrate the rock.

While the occurrence of vertical to sub-vertical tension gashes and sub-horizontal slickensides indicate that strike-slip faulting occurred, the sub-vertical displacement associated with some quartz-carbonate veins indicates that dip-slip movement also occurred. Dip-slip displacement is also suggested by the N.S.D.M.E. drilling in which the stratigraphy appears to be offset vertically approximately 30m between two drill holes. However, the possibility of a fold or kink in the stratigraphy cannot be discounted, as such features have been suggested by Coxheath geologists based on bedding orientations observed in drill core and underground mapping to the east. (Forgeron, pers.comm).

8. LOCALIZATION OF GOLD

As mentioned above, free native gold occurs as small ($<<$ 1mm) to very large (6x2x5cm) nuggets in massive milky quartz (Plate 12j) portions of bedding parallel quartz veins. There does not appear to be a correlation between the occurrence of gold with either the number of quartz veins present within a particular zone or the thickness of an individual quartz vein. Gold does however appear to show a preference with the hanging wall vein in zones of multiple quartz veins or to the the hanging wall portion of a single bedding parallel vein adjacent to the pelite contact. The gold is commonly associated with galena, pyrrhotite and arsenopyrite. The close association of gold and galena has been observed at other Meguma-type gold deposits (Smith, pers comm., 1991). The paragenetic sequence of the various sulphides observed within the Tangier samples is presented in Table 6. As shown in the table, arsenopyrite has the widest range of crystallization followed by chalcopyrite and pyrrhotite. Galena, sphalerite and gold appear to have crystallized at roughly the same period. The stages listed do not represent well-defined mineralizing events but instead reflect petrographic evidence indicating three distinct periods of sulphide growth.

Another preferred location for visible gold appears to be proximal to minor folds or rolls within the bedding parallel stratabound quartz veins. Coxheath geologists report many instances of gold concentrated or occurring within a fold crest or limb. Particularly good examples occur within the Marker and Twin veins exposed in sub-drifts on the 50m level. As mentioned above these folds appear to plunge 12° - 15° to the west, sympathetic to that of the anticline. Evidence of syndeformation gold is provided by the occurrence of crenulated gold within S_3 - S_4 deformed pelite at the contact with a BP quartz vein. Coxheath geologists also report several instances of gold enrichment proximal to northwest brittle-ductile faults and other D_5 structures which post-date quartz vein development and gold mineralization. These features suggest that although a 370 ca. period of gold deposition is suggested by

TABLE 6. Sulphide paragenetic sequence.

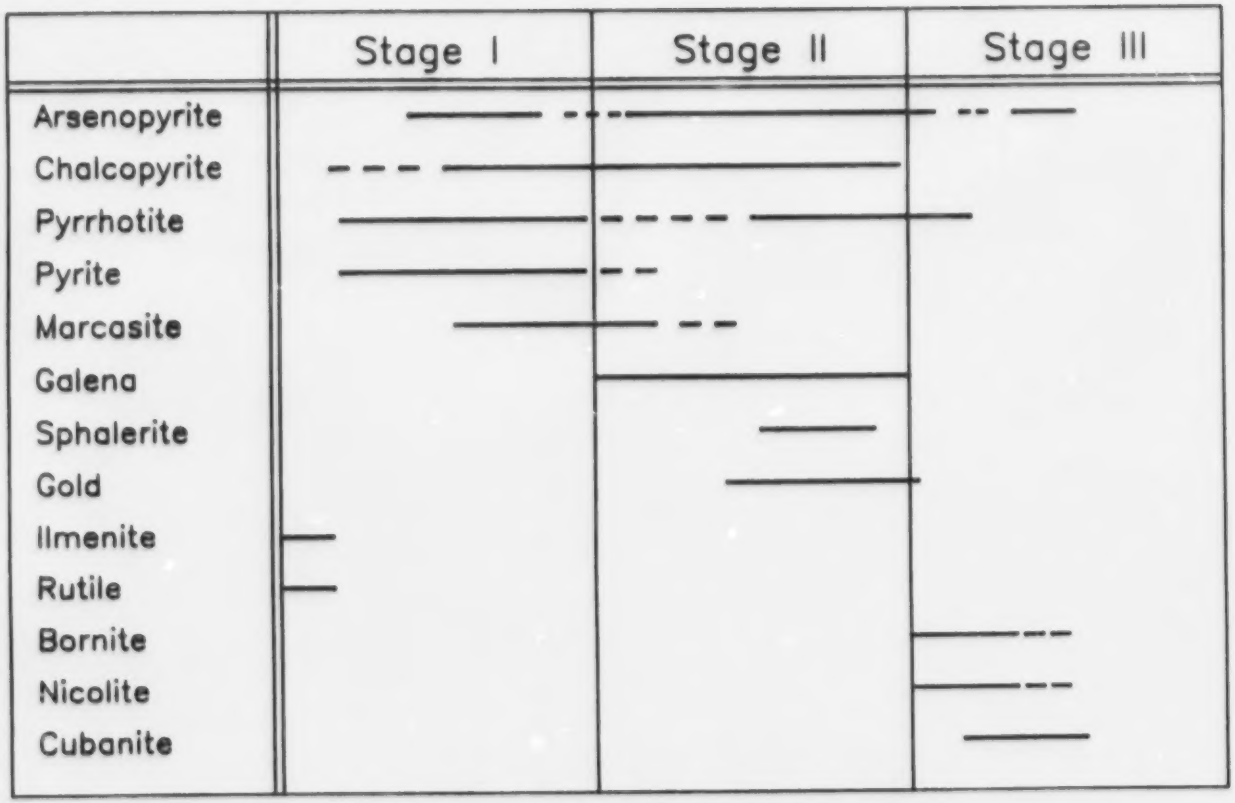

(after P.K.Smith; unpublished data)

its occurence within structurally late sites the case against remobilized, syngenetic gold cannot be discounted.

As mentioned above gold enrichment is also apparent associated with the quartz-carbonate angulars. Examples include a zone of intense quartz-carbonate veining near the base of the Marker psammite which was intersected in two adjacent holes approximately 50m below the North decline in a area of sinistral faulting. The histogram in Figure 25 shows that the quartz-carbonate angular veins associated with gold enrichment have orientations similar to quartz-carbonate angulars throughout the deposit. As reported by Coxheath, these zones returned 1.46 ppm Au over 13m and 5.3 ppm over 6-8m. In addition, recent drilling by N.S.D.M.E. encountered finely disseminated native gold intimately associated with galena, pyrrhotite, arsenopyrite and pyrite in sub-vertical quartz-carbonate stringers. These are hosted by intercalated black pelite and psammite which show intense shear deformation (Plates 25a-f). The gold is attached to pyrrhotite which is oriented parallel to the veins and is also intergrown with galena which infills D_5-fractures within large, euhedral arsenopyrite crystals.

Perhaps the most important structural feature regarding localization of gold at Tangier are the presence of 'jump-overs'. A 'jump-over' is characterized by a series of small angulars which range in width from 1mm - 10mm and cross from one bedding parallel vein to another. The "jump-over" sequence in Figure 26 occurs within the Whin zone near the fold hinge and consists of 5 narrow angular veins which jump up stratigraphy from a series of folded footwall B.P. veins in a 20cm pelite across a psammite bed into a narrow folded B.P. veins within a 20cm wide foot wall pelite bed. The point of jump-over also marks the beginning of the hanging wall vein. It is important to note that the point of exit of the jump-over veins into the hanging wall vein is marked by an increase in visible gold. At the time of mining and development (May, 1989) three confirmed "jump-overs" were documented within the Whin zone; two of which are associated with dramatic gold enrichment from 6-8 g/tonne to 24-30 g/tonne over a mining width (1.5m) immediately after the 'jump-over' (Coxheath, 1989). These "jump-overs" were mapped as striking 36° southwest relative to the Whin vein (74°) and plunging 45° west within the plane of the vein. These structures are thought to form within a shear zone (D_5 ?) which in the case of Figure 26 reflects sinistral movement. Although not confirmed, other similar structures occur; the extensions of which may delineate similar 'ore shoots' in other veins at Tangier. The process whereby some 'jump-overs' are sites of considerable gold enrichment while others are not is unknown.

9. DISCUSSION

Stratabound, bedding parallel quartz veins are the primary site of free, nuggets of gold within the Tangier deposit. These veins can display radical textural changes both along strike and with depth. Examples are the Nugget vein which ranges from massive en echelon tension-gap veins to a typical bedding-parallel vein which varies in thickness; and the Marker vein which is normally a wide crack-seal textured vein splits into two veins in the western portion of the deposit. In addition, bedding parallel veins pinch and swell with depth and along strike, in some cases pinching out entirely as observed within the Whin, Twin and Nugget veins. These variations likely reflect variable degrees of faulting and shearing within the mine. Another characteristic of these veins is that they appear to thicken within the westernmost undergound workings and also with depth. These thickening is coincident with overall stratigraphic thickening and may be related to compression of strata proximal to the anticlinal axis.

The occurrence of micron-sized, disseminated gold associated with galena, pyrrhotite and arsenopyrite within carbonatized psammite has important economic implications. Similar zones,

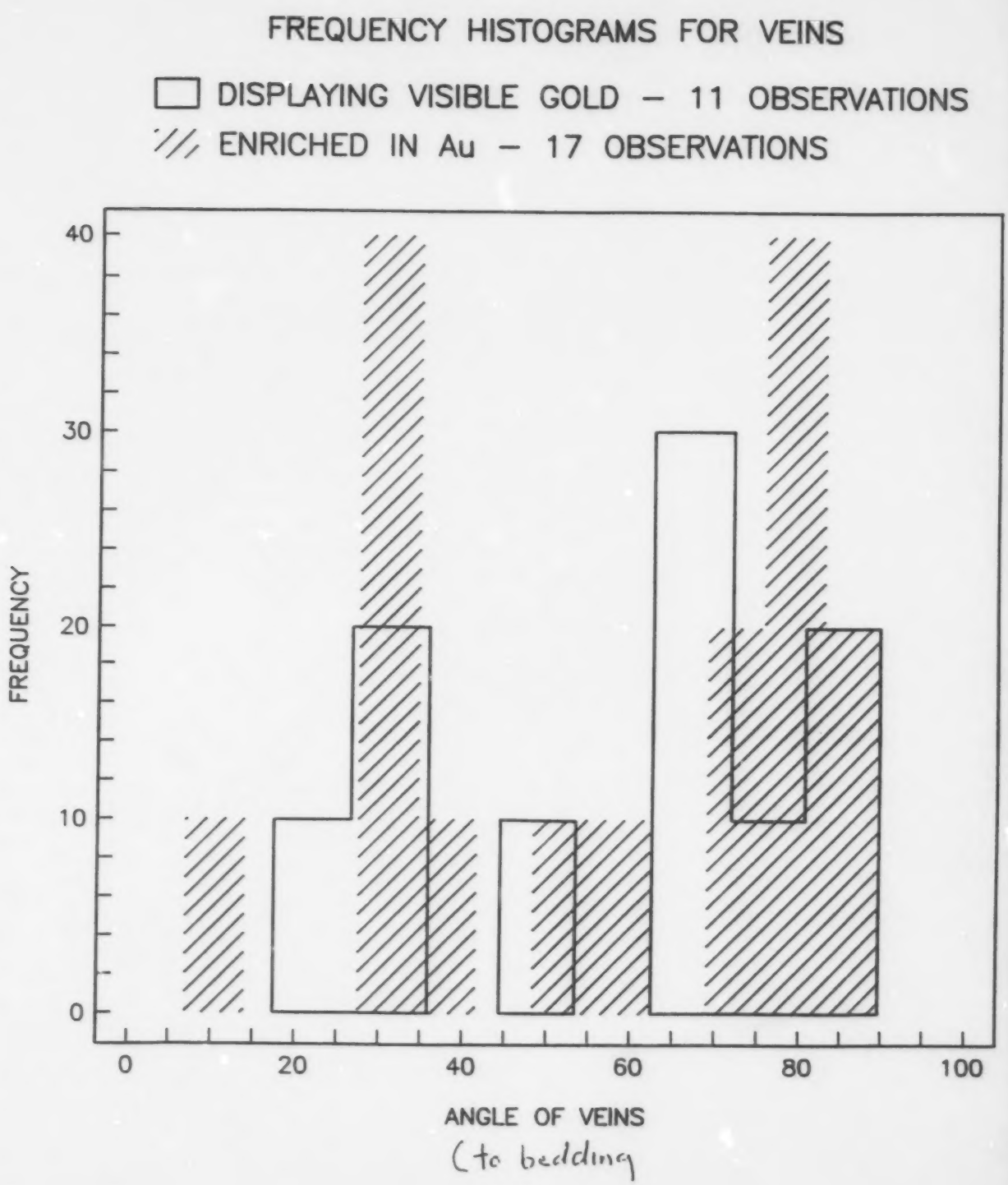

FIGURE 25. Histogram showing orientations of gold-enriched quartz-carbonate angulars within the Tangier deposit.

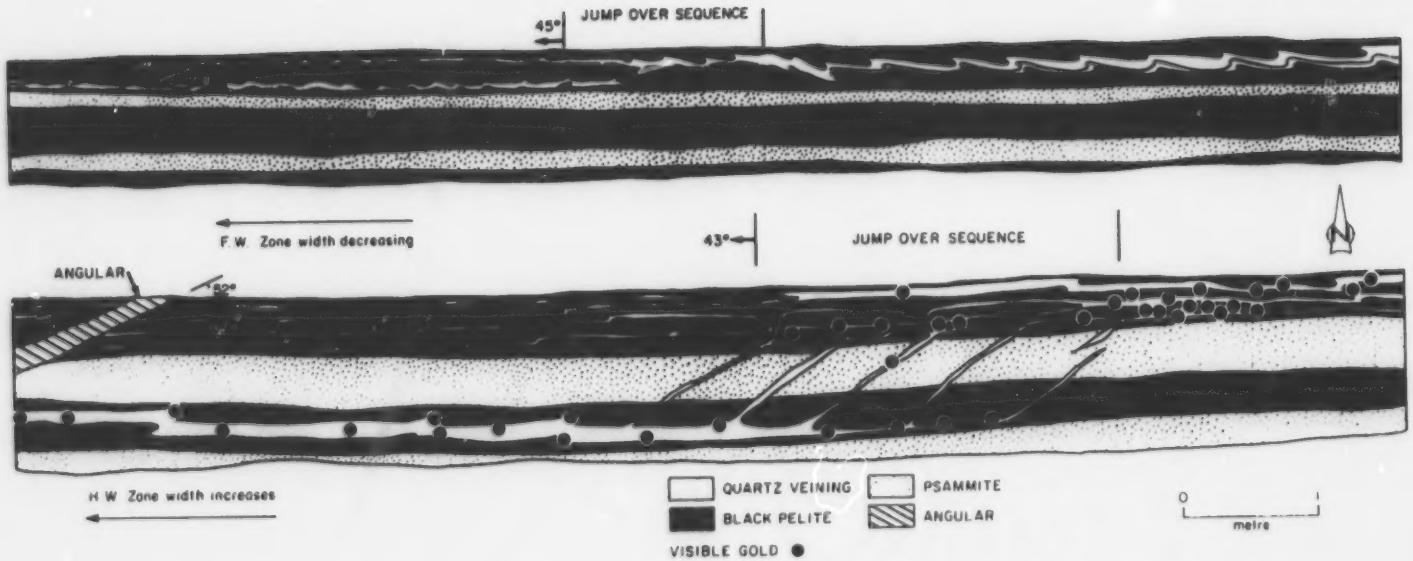

FIGURE 26. Diagram of "jump over" feature observed within the Whin vein after Hanson (1989).

particularly those with a high concentration of quartz-carbonate angular veins (some of which display geochemical gold enrichment) occur sporadically throughout deposit stratigraphy.

Best pathfinders for Au appear to be Pb and W. Petrographic and geochemical studies indicate that gold has a close association with galena and sphalerite within quartz veins and host rock (Table 5). It is interesting to note that these sulphide phases often show evidence of deformation. Although gold is also associated with arsenopyrite, the association appears more spatial than genetic since observations by Coxheath geologists indicate that arsenopyrite-rich zones commonly show no associated gold enrichment (Forgeron *et al.*, 1988). This is also shown by Table 5 which shows that arsenopyrite formation coincided with gold precipitation for only a relatively short period.

Geochemical data indicates major-oxide and trace element concentrations within a particular unit can vary due to inherent lithologic-stratigraphic diversity in addition to superimposed hydrothermal-metasomatic modification. This variation indicates that sample comparisons must be done on samples from the same bed or from the same stratigraphic level.

Relative geochemical variability within the veins and the pelites which host them suggests; 1) that chemically distinct fluid phases were injected during multi-phase quartz veining and/or 2) that the composition of the wall-rock may have been a contributing factor regarding the subsequent mineralogy (including gold) and geochemistry of the quartz vein during fluid-rock interaction. The presence of compositionally unique quartz veins in addition to clear evidence of pervasive wall rock replacement by quartz through progressive silicification, indicates that both processes were probably involved during quartz veining and mineral deposition.

Figure 21, suggests that the major-oxide and trace element concentrations of a pelite host rock may be modified by interaction with vein forming fluids. Conversely, the quartz vein does not reflect any evidence of geochemical modification due to wall rock assimilation. This may be because the fluid effectively pervaded the pelite along primary and structural pathways such as fractures, shear zones and perhaps cleavage planes.

The compositional difference between hydrothermal and metamorphic chlorites within quartz veins and host rock is also evidence of rock interaction with chemically distinct fluids.

It is interesting to note that the plunge of the boudins is the same as that determined for minor folds in the stratabound quartz veins and also for the plunge of the Tangier anticlinal axis. This would suggest that the development of local secondary structural features were controlled by the regional structures.

10. CONCLUSIONS

The Tangier gold deposit is similar in many respects to other Meguma Group gold deposits as described by other investigators with respect to:

- types and styles of quartz veins
- vein mineralogy
- presence of repeated and superimposed hydrothermal alteration associated with quartz veining and sulphide and gold mineralization
- evidence of multiple deformation

- apparent kink or minor fold in the stratigraphy on both limbs of the Tangier anticline
- faults/shear zones are common and display spatial segregation, (the reason however is presently unknown)
- evidence of significant strike and dip-slip displacement associated with faulting
- gold mineralization shows affinity for massive milky quartz within quartz veins
- occurrence of structurally controlled gold-rich, ore-shoots which reflect orientation different to other secondary structural features.

The Tangier deposit differs in that it lacks a metamorphic mineral assemblage indicative of thermal doming; a feature documented at other gold deposits.

Although no conclusions can be drawn regarding the fluid source for the quartz veins at Tangier, their similar textural and structural characteristics with other Meguma-hosted gold deposits suggest a method and time of emplacement analogous to that postulated for them (Kontak *et al.*, 1990a,b). Specifically, that the quartz veins formed from metamorphic fluids originating outside of the Meguma Group and were emplaced along sub-vertical shear zones. Their development post-dates regional Acadian deformation and is coincident with extensive plutonism throughout the Meguma Terrane at ca. 370 Ma.

ACKNOWLEGEMENTS

This study would not have been possible without the co-operation of Mike Riddell and Dennis Forgeron of Coxheath Gold Holdings Limited. They are thanked for providing the results of extensive exploration work conducted by Coxheath Gold Holdings Ltd. This report for a large part reflects the observations of them and geologists employed by them during development. The authors also benefitted greatly by the experience and advice of Paul Smith and Dan Kontak of the Nova Scotia Department of Natural Resources. The project was conceived by Paul K. Smith, but the authors assume full responsibility for the contents herein. Funding for this project was provided by the 1990-1992 Canada-Nova Scotia Mineral Development Agreement.

REFERENCES

Boyle, R.W.,
1979: The Geochemistry of Gold and Its Deposits: Bull. Geol. Surv. Can. No. 280, 584 p.

Boyle, R.W.,
1986: Gold deposits in turbidite sequences: their geology, geochemistry and history and theories and their origin; in Keppie, J.D., Boyle, R.W. and Haynes, S.J., eds. Turbidite-Hosted Gold Deposits: Geol. Assoc. Can. Special paper 32, p.1-13

Chatterjee, A.K. and Giles, P.S.,
1987: Lower Crustal Xenocrysts and Xenoliths in the Tangier Dyke, Eastern Meguma Zone Nova Scotia; in Mines and Minerals Branch Report of Activities 1987, Part A; Nova Scotia Department of Mines and Energy.Report 87-5, p.85-88.

Chatterjee, A.K. and Smith, P. K.,
1991: Potential source rocks for gold in Meguma-hosted auriferous vein deposits; abstract presented at the 1991 Atlantic Geoscience Society Colloquim, Amherst, Nova Scotia, February 8 to 10, 1991.

Chatterjee, A.K. and Giles, P.S.,
1991: An Occurrence of Sub-Silicic Orthopyroxene and Opx-Sp-Ru-Qtz Assemblage in Xenoliths of the Tangier Dyke, Southern Nova Scotia; abstract presented at the 1991 Atlantic Geoscience Society Colloquim, Amherst, Nova Scotia, February 8 to 10, 1991.

Coxheath Gold Holdings Ltd.,
1987: Annual Report for 1987; Bedford, Halifax County, Nova Scotia, 24 p.

Coxheath Gold Holdings Ltd.,
1988: Report on Geological, Geochemical, Diamond Drilling and Underground Exploration of the Tangier Gold Deposit, Halifax County, Nova Scotia. Nova Scotia Dept. Mines and Energy Assessment Report No. 11D/15A-88-03.

Coxheath Gold Holdings Ltd.,
1989: Annual Report for 1989; Bedford, Halifax County, Nova Scotia, 28 p.

Forgeron, D., Belliveau, P. J., McIntyre, W. A., Carle, D., Telford, W. M. and Becker, A.,
1988: Report on soil and till geochemical surveys, airborne magnetic, EM and VLF-EM surveys, a ground-probing radar survey, surface and underground drilling with drill core and drill sludge assays and underground excavations at the Tangier gold deposit, Tangier, Halifax County, Nova Scotia. Nova Scotia Dept. of Mines and Energy Assessment Report No. 88-033.

Douma, S.L.,
1988: Preliminary Report on the Metamorphic History of Meguma Group Metasediments in Eastern Nova Scotia; in Mines and Minerals Branch Report of Activities 1987, Part B; Nova Scotia Department of Mines and Energy. Report 87-5, p.121-129.

Douma, S.L.,
in prep: Structure and Metamorphic Evolution of the Eastern Meguma Terrane, Nova Scotia; Nova Scotia Dept Mines and Energy report in preparation. approx. 181 p.

Giles, P.S.,
1985: A Major Post - Visean Sinistral Shear Zone - New Perspectives on Devonian and Carboniferous Rocks of Southern Nova Scotia, eds. A.K. Chatterjee and D.B. Clark; Nova Scotia Dept. of Mines and Energy, preprint of paper 85-3.

Graves, M.C. and Zentilli, M.,
1982: A Review of the Geology of Gold in Nova Scotia; in Hodder, R.W. and Petruk, W., eds., Geology of Canadian Gold Deposits: CIMM Special Vol. 24, p.233-242.

Greenough, J.D., Ruffman, A. and Owen, V.,
1988: Subhorizontal Injection of Magma Forming the Popes Harbour Dyke; abstract presented at the 1988 Atlantic Geoscience Society Colloquim, Antigonish, Nova Scotia, February 5 to 7, 1988.

Haynes, S.J.,
1986: Geology and Chemistry of Turbidite-Hosted Gold Deposits, Greenschist Facies, Eastern Nova Scotia; in Keppie, J.D., Boyle, R.W. and Haynes, S.J., eds. Turbidite-Hosted Gold Deposits: Geol. Assoc. Can. Special paper 32, p. 161-178.

Henderson, M.N., and Henderson, J.R.,
1986: Constraints on the Origin of Gold in the Meguma Zone, Ecum Secum Area, Nova Scotia: Maritime Sediments and Atlantic Geology, Vol. 22, p1-14.

Hey, M.H.,
1954: A new review for the chlorites; Mineral. Mag. 13, p.277-292.

Jowett, E.C.,
1991: Fitting iron and magnesium into the hydrothermal chlorite geothermometer. GAC-MAC Program Abstr. 16, A62.

Keppie, J.D.,
1979: Geological Map of the Province of Nova Scotia, scale 1:500,000, compiled by J.D. Keppie; Nova Scotia Dept. Mines and Energy Publication.

Keppie, J.D., and Muecke, G. K.,
1979: Metamorphic map of Nova Scotia , scale 1:2,000,000, compiled by J.D. Keppie and G.K. Muecke; Nova Scotia Dept. Mines and Energy Publication.

Kontak, D.J. and Smith P.K.,
1988.a: Meguma Gold Studies IV: Chemistry of Vein Mineralogy; in Mines and Minerals Branch Report of Activities 1987, Part B; Nova Scotia Department of Mines and Energy. Report 87-5, p.85-101.

Kontak, D.J. and Smith P.K.,
1988.b: Meguma Gold Studies VI: An Integrated Model for the Genesis of Meguma Hosted Lode Gold Deposits; in Mines and Minerals Branch Report of Activities 1987, Part B; Nova Scotia Department of Mines and Energy. Report 87-5, p.111-121.

Kontak, D.J., Smith, P.K. and Reynolds, P.H.,
1988.c: Meguma Gold Studies III: Timing of Mineralization at the Beaver Dam Gold Deposit, Eastern Meguma Terrain, Nova Scotia - Implications for Meguma Gold Deposits; in Mines and Minerals Branch Report of Activities 1987, Part B; Nova Scotia Department of Mines and Energy. Report 87-5, p.77-85.

Kontak, D.J., Smith P.K. and Kerrich, R.,
1988.d: Meguma Gold Studies V: Carbon, Strontium, Oxygen and Sulphur Isotopic Compositions of Vein Minerals: Implications for Source Reservoirs and Fluid Rock Ratios Attending Vein Formation; in Mines and Minerals Branch Report of Activities 1987, Part B; Nova Scotia Department of Mines and Energy. Report 87-5, p.101-111.

Kontak, D.J., Smith P.K., Kerrich R. and Williams, P.F.,
1990.a: An Integrated Model for Meguma Group Lode Gold Deposits, Nova Scotia, Canada; Geology, Vol. 18, 238-242.

Kontak, D.J., Smith P.K., Reynolds, P. and Taylor, T.,
1990.b: Geological and $^{40}Ar/^{39}Ar$ Geochronological Constraints on the Timing of Quartz Vein Formation in Meguma Group Lode Gold Deposits, Nova Scotia; Atlantic Geology, Vol. 26, 201-227.

Malcom, W.,
1976: Gold Fields of Nova Scotia. Geological Survey of Canada, Memoir 385, 253p.

Mawer, C.K.,
1986: The Bedding-Concordant Quartz-Veins of the Meguma Group, Nova Scotia; in Keppie, J.D., Boyle, R.W. and Haynes, S.J., eds. Turbidite-Hosted Gold Deposits: Geol. Assoc. Can. Special paper 32, p. 135-148.

Mawer, C.K.,
1987: Mechanics of Formation of Gold-Bearing Quartz Veins, Nova Scotia; in Tectonophysics, Vol. 135, p.99-119.

Mills, R.F. and Corey, M.C.,
in prep: Results of N.S.D.M.E. diamond drilling at the Tangier gold deposit, Tangier, Nova Scotia.

O'Brien, B.H.,
1986: A Study of the Meguma Teranne in Lunenburg County, Nova Scotia; Geol. Surv. Can. Open File 1823. 80 p. with figures.

Sangster, A.L.,
1990: Metallogeny in the Meguma Terrane, Nova Scotia; in Mineral Deposit Studies in Nova Scotia, Vol 1.,Geol. Surv. Can. paper 90-8, p.115-163.

Smith, P.K.,
1988: Stop 1-3: Tangier; in Glacial Geology and Mineral Deposits of Mainland Nova Scotia, eds. R.R. Stea, R.M. Graves, and P.J. Rogers, Field Trip Guidebook, Prospecting in Areas of Glaciated Terrain; Symposium, Canadian Institute of Mining and Metallurgy, Halifax, Nova Scotia, August 29-31, p. 21-29.

Smith, P.K.; Haynes S.J. and Reilly, B.A.,
1985: Turbidite-hosted gold deposits, Meguma Domain, Eastern Nova Scotia; Geological Association of Canada, Field Book Excursion 11, 67p.

Smith, P.K. and Kontak, D.J.,
1987: Meguma Gold Studies: Some Basic Observations; in Mines and Minerals Branch Report of Activities 1986, Part A; Nova Scotia Department of Mines and Energy, Report 87-5, p.69-74.

Smith, P.K. and Kontak, D.J.,
1988.a: "Crack-Seal" Veins in Meguma Lode Gold Deposits: Hydraulic Fracturing or Replacement Phenomenon; Atlantic Geoscience Society Symposium, February 5 - 7, 1988; Antigonish, Nova Scotia. abstract.

Smith, P.K. and Kontak, D.J.,
1988.b: Meguma Gold Studies I: Generalized Geological Aspects of the Beaver Dam Gold Deposit, Eastern Meguma Zone, Nova Scotia; in Mines and Minerals Branch Report of Activities 1987, Part B; Nova Scotia Department of Mines and Energy. Report 87-5, p.45-61.

Smith, P.K. and Kontak, D.J.,
1988.c: Meguma Gold Studies II: Vein Morphology, Classification and Information, a New Interpretation of "Crack-Seal" Quartz Veins; in Mines and Minerals Branch Report of Activities 1987, Part B; Nova Scotia Department of Mines and Energy.Report 87-5, p.61-77.

Stea R.R. and Fowler J.H.,
1979: Minor and Trace Element Variations In Wisconsinian Tills, Eastern Shore Region, Nova Scotia. Nova Scotia Dept. Mines and Energy Paper 79-4, 30p. with maps.

Williams, P.F. and Hy, C.,
1990: Origin and Deformation and Metamorphic History of Gold Bearing Quartz Veins on the Eastern Shore of Nova Scotia; in Mineral Deposit Studies in Nova Scotia, Vol 1.,Geol. Surv. Can. paper 90-8, p.169-195.

TANGIER GOLD DEPOSIT - LITHOGEOCHEMISTRY

SAMPLE	90-3-24 PSAMMITE	90-3-53 PSAMMITE	90-3-149 PSAMMITE	90-3-184.6 PSAMMITE	90-3-315.4 PSAMMITE	90-3-465 PSAMMITE
OXIDES (WT. %)						
SiO2	78.25	76.32	77.15	70.32	71.98	77.40
TiO2	0.45	0.48	0.52	0.64	0.59	0.44
Al2O3	10.47	11.62	10.64	13.69	13.21	10.81
Fe2O3	0.67	0.50	0.35	0.95	1.01	0.32
FeO	1.65	2.24	1.78	3.13	2.51	2.51
MnO	0.029	0.034	0.040	0.039	0.050	0.034
MgO	1.35	1.67	1.37	2.15	1.90	1.23
CaO	0.69	0.74	1.15	0.73	0.87	0.78
Na2O	2.64	2.52	2.56	2.29	2.63	5.36
K2O	1.69	1.88	1.72	2.47	2.35	0.13
P2O5	0.113	0.109	0.121	0.146	0.159	0.130
CO2	0.70	0.81	1.00	0.82	1.35	0.61
H2O-	0.13	0.09	0.09	0.11	0.06	0.15
H2O+	1.22	1.22	1.12	2.11	1.71	0.90
C	N.D.	N.D.	0.08	0.05	0.05	N.D.
TOTAL OXIDES	100.05	100.24	99.69	99.65	100.43	100.81
TOTAL Fe (%)	2.51	3.00	2.33	4.44	3.81	3.12
TRACES (PPM)						
Ag	0.05	0.05	0.10	0.15	0.30	0.05
As	13	20	18	1300	290	7
Au (ppb)	7	2	200	55	9	5
B	74	76	80	87	82	3
Ba	440	420	340	360	360	17
Bi	0.05	0.07	0.07	0.09	0.08	0.09
Cd	0.02	0.05	0.98	1.52	0.91	0.01
Co	6	7	5	29	15	5
Cr	47	56	56	72	57	52
Cu	6	9	47	14	17	17
F	360	410	310	390	360	150
Ga	16	19	19	28	24	19
Hg	24	20	27	20	20	28
Li	29	42	34	52	40	17
Mo	1.8	1.8	2.5	2.1	2.1	2.7
Ni	16	14	13	41	26	16
Pb	7	5	9	25	123	6
Rb	59	65	53	88	78	8
S	10	62	500	1100	850	20
Sc	N.D.	4	7	N.D.	N.D.	8
Sn	2.0	2.3	2.3	2.4	2.3	1.4
Sr	103	98	90	75	60	85
V	49	57	61	68	68	48
W	1	1	1	1	1	9
Y	29	24	17	22	23	13
Zn	33	42	202	380	196	39
Zr	295	265	180	225	205	215

TANGIER GOLD DEPOSIT - LITHOGEOCHEMISTRY

SAMPLE	90-3-465.2 PSAMMITE	90-3-475 PSAMMITE	90-3-588 PSAMMITE	90-3-667 PSAMMITE	90-3-716 PSAMMITE	T-3-81.5 PSAMMITE
OXIDES (WT. %)						
SiO2	76.02	68.08	70.26	70.65	74.35	76.91
TiO2	0.46	0.60	0.54	0.53	0.56	0.60
Al2O3	11.49	14.95	13.08	12.40	12.40	10.10
Fe2O3	0.27	0.81	0.70	0.47	0.49	0.19
FeO	2.14	3.43	3.83	4.69	2.14	2.71
MnO	0.049	0.061	0.091	0.042	0.057	0.057
MgO	1.34	2.13	2.14	2.96	1.79	1.45
CaO	0.85	0.97	1.45	0.54	1.04	1.00
Na2O	2.71	2.59	2.52	3.43	2.70	2.47
K2O	2.04	2.97	2.20	1.24	2.19	1.94
P2O5	0.130	0.198	0.153	0.154	0.162	0.141
CO2	0.70	0.98	1.21	0.61	1.19	0.98
H2O-	0.04	0.04	0.05	0.03	N.D.	0.05
H2O+	1.07	2.25	1.72	2.16	1.09	0.80
C	0.05	0.05	0.09	N.D.	N.D.	0.16
TOTAL OXIDES	99.36	100.11	100.04	99.90	100.16	99.56
TOTAL Fe (%)	2.65	4.63	4.97	5.69	2.87	3.21
TRACES (PPM)						
Ag	0.05	0.13	0.10	0.15	0.10	0.10
As	63	51	2000	20	740	575
Au	11	<3	4	5	39	9
B	68	70	52	14	98	74
Ba	320	390	335	190	420	460
Bi	0.09	0.09	0.08	0.11	0.08	0.10
Cd	0.03	0.04	0.08	0.03	0.06	0.02
Co	4	10	15	12	9	9
Cr	73	75	68	55	54	49
Cu	12	7	5	20	7	35
F	280	410	320	280	310	260
Ga	17	22	14	18	18	22
Hg	28	16	20	24	20	12
Li	19	31	32	100	35	31
Mo	2.3	1.6	2.4	1.6	2.5	1.9
Ni	16	19	31	31	23	21
Pb	5	9	6	2	11	8
Rb	59	100	81	44	96	74
S	180	200	310	640	520	2200
Sc	2	4	8	7	7	9
Sn	2.1	2.7	2.5	3.8	2.4	2.7
Sr	50	95	96	145	90	95
V	55	67	61	65	62	50
W	2	2	1	4	4	10
Y	26	23	15	27	28	27
Zn	32	67	83	56	41	33
Zr	265	150	205	210	300	280

TANGIER GOLD DEPOSIT - LITHOGEOCHEMISTRY

SAMPLE	T-3-102.5 PSAMMITE	T-3-109 PSAMMITE	T-4-28.8 PSAMMITE	T-4-30.5 PSAMMITE	T-4-54.5 PSAMMITE	T-4-80.4 PSAMMITE
OXIDES (WT. %)						
SiO2	76.55	78.36	76.31	75.54	67.94	60.78
TiO2	0.65	0.56	0.54	0.64	0.69	0.80
Al2O3	11.14	9.98	11.01	10.69	14.39	17.73
Fe2O3	0.47	0.12	0.15	0.44	0.34	1.12
FeO	2.21	2.38	2.61	2.44	4.08	5.00
MnO	0.050	0.050	0.046	0.065	0.077	0.077
MgO	1.51	1.13	1.66	1.76	2.41	2.52
CaO	0.99	1.23	1.05	1.38	1.07	1.77
Na2O	2.45	2.48	2.63	2.33	1.98	1.89
K2O	1.90	1.47	1.73	1.75	2.73	3.81
P2O5	0.133	0.113	0.130	0.137	0.149	0.137
CO2	1.30	1.57	1.29	1.68	1.10	0.92
H2O-	0.05	0.03	0.06	0.04	0.05	0.08
H2O+	1.00	0.93	1.46	1.32	2.08	2.62
C	N.D.	N.D.	N.D.	N.D.	0.21	0.14
TOTAL OXIDES	100.40	100.40	100.68	100.21	99.30	99.39
TOTAL Fe (%)	2.93	2.77	3.06	3.16	4.89	6.69
TRACES (PPM)						
Ag	0.10	0.15	0.10	0.10	0.10	0.10
As	73	120	57	500	78	64
Au	2	2	2	2	4	17
B	66	57	16	27	80	85
Ba	340	320	360	390	570	700
Bi	0.09	0.11	0.09	0.11	0.09	0.09
Cd	0.01	0.02	0.02	0.08	0.04	0.04
Co	8	7	9	9	14	18
Cr	55	52	50	43	66	73
Cu	7	13	8	29	4	16
F	260	310	260	310	490	490
Ga	14	14	19	16	20	25
Hg	12	12	12	12	16	12
Li	34	24	35	30	46	51
Mo	1.6	2.7	1.9	1.8	1.4	1.0
Ni	17	17	16	18	30	39
Pb	5	6	12	13	20	3
Rb	77	61	72	80	110	144
S	180	580	100	820	48	590
Sc	4	5	5	11	12	12
Sn	2.0	2.7	2.1	2.3	2.4	2.9
Sr	55	58	62	65	98	140
V	53	43	57	53	76	91
W	390	10	14	10	6	4
Y	24	27	34	24	20	17
Zn	36	33	39	46	70	90
Zr	305	275	180	205	175	110

TANGIER GOLD DEPOSIT - LITHOGEOCHEMISTRY

SAMPLE	T-4-127 PSAMMITE	T-4-132 PSAMMITE	T-4-142.4 PSAMMITE	T-4-166 PSAMMITE	T-4-176 PSAMMITE	T-4-182 PSAMMITE
OXIDES (WT. %)						
SiO2	76.88	72.81	70.86	79.70	80.97	70.95
TiO2	0.49	0.59	0.65	0.44	0.31	0.64
Al2O3	10.84	13.56	13.10	10.30	9.84	14.11
Fe2O3	0.34	0.74	0.69	0.05	0.24	0.14
FeO	2.27	3.00	3.79	1.68	1.53	3.94
MnO	0.057	0.043	0.054	0.039	0.031	0.062
MgO	1.24	1.61	1.76	0.73	0.78	1.85
CaO	1.16	0.69	1.10	1.09	0.66	0.84
Na2O	2.61	2.79	2.36	2.77	2.36	2.36
K2O	1.82	2.10	2.08	1.65	1.48	2.34
P2O5	0.109	0.129	0.130	0.109	0.097	0.141
CO2	1.68	0.84	1.35	1.46	0.71	0.79
H2O-	0.05	0.03	0.04	0.03	0.04	0.02
H2O+	0.88	1.60	1.71	0.68	0.79	1.95
C	N.D.	0.09	N.D.	N.D.	N.D.	0.11
TOTAL OXIDES	100.43	100.62	99.67	100.73	99.83	100.24
TOTAL Fe (%)	2.87	4.08	4.91	1.92	1.94	4.53
TRACES (PPM)						
Ag	0.20	0.20	0.10	0.15	0.10	0.15
As	1000	2000	1100	300	290	620
Au	140	5	45	7	10	7
B	87	92	95	86	75	114
Ba	360	465	360	380	290	540
Bi	0.08	0.08	0.09	0.08	0.09	0.10
Cd	0.05	0.01	0.02	0.04	0.01	0.04
Co	8	11	14	5	5	11
Cr	40	52	63	31	34	58
Cu	26	8	12	22	12	4
F	210	360	340	360	280	390
Ga	20	20	18	15	14	20
Hg	16	12	12	16	16	12
Li	24	31	30	18	20	34
Mo	2.2	1.5	1.5	1.7	3.1	1.8
Ni	18	26	31	11	12	25
Pb	16	12	12	11	3	18
Rb	78	68	74	71	59	88
S	1700	970	1100	1500	170	430
Sc	12	10	12	9	6	11
Sn	2.1	2.1	2.4	1.8	2.9	2.4
Sr	128	115	142	130	85	110
V	51	64	57	47	44	69
W	20	2	2	12	30	12
Y	23	29	23	19	14	26
Zn	34	54	63	19	21	58
Zr	185	350	330	155	195	360

TANGIER GOLD DEPOSIT - LITHOGEOCHEMISTRY

SAMPLE	90-3-30.5 PELITE	90-3-168.5 PELITE	90-3-182.2 PELITE	90-3-286 PELITE	90-3-427 PELITE	90-3-444 PELITE	90-3-480 PELITE
OXIDES (WT. %)							
SiO2	51.84	54.43	56.25	55.82	58.84	48.25	57.47
TiO2	0.94	1.04	0.93	0.90	0.85	0.97	0.75
Al2O3	24.98	22.77	20.45	20.40	20.01	24.19	21.47
Fe2O3	1.41	1.21	1.22	1.69	1.81	1.26	1.69
FeO	4.62	4.22	4.62	4.52	3.63	6.30	4.29
MnO	0.050	0.054	0.060	0.057	0.059	0.063	0.080
MgO	3.42	3.27	3.52	3.39	2.92	3.69	2.63
CaO	0.77	1.00	1.21	1.00	0.68	0.74	1.25
Na2O	0.73	1.37	1.29	1.23	1.29	2.90	1.23
K2O	6.92	6.20	5.21	4.99	5.07	6.31	5.28
P2O5	0.154	0.170	0.231	0.206	0.173	0.259	0.194
CO2	0.74	1.26	1.73	1.43	1.02	0.37	1.26
H2O-	0.18	0.09	0.09	0.11	0.13	0.09	0.04
H2O+	3.43	3.33	3.10	3.54	3.21	4.32	2.56
C	0.23	0.16	0.23	0.19	0.25	0.51	0.12
TOTAL OXIDES	100.42	100.57	100.14	99.48	99.94	100.22	100.31
TOTAL Fe (%)	6.56	5.91	6.37	6.73	5.85	8.28	6.47
TRACES (PPM)							
Ag	0.15	0.05	0.15	0.15	0.50	0.10	0.10
As	104	54	310	670	420	1400	13
Au	9	2	4	2	20	7	5
B	85	90	85	104	75	86	72
Ba	2250	2400	800	890	770	1580	1350
Bi	0.05	0.08	0.07	0.08	0.09	0.07	0.07
Cd	0.05	0.24	0.97	1.53	0.09	0.13	0.05
Co	21	8	13	23	12	24	14
Cr	108	113	94	114	108	129	106
Cu	56	4	17	39	7	5	50
F	600	560	560	640	600	80	460
Ga	30	29	29	28	32	30	29
Hg	20	24	24	20	20	20	20
Li	63	61	75	74	38	54	42
Mo	0.9	1.2	2.3	1.2	1.4	1.2	1.3
Ni	42	16	34	43	27	46	36
Pb	5	13	9	6	30	16	7
Rb	171	168	177	165	152	209	173
S	280	1400	1100	2000	270	530	1400
Sc	24	13	6	11	N.D.	10	17
Sn	3.4	3.1	2.7	2.9	3.2	3.2	3.1
Sr	100	80	80	120	90	77	95
V	181	157	140	138	125	171	130
W	1	1	1	3	15	14	1
Y	34	35	26	40	23	15	29
Zn	88	141	236	429	86	140	93
Zr	170	210	245	130	106	155	115

TANGIER GOLD DEPOSIT - LITHOGEOCHEMISTRY

SAMPLE	90-3-512 PELITE	90-3-538.5 PELITE	90-3-590.5 PELITE	90-3-624 PELITE	90-3-646.5 PELITE	T-3-91.5 PELITE	T-3-96.2 PELITE
OXIDES (WT. %)							
SiO2	53.39	58.89	44.12	51.20	53.21	55.42	55.37
TiO2	0.80	0.89	1.07	0.99	0.91	0.96	1.00
Al2O3	23.61	19.63	27.00	23.98	22.98	19.72	21.41
Fe2O3	1.64	1.24	1.91	1.91	1.34	2.64	1.36
FeO	5.18	5.21	7.75	5.58	5.64	6.00	5.35
MnO	0.060	0.077	0.073	0.070	0.062	0.054	0.055
MgO	2.97	2.84	4.27	3.64	3.52	3.38	3.36
CaO	0.42	0.65	0.43	0.51	0.51	0.80	0.80
Na2O	1.31	1.99	0.56	1.04	0.76	0.76	0.68
K2O	5.65	4.09	6.70	5.70	5.60	4.82	5.51
P2O5	0.198	0.140	0.234	0.178	0.238	0.158	0.182
CO2	0.56	0.53	0.07	0.42	0.14	0.63	0.86
H2O-	N.D.	0.02	0.01	0.11	0.03	0.08	0.04
H2O+	3.39	3.18	4.37	3.67	3.94	3.76	3.72
C	0.37	0.09	0.53	0.41	0.49	0.46	0.41
TOTAL OXIDES	99.55	99.46	99.08	99.41	99.37	99.64	100.11
TOTAL Fe (%)	7.41	7.04	10.54	8.13	7.62	9.32	7.32
TRACES (PPM)							
Ag	0.10	0.15	0.80	0.20	0.10	0.20	0.10
As	1050	34	40	29	390	280	69
Au	<2	29	14	2	2	7	10
B	80	72	82	87	82	88	80
Ba	1600	460	2100	1680	1500	1320	1400
Bi	0.09	0.05	0.09	0.08	0.08	0.09	0.12
Cd	0.09	0.04	0.10	0.04	0.05	0.01	0.03
Co	23	19	25	20	23	17	19
Cr	128	109	140	119	106	83	89
Cu	14	14	65	37	16	75	16
F	520	180	600	520	520	560	600
Ga	30	32	32	36	35	31	29
Hg	20	20	24	20	20	12	16
Li	53	42	62	67	58	74	78
Mo	1.3	1.3	1.4	1.3	1.7	0.8	1.4
Ni	34	34	57	41	33	61	43
Pb	31	3	8	6	9	31	8
Rb	174	122	225	219	196	138	161
S	860	180	2300	870	170	12000	1800
Sc	16	6	13	11	13	13	15
Sn	3.6	3.0	3.3	3.8	3.4	3.2	3.5
Sr	95	61	57	35	47	48	53
V	141	96	159	144	141	106	126
W	2	1	4	1	2	20	11
Y	26	23	21	23	23	37	27
Zn	116	106	149	107	100	95	98
Zr	115	140	145	155	165	210	165

TANGIER GOLD DEPOSIT - LITHOGEOCHEMISTRY

SAMPLE	T-3-140.5 PELITE	T-4-37.55 PELITE	T-4-145 PELITE	T-4-134 PELITE	90-3-183 QV	90-3-285 QV	90-3-317 QV	90-3-435 QV
OXIDES (WT. %)								
SiO2	57.73	57.66	47.71	60.00	99.02	93.79	98.85	98.51
TiO2	0.85	0.88	0.93	0.78	0.003	0.05	0.005	N.D.
Al2O3	20.88	19.58	23.36	19.46	0.12	1.20	0.12	0.08
Fe2O3	1.21	1.07	1.94	1.26	0.15	0.28	0.05	0.01
FeO	4.82	4.65	5.71	4.57	0.33	0.83	0.59	0.66
MnO	0.068	0.077	0.079	0.054	0.005	0.046	0.008	0.006
MgO	2.81	2.38	3.48	2.47	0.046	0.24	0.063	0.035
CaO	0.86	2.64	1.85	1.07	0.09	1.47	0.13	0.053
Na2O	1.33	1.44	2.73	1.09	0.011	0.015	0.003	0.008
K2O	5.48	4.75	5.97	4.77	0.015	0.27	0.011	0.013
P2O5	0.154	0.174	0.190	0.149	0.004	0.012	0.024	0.004
CO2	0.77	2.28	2.27	1.68	0.13	1.46	0.23	0.02
H2O-	0.04	0.04	0.07	0.05	0.07	0.09	0.07	0.03
H2O+	3.22	2.71	3.74	2.17	0.14	0.41	0.14	1.13
C	0.39	0.25	0.57	0.32	N.D.	N.D.	N.D.	N.D.
TOTAL OXIDES	100.61	100.58	100.60	99.89	100.14	100.16	100.30	100.56
TOTAL Fe (%)	6.58	6.25	8.30	6.35	0.52	1.20	0.71	0.75
TRACES (PPM)								
Ag	0.15	0.15	0.25	0.25	0.05	0.80	0.20	0.20
As	40	40	5100	900	29	170	2	53
Au	4	5	5	34	9	4	3800	88
B	83	102	84	95	14	36	15	9
Ba	1300	820	1200	830	5	72	4	2
Bi	0.09	0.06	0.13	0.08	0.09	0.12	0.10	0.11
Cd	0.02	0.05	0.08	0.05	0.13	7.33	0.24	0.06
Co	18	16	17	12	1	5	1	1
Cr	100	82	104	74	26	49	76	76
Cu	10	12	40	48	34	45	10	12
F	640	1320	690	560	80	110	48	50
Ga	28	25	29	31	N.D.	5	N.D.	N.D.
Hg	10	12	12	12	19	16	24	19
Li	58	52	66	58	2	30	2	1
Mo	1.2	1.0	0.8	1.6	5.0	6.5	13.0	11.0
Ni	35	32	45	41	5	28	6	6
Pb	28	7	15	48	3	59	2	3
Rb	139	190	204	167	6	15	5	5
S	470	980	4100	5300	100	2600	39	14
Sc	14	17	23	18	N.D.	N.D.	N.D.	N.D.
Sn	3.2	3.2	3.4	3.3	2.4	1.7	2.3	2.1
Sr	50	150	170	130	N.D.	21	N.D.	N.D.
V	125	110	150	110	N.D.	7	N.D.	N.D.
W	15	9	5	2	1	3	3	1
Y	21	17	24	22	16	31	20	14
Zn	91	92	113	83	22	1206	27	11
Zr	170	100	115	80	95	70	100	50

TANGIER GOLD DEPOSIT - LITHOGEOCHEMISTRY

SAMPLE	90-3-450.6 QV	90-3-592 QV	T-4-37.5 QV	T-4-143.6 QV	T-4-145.6 QV	T-4-169 QV
OXIDES (WT.%)						
SiO2	96.95	97.81	96.78	98.85	98.43	99.03
TiO2	N.D.	N.D.	0.006	0.008	0.004	0.003
Al2O3	0.23	0.23	0.23	0.20	0.12	0.12
Fe2O3	0.01	0.03	0.37	0.11	0.02	0.01
FeO	0.65	0.82	0.69	0.46	0.59	0.46
MnO	0.024	0.015	0.007	0.005	0.017	0.003
MgO	0.31	0.24	0.044	0.023	0.109	0.019
CaO	0.64	0.36	0.12	0.066	0.34	0.037
Na2O	0.011	0.009	0.008	0.008	0.009	0.007
K2O	0.086	0.014	0.047	0.044	0.023	0.016
P2O5	0.072	0.012	0.012	0.008	0.008	0.008
CO2	0.72	0.56	0.52	0.14	0.46	0.07
H2O-	0.06	0.02	0.10	0.11	0.11	0.01
H2O+	0.25	0.02	0.19	0.18	0.17	0.15
C	N.D.	N.D.	N.D.	N.D.	N.D.	N.D.
TOTAL OXIDES	100.01	100.14	99.13	100.21	100.41	99.93
TOTAL Fe (%)	0.73	0.94	1.14	0.62	0.68	0.52
TRACES (PPM)						
Ag	0.20	0.20	0.73	0.07	0.13	0.05
As	2	3	12	3	16	4
Au	94	4	313	50	10	2
B	16	14	104	16	12	15
Ba	13	2	11	19	10	10
Bi	0.11	0.12	0.50	0.11	0.10	0.11
Cd	0.03	0.10	0.04	0.03	0.05	0.02
Co	1	1	7	1	1	2
Cr	58	56	61	74	56	48
Cu	10	14	294	12	11	10
F	280	38	52	48	58	37
Ga	N.D.	N.D.	1	1	1	1
Hg	20	23	16	20	12	16
Li	5	1	1	3	1	1
Mo	11.0	12.0	8.3	9.6	8.0	9.9
Ni	7	8	15	4	4	4
Pb	5	1	131	2	1	1
Rb	7	5	7	7	8	3
S	24	43	2700	49	92	83
Sc	1	2	N.D.	N.D.	1	N.D.
Sn	2.0	2.5	2.9	2.0	2.4	4.1
Sr	N.D.	N.D.	N.D.	N.D.	8	5
V	N.D.	N.D.	N.D.	N.D.	N.D.	N.D.
W	1	1	1	1	1	2
Y	19	17	19	19	19	17
Zn	8	8	12	8	14	6
Zr	350	30	55	60	58	58

APPENDIX B: BIOTITE MINERAL CHEMISTRY

Texture	PORPH	PORPH	PORPH	PORPH	PORPH	PORPH	PORPH	PORPH	PORPH	PORPH	LATH	LATH
(wt. %)SiO2	34.584	35.168	35.36	34.875	36.061	35.263	35.391	33.023	36.412	35.704	34.831	35.379
TiO2	1.795	2.237	1.848	1.781	1.94	1.774	1.859	1.826	2.043	1.933	1.931	1.662
Al2O3	14.311	16.441	16.462	15.059	16.434	17.33	16.596	15.645	15.716	16.486	16.186	15.849
FeO	19.112	21.829	21.564	20.586	21.537	21.655	21.391	20.446	21.67	21.952	21.529	21.091
MnO	0.097	0.109	0.117	0.102	0.092	0.114	0.097	0.094	0.112	0.086	0.1	0.099
MgO	7.902	8.265	7.979	7.417	8.713	8.284	8.479	7.647	8.856	8.57	8.48	8.104
CaO	0.018	0.037	0.02	0.014	0	0.016	0.091	0.026	0.018	0.047	0.062	0.019
Na2O	0.044	0.039	0.055	0.089	0.069	0.071	0.144	0.046	0.032	0.071	0.077	0.059
K2O	8.192	8.036	8.572	8.405	8.114	8.571	8.236	8.307	8.382	8.233	8.206	8.252
TOTAL	86.06	92.16	91.98	88.33	92.96	93.08	92.28	87.06	93.24	93.08	91.4	90.51
Si	5.838	5.579	5.629	5.773	5.649	5.542	5.599	5.57	5.7	5.608	5.58	5.704
Aliv	2.162	2.421	2.371	2.227	2.351	2.458	2.401	2.43	2.3	2.392	2.42	2.296
Alvi	0.683	0.651	0.715	0.709	0.68	0.75	0.692	0.678	0.598	0.657	0.634	0.714
Ti	0.23	0.27	0.223	0.224	0.231	0.212	0.223	0.234	0.243	0.231	0.235	0.204
Fe	2.698	2.896	2.871	2.85	2.821	2.846	2.83	2.884	2.837	2.883	2.885	2.844
Mn	0.014	0.015	0.016	0.014	0.012	0.015	0.013	0.013	0.015	0.011	0.014	0.014
Mg	1.988	1.954	1.893	1.83	2.034	1.94	1.999	1.922	2.066	2.006	2.025	1.947
Ca	0.003	0.006	0.003	0.002	0	0.003	0.015	0.005	0.003	0.008	0.011	0.003
Na	0.014	0.012	0.017	0.029	0.021	0.022	0.044	0.015	0.01	0.022	0.024	0.018
K	1.764	1.626	1.741	1.775	1.622	1.719	1.662	1.788	1.674	1.65	1.677	1.697
SUM CATS	15.395	15.43	15.479	15.433	15.421	15.507	15.48	15.539	15.446	15.468	15.504	15.441
Fe/(Fe+Mg)	0.58	0.6	0.6	0.61	0.58	0.59	0.59	0.6	0.58	0.59	0.59	0.59
Mg/(Fe+Mg)	0.42	0.4	0.4	0.39	0.42	0.41	0.41	0.4	0.42	0.41	0.41	0.41

BASED ON 22 OXYGEN

APPENDIX B: BIOTITE MINERAL CHEMISTRY

Texture	LATH	LATH	LATH	LATH	LATH	LATH	LATH
(wt.%)SiO2	35.96	35.136	36.379	35.289	35.41	35.349	34.907
TiO2	2.181	1.904	1.889	1.791	1.83	1.898	1.825
Al2O3	16.518	16.913	17.488	16.412	17.082	17.057	17.041
FeO	21.725	21.359	21.74	21.188	21.407	21.802	21.748
MnO	0.101	0.119	0.094	0.102	0.097	0.096	0.09
MgO	8.446	8.31	8.729	7.784	8.278	8.616	8.247
CaO	0.083	0.019	0.065	0.042	0.033	0.015	0.019
Na2O	0.371	0.074	0.121	0.05	0.058	0.063	0.058
K2O	8.448	8.469	0.8337	8.315	8.667	8.353	8.314
TOTAL	93.83	92.3	87.34	90.97	92.86	93.25	92.25
Si	5.606	5.564	5.777	5.662	5.574	5.543	5.538
Aliv	2.394	2.436	2.223	2.338	2.426	2.457	2.462
Alvi	0.639	0.719	1.047	0.763	0.741	0.693	0.723
Ti	0.258	0.229	0.228	0.218	0.219	0.226	0.22
Fe	2.832	2.829	2.887	2.843	2.818	2.859	2.886
Mn	0.013	0.016	0.013	0.014	0.013	0.013	0.012
Mg	1.962	1.961	2.066	1.861	1.942	2.013	1.95
Ca	0.014	0.003	0.011	0.007	0.006	0.003	0.003
Na	0.112	0.023	0.037	0.016	0.018	0.019	0.018
K	1.68	1.711	0.169	1.702	1.741	1.671	1.683
SUM CATS	15.511	15.491	14.458	15.424	15.498	15.497	15.495
Fe/(Fe+Mg)	0.59	0.59	0.58	0.6	0.59	0.59	0.6
Mg/(Fe+Mg)	0.41	0.41	0.42	0.4	0.41	0.41	0.4

BASED ON 22 OXYGEN

TABLE : CHLORITE MINERAL CHEMISTRY

Texture	WORM	WORM	WORM	PORPH	PORPH	PORPH	PORPH	PORPH	PORPH	PORPH	PORPH	PORPH	PORPH
(wt.%)SiO2	27.483	28.108	28.575	25.76	24.948	24.797	24.229	24.743	24.035	24.042	23.906	24.056	23.987
TiO2	0.023	0	0.056	0.068	0.068	0.066	0.06	0.057	0.045	0.066	0.007	0.032	0.057
Al2O3	18.588	19.043	19.048	20.797	21.676	21.141	20.335	21.715	20.994	21.358	21.455	20.54	20.793
FeO	22.958	22.553	22.034	28.254	27.938	27.145	26.641	27.625	27.729	28.044	28.771	27.959	27.987
MnO	0.152	0.162	0.169	0.1	0.162	0.174	0.157	0.162	0.179	0.208	0.269	0.204	0.224
MgO	16.329	16.993	17.112	12.334	11.227	10.97	10.504	11.641	12.012	11.464	11.456	11.948	11.386
CaO	0.013	0	0	0.021	0.009	0.009	0.042	0	0.029	0.031	0.024	0.019	0.019
Na2O	0.014	0	0	0.03	0.043	0	0.034	0	0.056	0.057	0.01	0.104	0
K2O	0	0	0	0	0	0	0	0	0.569	0	0.011	0	0
F	0	0	0	0	0	0	0	0	0	0	0	0	0
CL	0.025	0	0.015	0.008	0.034	0.013	0.806	0.402	0	0	0	0	0
TOTAL	85.58	86.86	87.01	87.37	86.11	84.32	82.81	86.35	85.65	85.27	85.91	84.86	84.45
Si	5.849	5.864	5.927	5.525	5.431	5.498	5.531	5.389	5.301	5.311	5.264	5.347	5.355
Aliv	2.151	2.136	2.073	2.475	2.569	2.502	2.469	2.611	2.699	2.689	2.736	2.653	2.645
Alvi	2.508	2.543	2.58	2.778	2.989	3.018	2.998	2.959	2.754	2.867	2.827	2.724	2.823
Ti	0.004	0	0.009	0.011	0.011	0.011	0.01	0.009	0.008	0.011	0.001	0.005	0.01
Fe	4.086	3.935	3.822	5.068	5.087	5.033	5.086	5.032	5.115	5.181	5.298	5.198	5.226
Mn	0.027	0.029	0.03	0.018	0.03	0.033	0.03	0.03	0.033	0.039	0.05	0.038	0.042
Mg	5.179	5.283	5.29	3.943	3.643	3.625	3.574	3.778	3.948	3.774	3.759	3.958	3.788
Ca	0.003	0	0	0.005	0.002	0.002	0.01	0	0.007	0.007	0.006	0.005	0.005
Na	0.006	0	0	0.012	0.018	0	0.015	0	0.024	0.024	0.004	0.045	0
K	0	0	0	0	0	0	0	0	0.16	0	0.003	0	0
SUM CATS	19.814	19.79	19.731	19.836	19.779	19.722	19.724	19.808	20.049	19.904	19.949	19.973	19.893
Fe/(Fe+Mg)	0.44	0.43	0.42	0.56	0.58	0.58	0.59	0.57	0.56	0.58	0.58	0.57	0.58
Mg/(Fe+Mg)	0.56	0.57	0.58	0.44	0.42	0.42	0.41	0.43	0.44	0.42	0.42	0.43	0.42
Temp C	281.1025	278.5505	268.3425	334.6945	350.0065	339.32	334.216	356.546	370.4225	369.1465	376.643	363.245	362.1285
Aliv corr.	1.0975	1.0895	1.0575	1.2655	1.3135	1.28	1.264	1.334	1.3775	1.3735	1.397	1.355	1.3515

TABLE : CHLORITE MINERAL CHEMISTRY

Texture	PORPH	PORPH	PORPH	PORPH	LATH	LATH	LATH	LATH	LATH	LATH	LATH	LATH	LATH
(wt.%)SiO2	23.926	24.34	23.953	23.46	28.818	28.061	27.656	28.159	23.876	24.975	24.33	28.484	27.705
TiO2	0.049	0.058	0.059	0.049	0.023	0.069	0.041	0.036	0.046	0.066	0.045	0	0.023
Al2O3	21.098	19.315	21.211	20.102	18.912	19.85	20.731	19.151	21.362	21.22	20.741	20.111	18.102
FeO	28.09	28.322	27.824	28.356	21.048	21.307	22.299	21.58	28.171	27.451	26.797	21.646	27.891
MnO	0.208	0.179	0.237	0.168	0.176	0.197	0.191	0.137	0.21	0.17	0.17	0.154	0.172
MgO	11.789	12.194	11.263	10.744	18.139	16.816	16.712	17.695	11.662	11.521	11.452	14.671	14.142
CaO	0	0.047	0.013	0.065	0	0.013	0	0	0.037	0.016	0.024	0.048	0.033
Na2O	0	0	0	0	0	0	0	0	0	0.035	0.059	0.029	0
K2O	0	0	0	0	0	0	0	0	0	0	0	0	0
F	0	0	0	0	0	0	0	0	0	0	0	0	0
CL	0	0	0	0	0.016	0.009	0	0.011	0	0.167	0.731	0.058	0.014
TOTAL	85.16	84.46	84.56	82.94	87.13	86.32	87.63	86.77	85.36	85.62	84.35	85.2	88.08
Si	5.297	5.453	5.332	5.363	5.937	5.846	5.704	5.85	5.274	5.468	5.445	6.01	5.875
Aliv	2.703	2.547	2.668	2.637	2.063	2.154	2.296	2.15	2.726	2.532	2.555	1.99	2.125
Alvi	2.798	2.549	2.894	2.775	2.527	2.717	2.74	2.536	2.832	2.939	2.912	3.007	2.396
Ti	0.008	0.01	0.01	0.009	0.004	0.011	0.006	0.006	0.008	0.011	0.008	0	0.004
Fe	5.201	5.306	5.18	5.421	3.627	3.713	3.847	3.75	5.204	5.026	5.016	3.82	4.946
Mn	0.039	0.034	0.045	0.033	0.031	0.035	0.033	0.024	0.039	0.032	0.032	0.028	0.031
Mg	3.89	4.071	3.737	3.66	5.57	5.221	5.137	5.479	3.839	3.759	3.82	4.613	4.469
Ca	0	0.011	0.003	0.016	0	0.003	0	0	0.009	0.004	0.006	0.011	0.007
Na	0	0	0	0	0	0	0	0	0	0.015	0 026	0.012	0
K	0	0	0	0	0	0	0	0	0	0	0	0	0
SUM CATS	19.936	19.982	19.869	19.914	19.757	19.7	19.764	19.794	19.931	19.785	19.818	19.49	19.854
Fe/(Fe+Mg)	0.57	0.57	0.58	0.6	0.39	0.42	0.43	0.41	0.58	0.57	0 57	0.45	0.53
Mg/(Fe+Mg)	0.43	0.43	0.42	0.4	0.61	0.58	0.57	0.59	0.42	0.43	0.43	0.55	0.47
Temp C	371.22	346.338	365.797	361.1715	266.269	281.262	304.0705	280.4645	375.048	343.9455	347.614	255.5825	278.391
Aliv corr.	1.38	1.302	1.363	1.3485	1.051	1.098	1.1695	1.0955	1.392	1.2945	1.306	1.0175	1.089

TABLE : CHLORITE MINERAL CHEMISTRY

Texture	LATH	LATH	LATH	LATH	LATH
(wt. %)SiO2	27.653	29.208	28.192	24.236	24.233
TiO2	0.018	0	0.031	0.066	0.06
Al2O3	18.294	22.742	17.788	20.754	19.284
FeO	25.781	18.03	25.99	28.383	28.062
MnO	0.139	0.066	0.129	0.245	0.213
MgO	13.792	14.686	15.454	11.918	12.334
CaO	0.042	0.121	0.035	0.047	0.019
Na2O	0.07	0.217	0.035	0.046	0.058
K2O	0	0	0	0	0
F	0	0	0	0	0
CL	0.067	0.224	0.021	0	0
TOTAL	85.86	85.29	87.67	85.7	84.26
Si	5.955	6.014	5.943	5.34	5.438
Aliv	2.045	1.986	2.057	2.66	2.562
Alvi	2.594	3.528	2.358	2.726	2.535
Ti	0.003	0	0.005	0.011	0.01
Fe	4.643	3.105	4.582	5.23	5.267
Mn	0.025	0.012	0.023	0.046	0.04
Mg	4.426	4.506	4.855	3.914	4.125
Ca	0.01	0.027	0.008	0.011	0.005
Na	0.029	0.087	0.014	0.02	0.025
K	0	0	0	0	0
SUM CATS	19.73	19.264	19.845	19.958	20.008
Fe/(Fe+Mg)	0.51	0.41	0.49	0.57	0.56
Mg/(Fe+Mg)	0.49	0.59	0.51	0.43	0.44
Temp C	265.312	254.3065	266.907	364.3615	348.571
Aliv corr.	1.048	1.0135	1.053	1.3585	1.309

PYRROTITE GEOCHEMISTRY (Tangier)

Element	* Sample Number TAN-88-1	TAN-88-2
FeO (%)	63.40	67.67
Fe2O3	12.17	2.82
Mn (ppm)	100	98
Ag	<0.1	4.0
As	32	22
Bi	0.2	82
Co	117	143
Cu	550	2600
Pb	37	470
Zn	65	67
Cd	<1	<1
Ni	1660	2000
Au (ppm)	<5	<5
Total iron as Fe2O3	82.80	78.20

Sample Description:

TAN-88-1 -magnetic pyrrotite from laminated quartz texture in the Marker Vein

TAN-88-2 -magnetic pyrrotite from massive quartz texture; exact location is uncertain but it is not from the Marker Vein.

* Both samples were acquired from A. MacIntyre during the 1987 NSDME Open House. Samples were collected during the second round of underground exploration at the Tangier property.

LIST OF PLATES

1a. Black-graphitic pelite containing abundant carbonate oikocrysts oriented parallel to shear cleavage (S_4).

1b. Black pelite containing disseminated biotite, tourmaline and S_4 oriented chlorite and carbonate porphroblasts. Field of view = 3.1 x 2.2 mm.

1c. Black-graphitic pelite showing common bedding-parallel carbonate-rich bands and S_2 oriented carbonate oikocrysts.

1d. Close-up of 1c showing concentration of carbonate oikocrysts. Field of view = 20 x 26mm

2a. Pyrrhotite + pyrite + chalcopyrite stringers in pelite oriented parallel to S_4 cleavage (as shown by arrow)

2b. Carbonate oikocrysts and pyrrhotite blebs oriented parallel to S_4 cleavage. Field of view = 16 x 20mm.

1a.

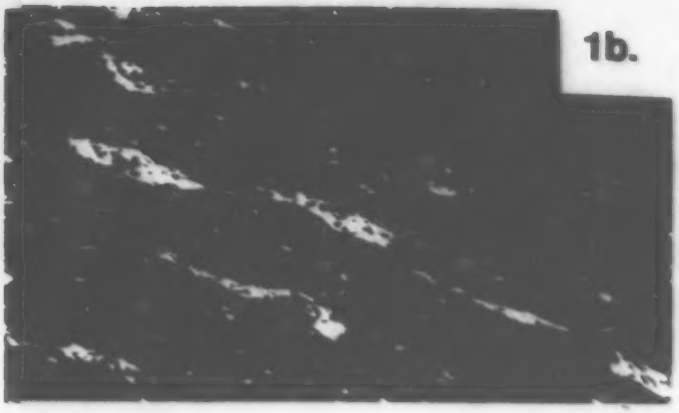

1b.

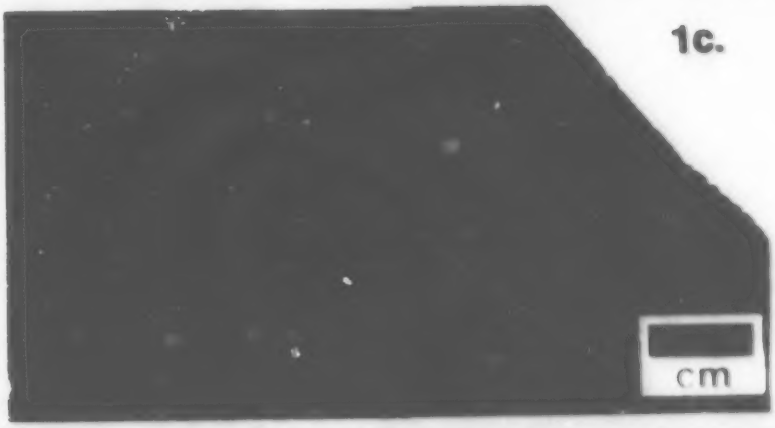

1c.

1d.

2a.

cm

2b.

2c. S_4-oriented quartz-carbonate pods in pelite containing two generations of sulphides. Field of view = 6 x 8mm.

2d. Close-up of 2c showing early S_4 (?) deformed pyrrhotite + pyrite + sphalerite crystals overgrown by coarse euhedral-subhedral arsenopyrite crystals. Field of view = 3.1 x 2.2mm

3. $1cm^2$ black pelite rip-up clast (to left of dime), within a grey pelite.

4a. Typical bedding parallel, crack-sealed textured quartz-vein, sandwiched between an upper more massive quartz vein and a lower carbonate + chlorite + pyrrhotite vein. Note the intense development of carbonate oikocrysts (carb) in the pelite adjacent to the lower vein whereas the upper pelite is virtually barren of oikocrysts. The dashed white line marks the limit of oikocryst development.

4b. Close-up of 4a showing carbonate oikocrysts which formed in response to superimposed alteration. The carbonate displays an orientation (S_4 ?) different to that shown by the two chlorite porphyroblasts located in the lower right and top left of the plate. Field of view = 3.1 x 2.2mm

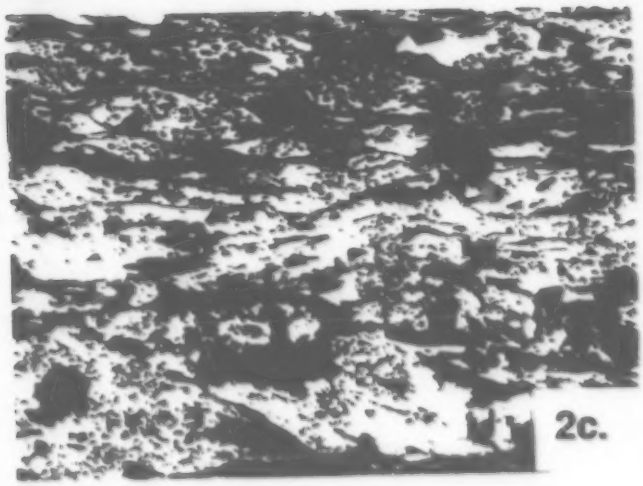

2c.

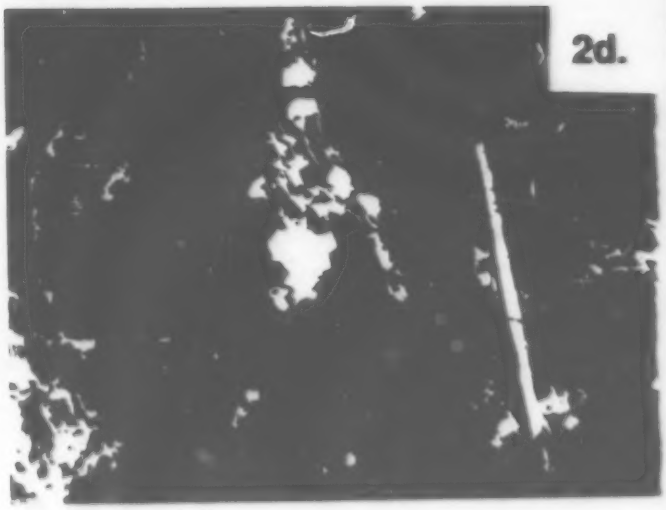

2d.

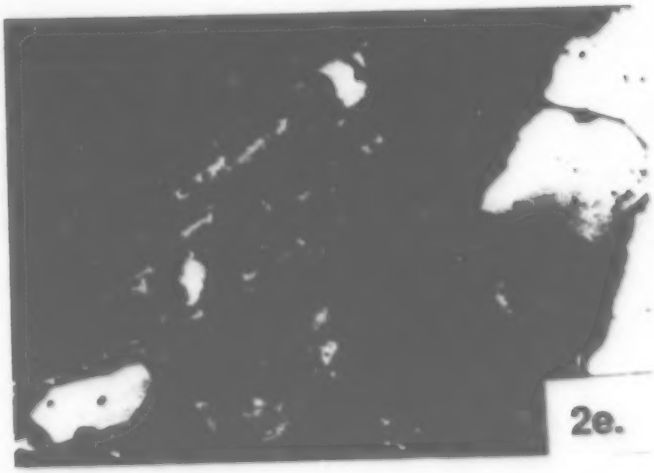

2e.

3.

4a.

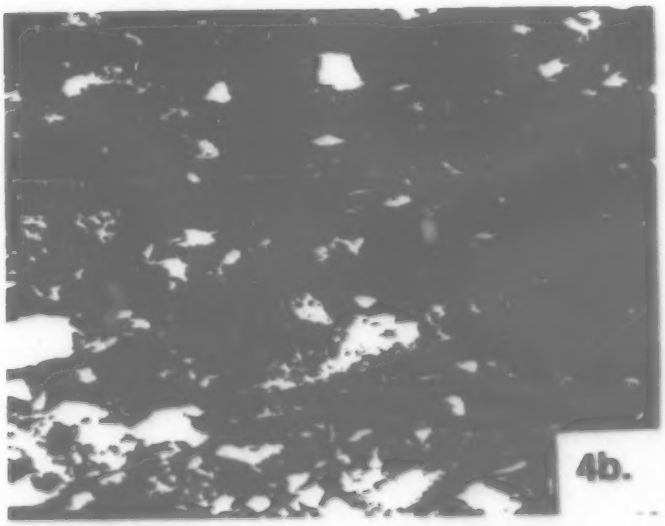

4b.

5a. Medium-grained psammite containing accessory tourmaline, carbonate, muscovite, pyrrhotite and rare biotite. The pyrrhotite (opaque) shows a strong S_4 alighnment. Field of view = 3.1 x 2.2mm.

5b. Psammite with abundant fine-grained, S_2-oriented muscovite. Field of view = 3.1 x 2.2mm.

5c. Psammite containing S_2-oriented chlorite porphyroblasts. Field of view = 6 x 8mm.

5d. Psammite showing S_2-oriented chlorite overgrown by S_4-oriented carbonate oikocrysts which contain biotite. Field of view = 3.1 x 2.2mm.

5e. Large S_4-oriented pyrrhotite-chalcopyrite-pyrite lenses within psammite adjacent to contact with pelite. The contact is amrked by several folded bedding-parallel quartz veins. Note that the orientation of the sulphide lenses are parallel to the axis of the minor folds (F_2 ?) within the veins.

6. Psammite displaying well-developed pressure solution cleavage (S_2).

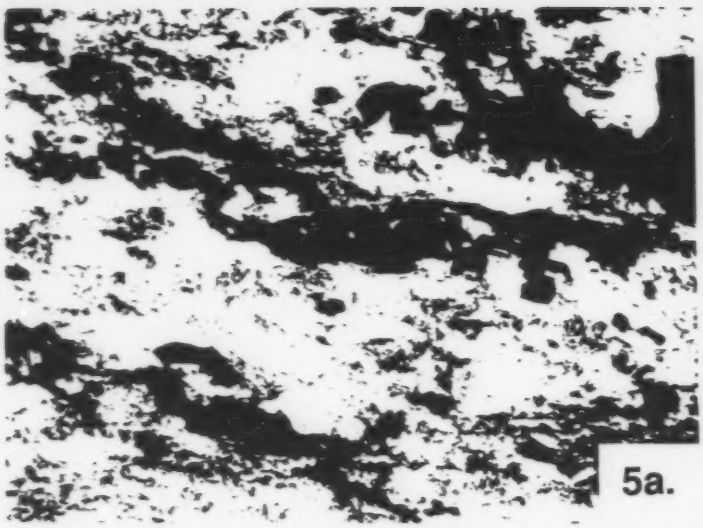

5a.

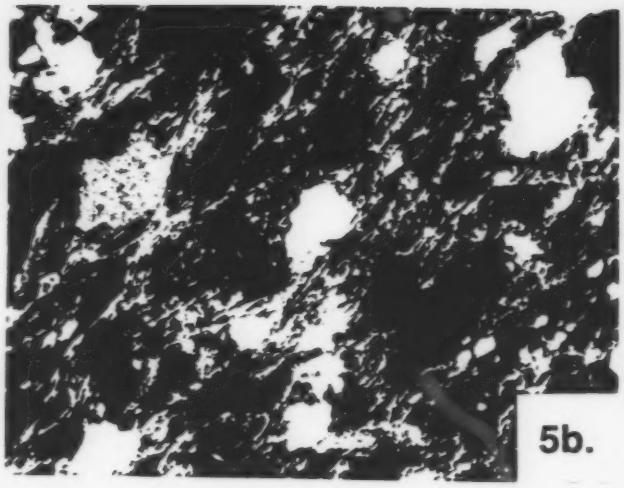

5b.

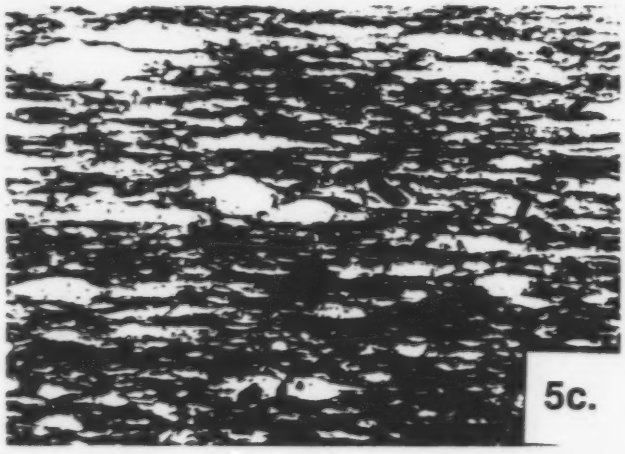

5c.

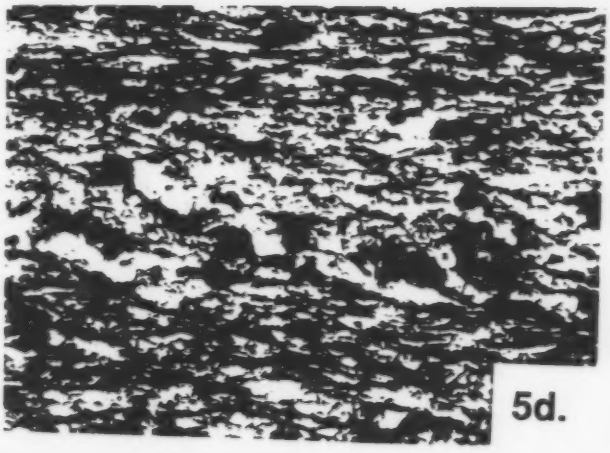

5d.

5e.

6.

7. Psammite containing large, euhedral arsenopyrite crystals with quartz-carbonate filled pressure shadows cut by series of mm-thick quartz-carbonate angular veins.

8a. Well developed flame-structures at psammite-pelite contact.

8b. Pelite rip-up clast in psammite showing S_2 attenuation at lower end. Irregular opaque blebs consists of pyrrhotite and pyrite. Field of view = 26 x 20mm.

8c. Plate shows stylolite (?) at pelite/psammite contact indicating dissolution at lithological boundary.

8d. Intercalated pelite (dark) and psammite (light) showing intense S_2 cleavage attenuation of bedding. Dislocation is less than 1 cm., field of view = 20 x 26mm.

9. Sulphide-bearing psammite dyke within black-graphitic pelite.

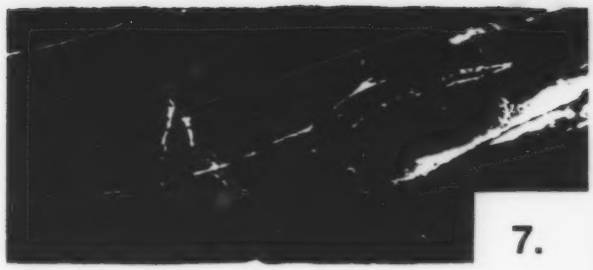

7.

8a.

8b.

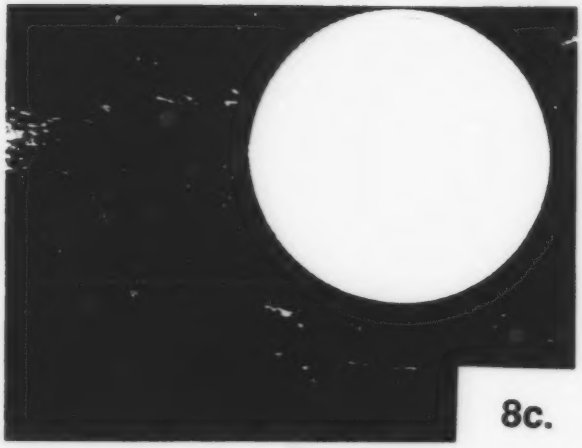

8c.

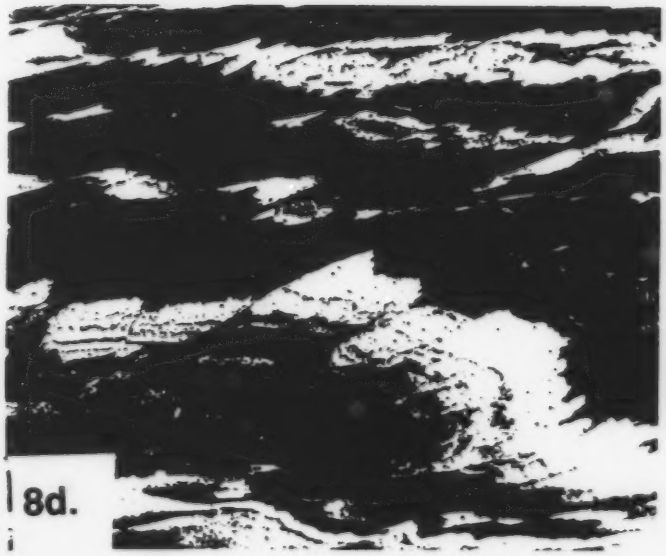

8d.

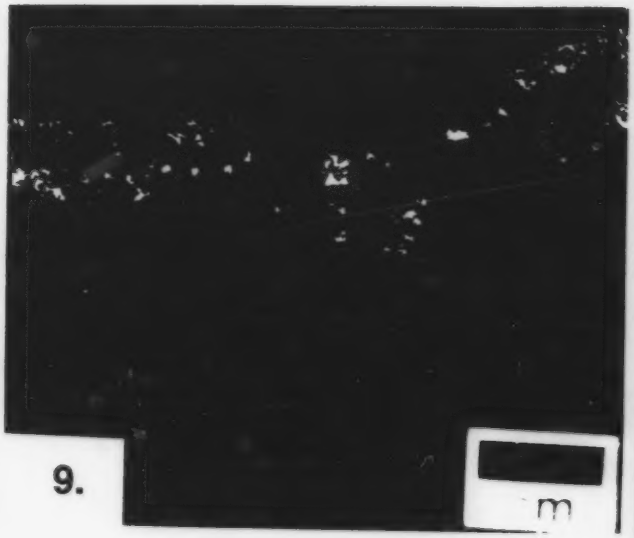

9.

10a. Psammite displaying gradation from mottled, light green silicified part on the left to an unaltered medium-grey part on the right. The latter is also in diffuse contact with dark-grey pelite at far right.

10b. Psammite showing mottled texture and increased fracturing in response to intense silicification.

11. Finely bedded semi-pelite containing abundant subrounded biotite grains. Field of view = 20 x 26mm.

12a. Typical crack-seal textured stratabound quartz vein. The lower half of the vein contains coarse black-graphitic pelite clasts oriented parallel to the shear cleavage and small clots of carbonate and chlorite. In contrast the upper half of the vein contains coarse-grained disseminated pyrrhotite and thin pale-grey pelite inclusions. The different vein textures may be due to progressively intense silicification from the bottom of the plate to the top and or the presence of two discrete veins. The circle encloses a small nugget of gold.

12b. Massive milky quartz vein containing disseminated pyrrhotite grains.

12c. Massive milky quartz vein showing well developed columnar quartz crystals oriented perpendicular to vein wall. This is locally known as "speckled hen texture".

10a.

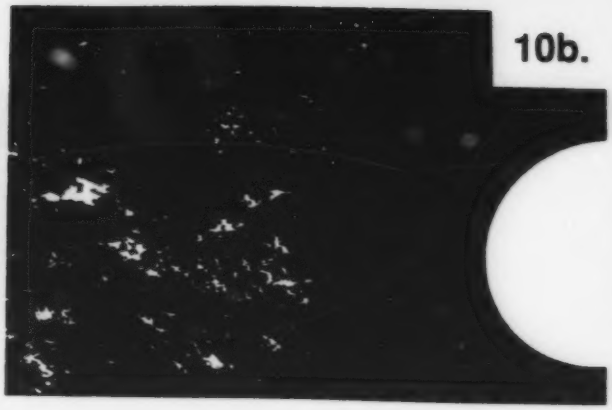

10b.

11.

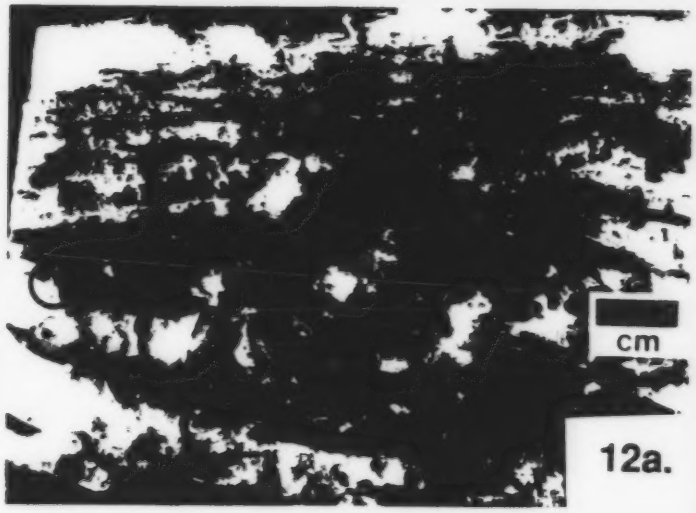

12a.

12b.

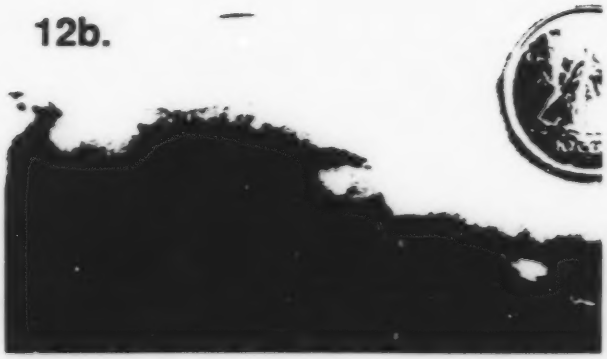

12c.

12d. Quartz vein showing inclusion-rich quartz platelets which comprise individual quartz columns. Field of view = 20 x 26mm.

12e. Crossed-polar photograph of 12c showing outline of quartz columns. The quartz grains show undulose extinction and recrystallized grain boundaries which are evidence of deformation. Field of view = 20 x 26mm.

12f. Crack-seal textured bedding parallel vein containing euhedral ilmenite crystals (indicated by arrow) alighned parallel to vein wall. The upper half of the vein contains coarse carbonate and chlorite grains. Field of view = 3.1 x 2.2mm.

12g. Quartz vein containing subhedral chlorite laths (indicated by arrow) of probable hydrothermal origin. Sulphide-bearing pelite inclusions within the vein reflect advanced degree of silicification compared to wall rock. Field of view = 10 x 14mm.

12h. Quartz vein containing euhedral apatite (ap) in contact with pyrrhotite and boudinaged chloritic pelite inclusion. Field of view = 3.1 x 2.2mm

12i. Specimen of massive pink calcite from within a stratabound vein. The calcite reflects a crack-seal texture similar to that of the quartz veins as reflected by the thin ribbons of quartz.

12d.

12e.

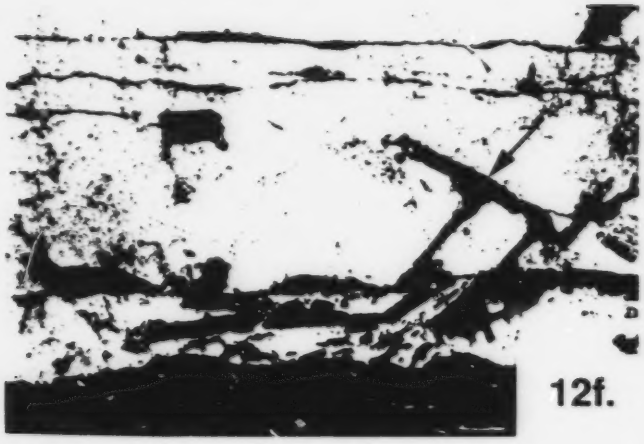

12f.

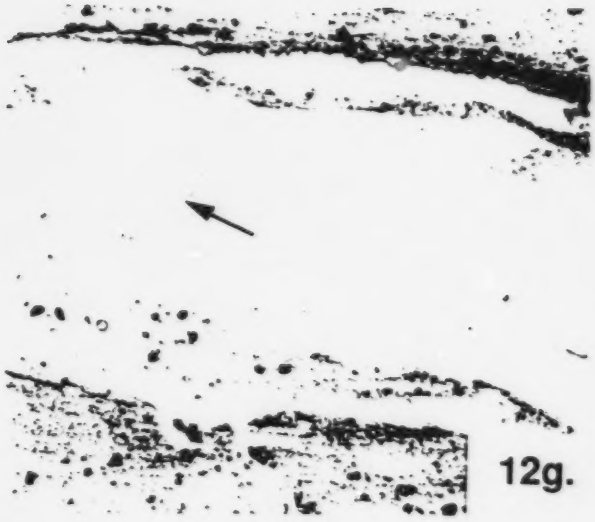

12g.

12h.

12i.

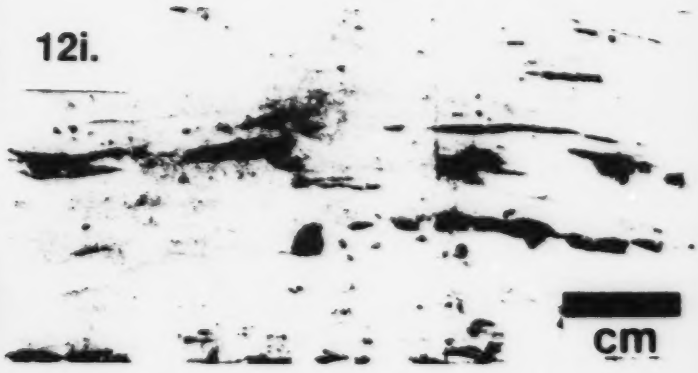

12j. Nugget of gold intergrown with pyrrhotite within a massive milky quartz vein.

12k. A narrow angular vein traversing psammite shows abrupt diversion at the pelite contact to become a folded bedding-parallel vein. Note the similar orientation of the minor fold axis within the quartz vein and the pyrrhotite grains scattered along the contact, probably reflecting presence of shear cleavage (S_4).

13 a-o. Examples of the bedding parallel Marker vein(s) package. Refer to Fig. 8 for plate locations. Top is at top of plate. The plates show the variation of the Marker vein(s) from a characteristic single, wide crack-seal textured vein with well developed "speckled hen" texture, to variations which include; several rolled veins and a intensely sheared vein(s) cross-cut by massive, milky quartz angular veins (13o). Ruler is 15cm long.

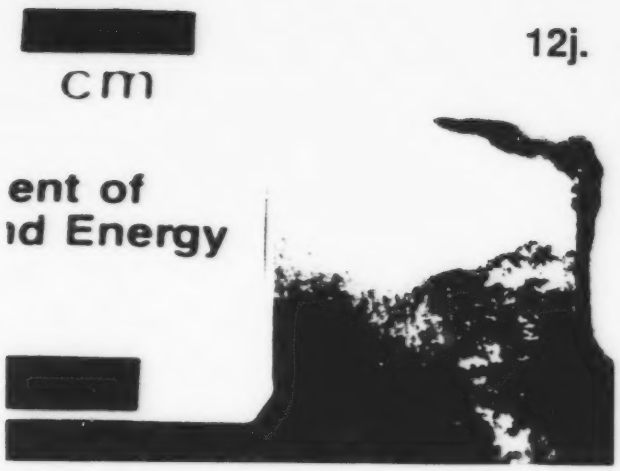

12j.

12k.

13a.

13b.

13c.

13d.

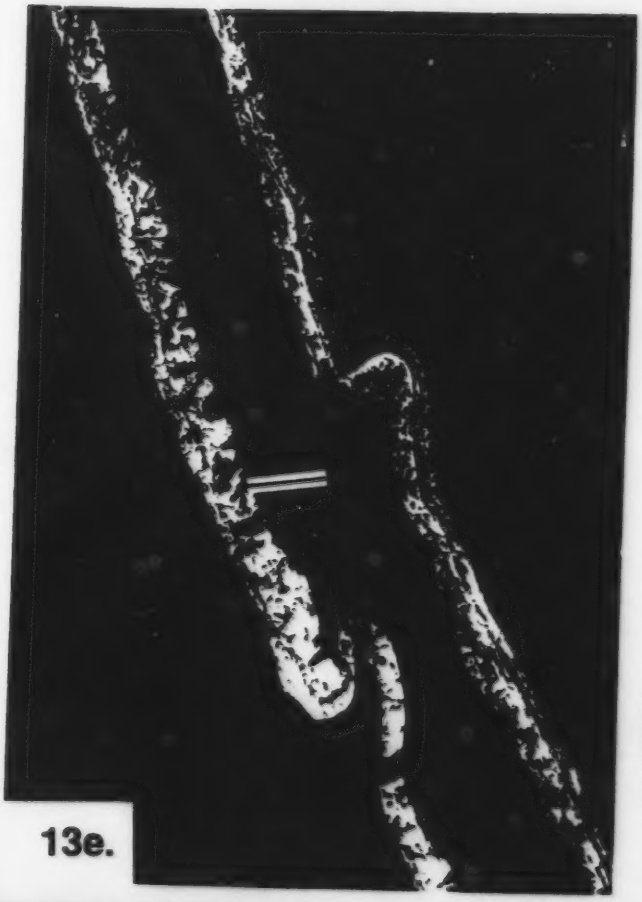

13e.

13f.

13g.

13h.

13i.

13j.

13k.

13l.

13m.

13n.

14 a-f. Examples of the Whin vein package. This vein package typically contains 4-7, intensely folded, bedding parallel, crack-seal textured veins.

13o.

14a.

14b.

14c.

15 a-j. Examples of the Twin vein package, typified by two, folded bedding parallel, crack-seal textured veins. Plates 15e,i,j show massive quartz angular veins cross-cutting the Twin veins and also becoming a bedding parallel vein where it encounters the Twin vein (15e).

14d.

14e.

14f.

15a.

15b.

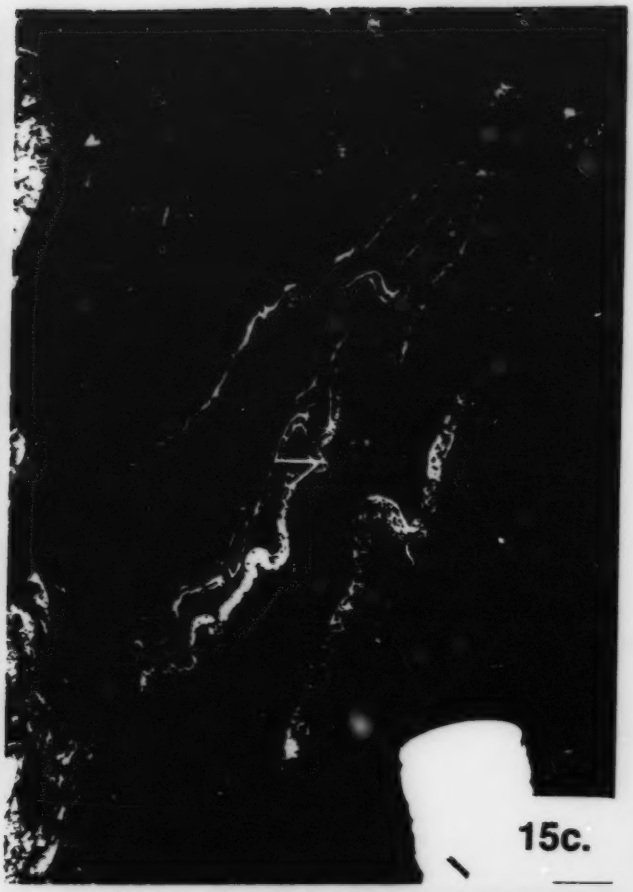

15c.

15d.

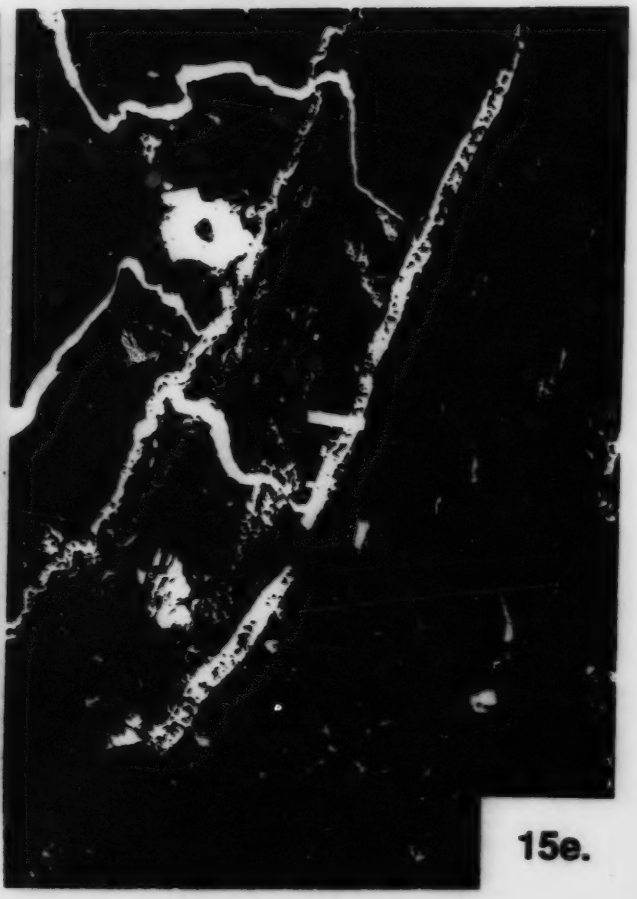

15e.

15f.

15g.

15h.

15i.

16 a-f. Examples of the Nugget vein package. Zone is typified by massive, en echelon and tension-gap quartz veins which can contain angular pelite fragments. However as shown in Plate 16d this vein may also show features typical of other bedding-parallel veins.

15j.

16a.

16b.

16c.

16d.

16e.

16f.

17a. Stratabound quartz vein containing boudinaged pelite inclusion alighned parallel to vein wall and also similarly oriented coarse pyrrhotite grains (opaques). The pelite wall rock at the bottom of the plate displays well developed slatey cleavage (S_2) marked by oriented chlorite porphyroblasts. In contrast the pelite adjacent to the quartz vein shows abundant S_4-oriented carbonate oikocrysts. Note the kinked thin dark bedding laminations indicated by the arrow within the pelite near the center of the plate. Field of view = 12 x 15mm.

17b. Folded quartz veins within black-graphitic pelite. The veins contain pyrrhotite blebs oriented parallel to the F_2 axial plane. Note that the carbonate oikocrysts in the pelite are similarly oriented with the exception of large undeformed carbonate at the hinge which presumably formed in the pressure shadow.

17c. S_4-oriented pyrrhotite striping cross-cut and deformed by a 1cm. wide D_5 shear zone within a black, graphitic pelite.

17d. Surface of stratabound quartz vein displaying prominent strike-parallel shearing with superimposed crenulation cleavage visible (indicated by arrow). The crenulations appear to trend perpendicular to that of the shearing.

17e. Close-up of 17d showing tightly crenulated stylolites and pyrrhotite ribbons (opaque). Field of view = 20 x 26mm.

17f. Statabound quartz vein showing disrupted and deformed stylolites, pyrrhotite and faint wall rock inclusions.

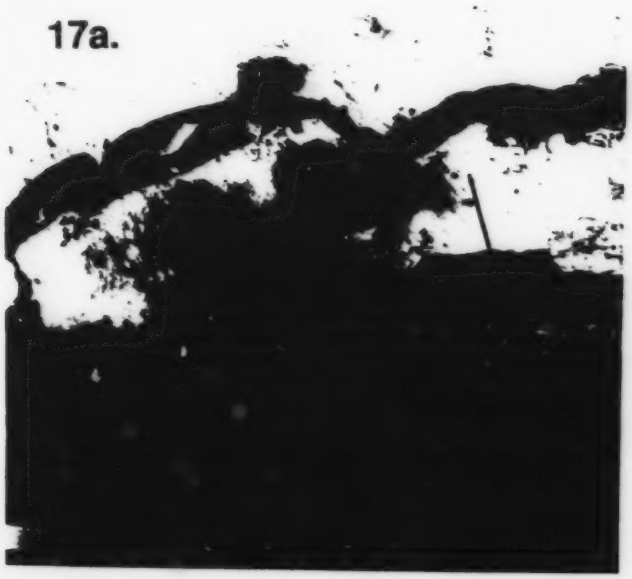
17a.

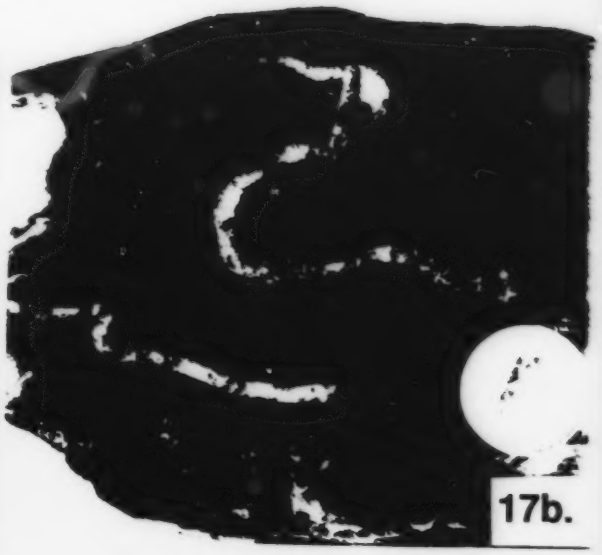
17b.

17c.

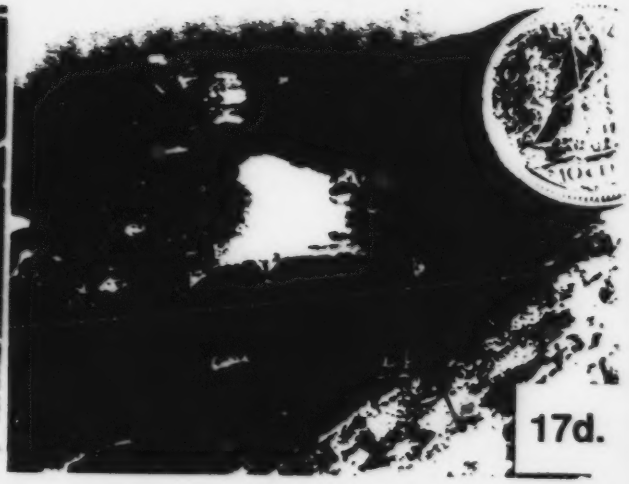
17d.

17e.

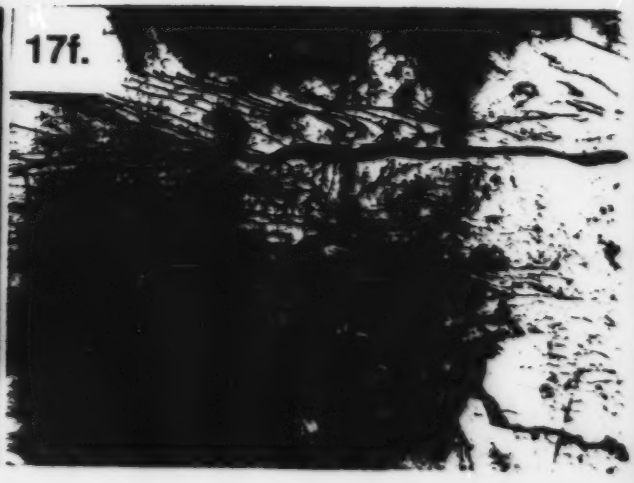
17f.

17g. Two narrow bedding parallel veins showing intense S_4 shear deformation.

18. Pelite wall rock inclusions within crack-seal textured quartz vein showing folding sympathetic to minor folds.

19. Boudinaged Marker vein showing characteristic massive milky quartz + carbonate infilling tension gashes at the boudin necks. The white painted stripes are approximately 1m apart.

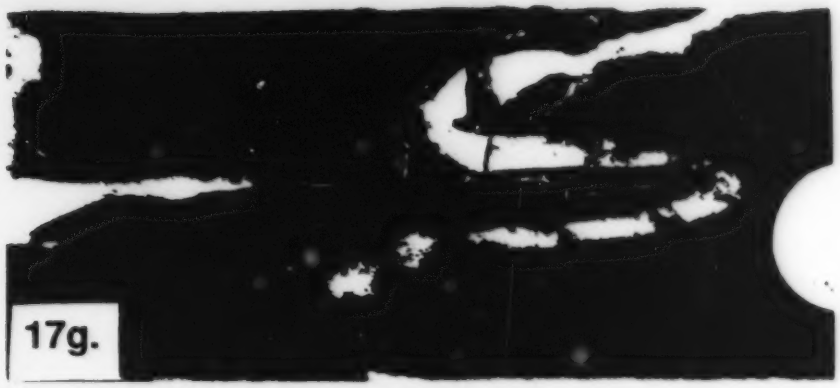

17g.

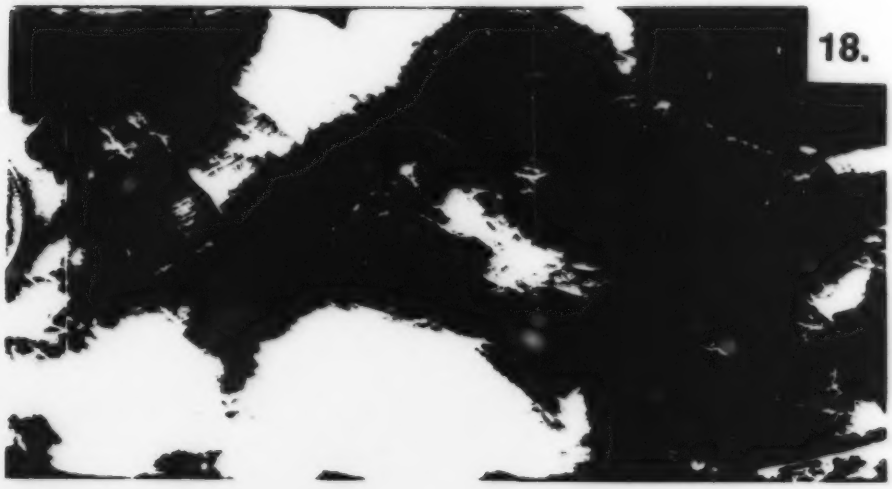

18.

19.

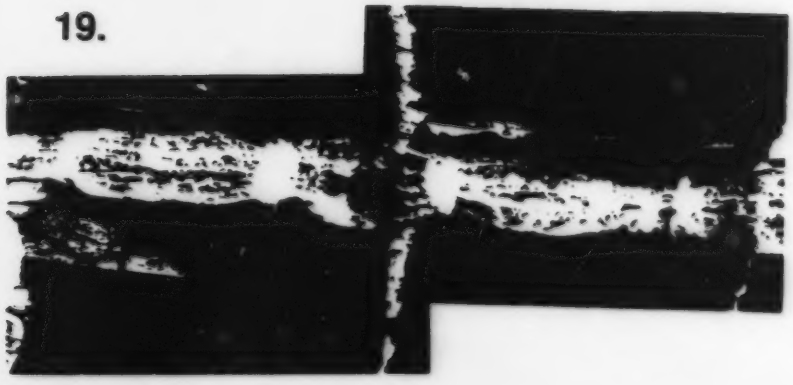

20a. Brecciated dark -green psammite cemented by quartz + carbonate. These breccias can be quite wide and locally very intense resulting in a microbreccia texture. This particular sample taken from N.S.D.M.E. drill core (TAN90-3) is part of a 5'wide breccia zone.

20b. Carbonate + chlorite breccia containing finely disseminated pyrite, commonly associated with NW-fault and shear zones.

20c. Pelite-hosted, folded bedding-parallel veins, cross-cut and displaced by a sub-vertical quartz + carbonate + pyrite stockwork system.

21. Marker vein showing approximately 1m of apparent dip-slip displacement.

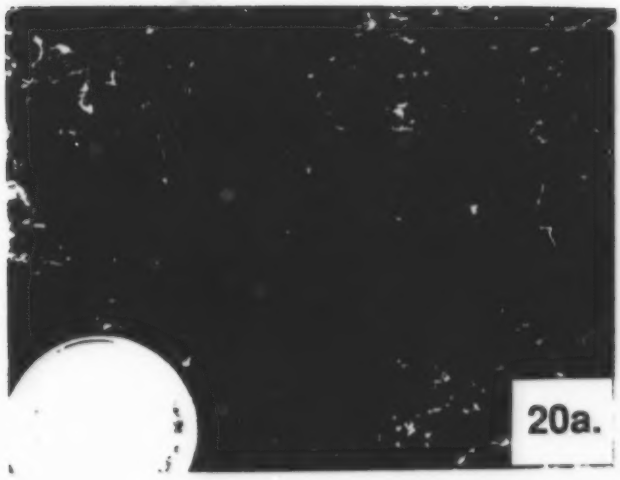

20a.

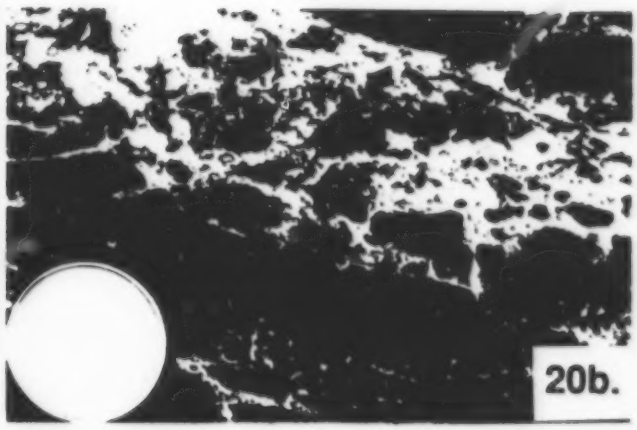

20b.

20c.

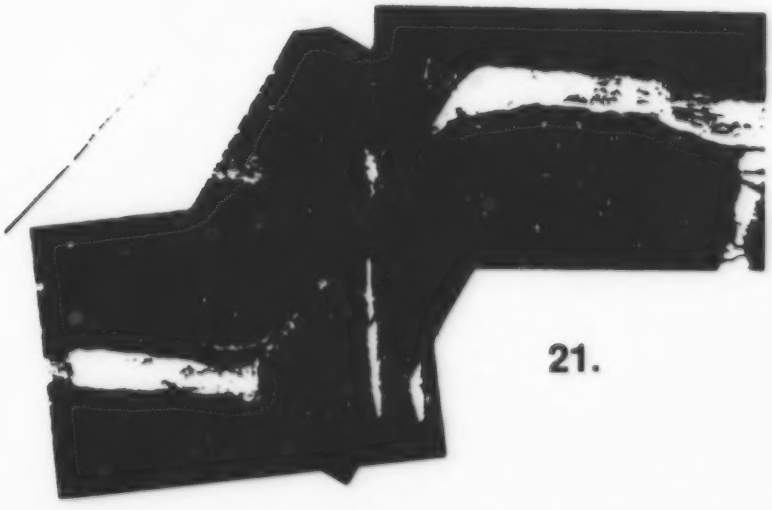

21.

22a. Approximately 1cm wide ductile shear zone within a pale-green silicified psammite. The margins of the shear zone are chlorite-rich and contain several < 1mm thick ribbons of pyrrhotite. A vuggy quartz-carbonate-chlorite vein occupies the interior of the shear zone.

22b. Close-up showing the ductile nature of the shear zone in contrast to the relatively undeformed psammite wall-rock. The abundant light grey mineral within the quartz vein is chlorite of probable hydrothermal origin. Field of view = 20 x 26 mm.

23a. Example of quartz-carbonate filled tension gashes associated with sub-vertical fault zone.

23b. Interbedded carbonate-rich psammite and black, graphitic pelite showing displacement by sub-vertical quartz-carbonate angulars. Distance of offset is unknown.

24. Well developed penetrative crenulation cleavage (S_c) within black, graphitic pelite.

25a. Core specimen (4.5cm wide) showing sulphide-clots within intensely sheared intercalated black pelite and carbonate+chlorite bearing psammite.

25b. Example of gold-bearing sulphide-clots oriented parallel to shear cleavage. Sulphides present include, arsenopyrite, pyrrhotite, chalcopyrite, galena and pyrite.

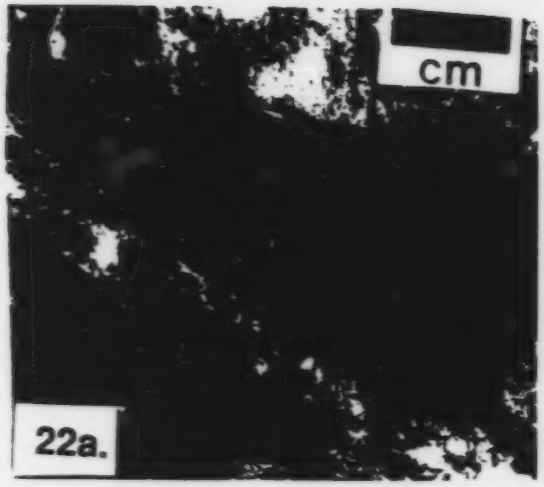

22a.

22b.

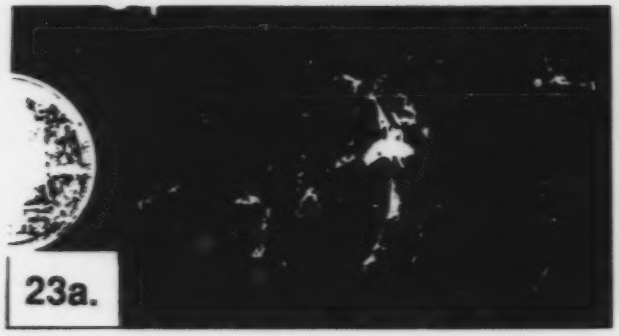

23a.

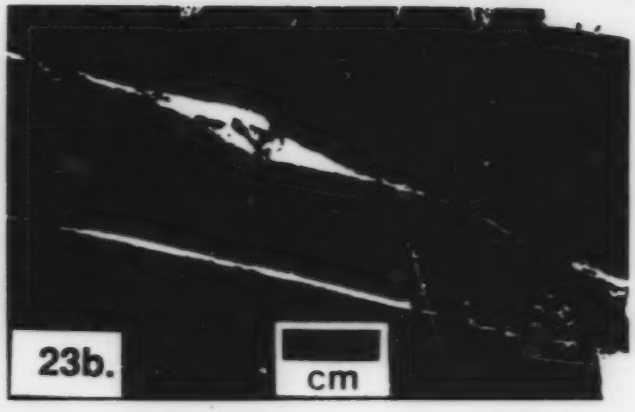

23b.

24.

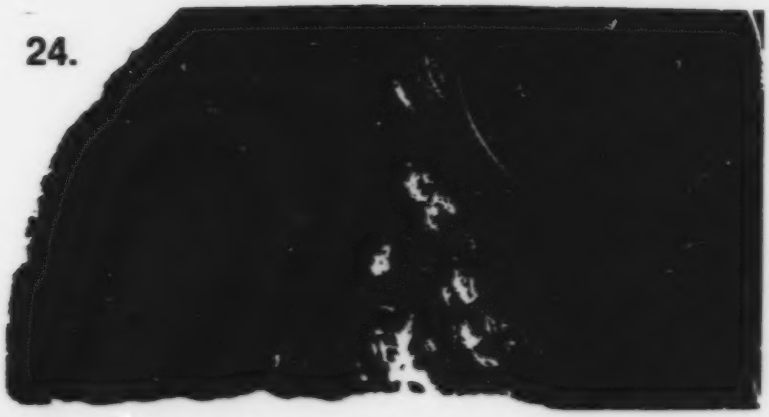

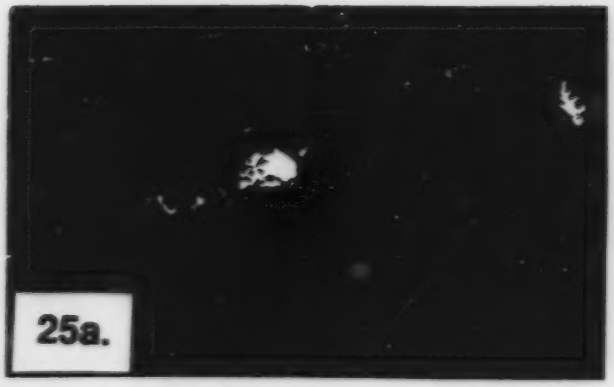

25a.

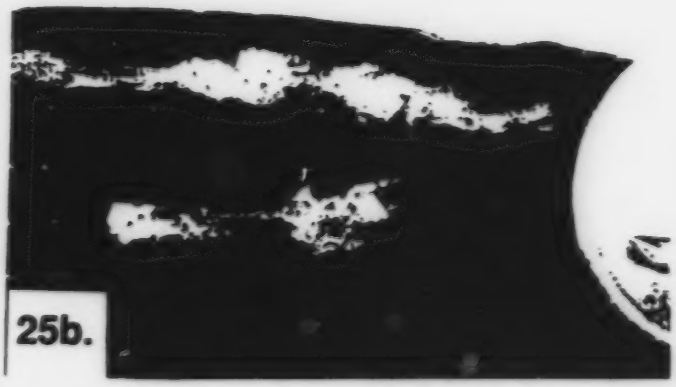

25b.

25c. Close-up of 25b showing S_4-oriented, strained quartz-carbonate filled pressure shadows flanking the sulphide clots. The psammite host rock contains abundant chlorite and carbonate porphyroblasts also parallel to the shear cleavage. Field of view = 20 x 26mm

25d. Typical sulphide clot showing large euhedral arsenopyrite (asp) crystals overgrowing pitted pyrrhotite (po) and chalcopyrite (cpy). Galena (gn) is also present as a grain within chalcopyrite and as fracture-filling within arsenopyrite. See 25e.

25e. Galena-filled fractures within arsenopyrite. Small grains of gold can be seen within a fracture in the top right and lower left.

25f. Gold-bearing pyrrhotite grains showing elongation parallel to the shear cleavage. Field of view = 3.1 x 2.2mm

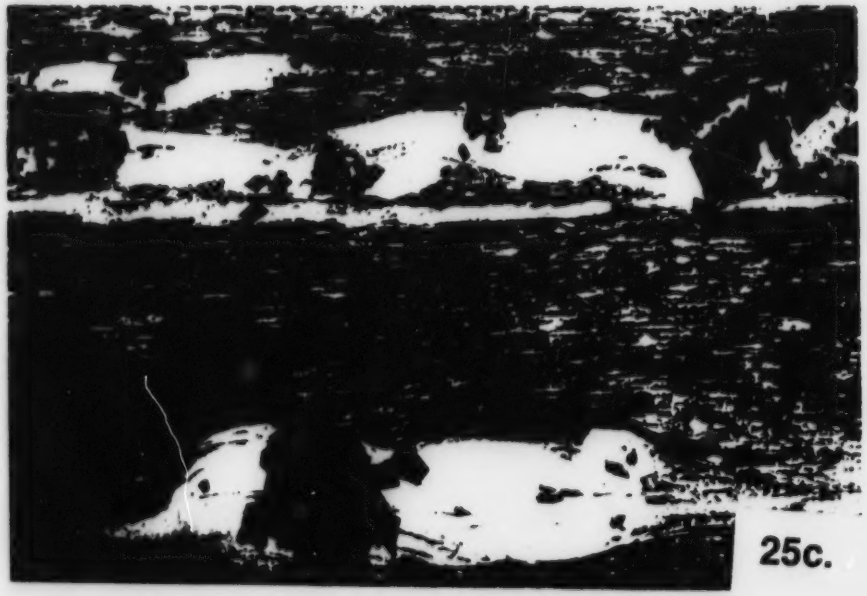

25c.

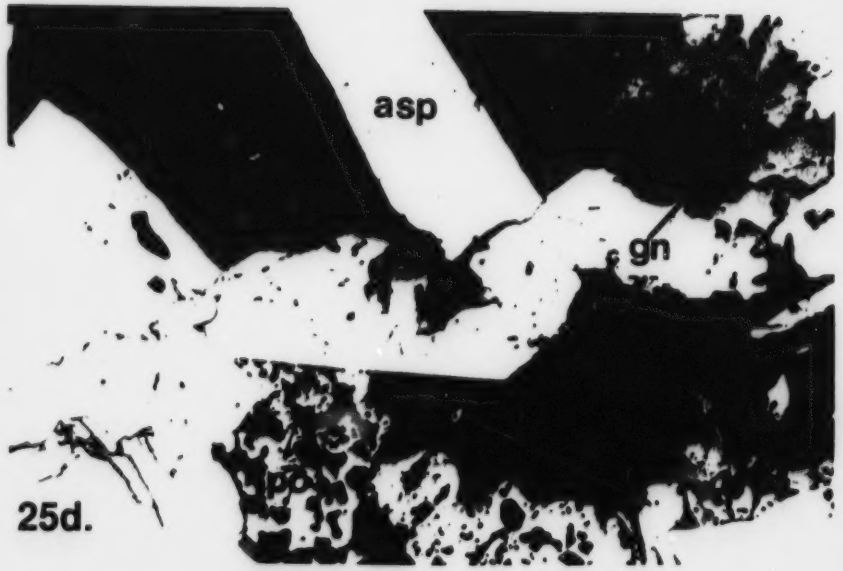

25d.